AD-A171 329 THE EFFECTS OF IMPLANTED DELAMINATIONS ON THE TENSILE STRENGTH OF GRAPHITE/EPOXY LAMINATES(U) AIR FORCE INST OF TECH WRIGHT-PATTERSON AFB OH L M ROBICHAUX 1986 1/2

UNCLASSIFIED AFIT/CI/NR-86-130T F/G 11/4 NL

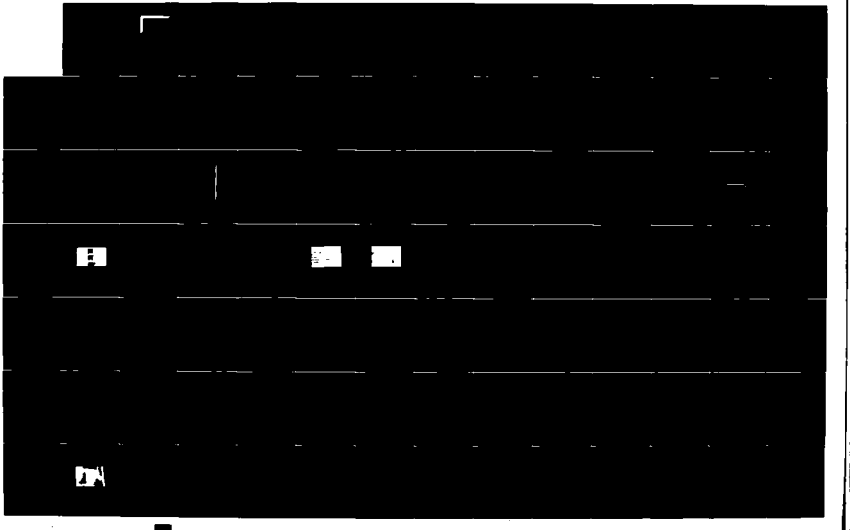

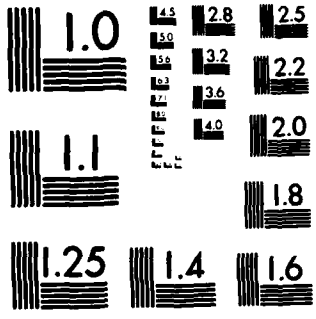

LEONARD MARK ROBICHAUX

B.S., United States Air Force Academy
(1978)

SUBMITTED TO THE DEPARTMENT OF
AERONAUTICS AND ASTRONAUTICS
IN PARTIAL FULFILLMENT OF THE
REQUIREMENTS OF THE DEGREE OF

MASTER OF SCIENCE IN
AERONAUTICS AND ASTRONAUTICS

DEPARTMENT OF
AERONAUTICS AND ASTRONAUTICS
MASSACHUSETTS INSTITUTE OF TECHNOLOGY
CAMBRIDGE, MASSACHUSETTS 02139

THE EFFECTS OF IMPLANTED DELAMINATIONS ON THE TENSILE BEHAVIOR OF GRAPHITE/EPOXY LAMINATES

by

LEONARD MARK ROBICHAUX

B.S., United States Air Force Academy
(1978)

SUBMITTED TO THE DEPARTMENT OF
AERONAUTICS AND ASTRONAUTICS
IN PARTIAL FULFILLMENT OF THE
REQUIREMENTS OF THE DEGREE OF

MASTER OF SCIENCE IN
AERONAUTICS AND ASTRONAUTICS

at the

MASSACHUSETTS INSTITUTE OF TECHNOLOGY

FEBRUARY 1986

Signature of Author Leonard M. Robichaux
Department of Aeronautics and Astronautics
January 17, 1986

Certified by Paul A. Lagace
Professor Paul A. Lagace
Thesis Supervisor

Accepted by Harold Y. Wachman
Professor Harold Y. Wachman
Chairman, Departmental Graduate Committee

SECURITY CLASSIFICATION OF THIS PAGE *(When Data Entered)*

REPORT DOCUMENTATION PAGE		READ INSTRUCTIONS BEFORE COMPLETING FORM
1. REPORT NUMBER AFIT/CI/NR 86-130T	2. GOVT ACCESSION NO.	3. RECIPIENT'S CATALOG NUMBER
4. TITLE *(and Subtitle)* The Effects Of Implanted Delaminations On The Tensile Strength Of Graphite/Epoxy Laminates		5. TYPE OF REPORT & PERIOD COVERED THESIS/DISSERTATION 6. PERFORMING ORG. REPORT NUMBER
7. AUTHOR(s) Leonard Mark Robichaux		8. CONTRACT OR GRANT NUMBER(s)
9. PERFORMING ORGANIZATION NAME AND ADDRESS AFIT STUDENT AT: Massachusetts Institute of Technology		10. PROGRAM ELEMENT, PROJECT, TASK AREA & WORK UNIT NUMBERS
11. CONTROLLING OFFICE NAME AND ADDRESS AFIT/NR WPAFB OH 45433-6583		12. REPORT DATE 1986 13. NUMBER OF PAGES 150
14. MONITORING AGENCY NAME & ADDRESS*(if different from Controlling Office)*		15. SECURITY CLASS. *(of this report)* UNCLAS 15a. DECLASSIFICATION/DOWNGRADING SCHEDULE

16. DISTRIBUTION STATEMENT *(of this Report)*

APPROVED FOR PUBLIC RELEASE; DISTRIBUTION UNLIMITED

17. DISTRIBUTION STATEMENT *(of the abstract entered in Block 20, if different from Report)*

18. SUPPLEMENTARY NOTES

APPROVED FOR PUBLIC RELEASE: IAW AFR 190-1

LYNN E. WOLAVER
Dean for Research and Professional Development
AFIT/NR

19. KEY WORDS *(Continue on reverse side if necessary and identify by block number)*

20. ABSTRACT *(Continue on reverse side if necessary and identify by block number)*

ATTACHED.

DD FORM 1 JAN 73 1473 EDITION OF 1 NOV 65 IS OBSOLETE

SECURITY CLASSIFICATION OF THIS PAGE *(When Data Entered)*

THE EFFECTS OF IMPLANTED DELAMINATIONS ON THE TENSILE STRENGTH OF GRAPHITE/EPOXY LAMINATES

by

LEONARD MARK ROBICHAUX

Submitted to the Department of Aeronautics and Astronautics on January 29, 1986 in partial fulfillment of the requirements for the Degree of Master of Science

ABSTRACT

The fracture of graphite/epoxy laminates implanted with materials to cause local delaminations was investigated both experimentally and analytically to assess the effects of the implants on the stress-strain behavior and ultimate tensile strength. Two different stacking sequences were examined: $[\pm 45/0]s$ and $[0/\pm 45]s$ with a majority of the tests conducted on the first stacking sequence. Implant thickness, shape, size, and configuration, which describes the number and location of the implants, were varied. All implants were centered in the specimen. All these variables except implant shape were discovered to affect the fracture strength of the laminate. Implants with thicknesses below 0.0127 mm will not reduce the fracture stress as observed for the thin implants utilized. Reductions in strength for thicknesses greater than this are a result of the stress redistribution in the plies due, in part, to an induced bending moment as each ply is forced to bend around the implant. Significant stress redistributions predicted by the model occur when more than one implant is embedded in a laminate. Multiple implants which isolate plies prevent a path for three-dimensional load transfer within the delaminated region. Thus, cracks which form in this region will grow quickly into splits until arrested by the laminated plies. These cracks reduce the bending stiffness and strength of the delaminated plies. This will cause the laminate to fail at a reduced stress level than it would otherwise. Implant width was also found to reduce strength. The model could adequately simulate all these effects except for that due to the width.

Thesis Supervisor: Paul A. Lagace

Title: Charles Stark Draper Assistant Professor of Aeronautics and Astronautics

A-1

ACKNOWLEDGEMENTS

I cannot begin to recall all of the people who have helped me and befriended me during these past eighteen months. I'd like to extend a personal "thank-you" to all but with Uncle Sam banging at my door, I must rush off. Please pardon me for this.

My first thanks must go to the faculty and administration of MIT for accepting me into the Master's Program and providing me with an education above my expectations. Thanks for the challenge.

The department staff proved to be an invaluable asset. Special thanks must go to Al Supple and Carl Varnerin. Al always seemed to have the knowledge of God, the patience of Job, and proved to be a good friend as well. I'm sorry I can't compare you to God Carl, but your help and friendship I shall always remember. Carl's assistance proved to be a life-saver for me more than once and I couldn't have completed my manufacturing without him. Special thanks also go to Ping Lee for her assistance and Debra Smith as well.

I shall never forget my office mates! Their translation and explanations of the lectures got me through the course work. Thanks all of you: Masami, Pierre, Doug C., Gun-shing, Sim, Cheng, Ray, Mike; as well as the crew upstairs: Dave, Tony, John B., John S., Marc, Steve, Doug W., Hatem, and the rest of the gang. Extra thanks is reserved for Kevin. His advice, assistance, and friendship were just what I needed when the walls seemed to be coming down upon me. I cannot thank the delamination crew too much either: Doug F., Rikki, Mike, and Julie. They were the ones who had to do all of the "dirty" work. Their devotion and help in accomplishing the tedious chores were not overlooked.

I cannot forget my first friend and lab partner at MIT; Tom Grapes. Whether it was giving his time in explaining tough concepts, helping me with lab work, or just having a listening ear, Tom was there. Tom is a true brother and an eternal friend.

Paul, I didn't forget you but thought it fitting to thank you last since you had to work as hard drafting this thesis as I did. I didn't realize what iteration really was until I met Paul. His thoughful insight, hard work, and sound advice helped to bring this thesis together.

DEDICATION

To my beautiful and loving wife. Thanks for standing by me these past eighteen months. You make life worth living!

TABLE OF CONTENTS

LIST OF FIGURES

LIST OF FIGURES (Continued)

LIST OF FIGURES (Continued)

LIST OF TABLES

LIST OF DATA TABLES

NOMENCLATURE

C	circular (delamination)
CLPT	Classical Laminated Plate Theory
C_{PS}	plane stress correction factor
$E^{[\theta i]}_{\alpha\beta\sigma\gamma}$	2-D elasticity tensor for the ith ply
E^{D}_{L}	longitudinal stiffness in the delaminated region
E^{L}_{L}	longitudinal stiffness in the laminated region
h	laminate thickness
N	cycles
N_n	normal incidence fringe order
N_θ	oblique incidence fringe order
S	square (delamination)
TCGF	Teflon Coated Glass Fabric
t_{ply}	ply thickness
W	specimen width
W^D	width of the delaminated region
x_1	longitudinal direction
x_2	transverse direction
z^i	distance from the laminated region midplane
z_{il}	distance from the laminated region midplane to the upper surface of the ith ply
z_{iu}	distance from the laminated region midplane to the lower surface of the ith ply
ε°_{11}	longitudinal strain at the reference plane
ε^{i}_{11}	longitudinal at level z^i
ε_L	longitudinal strain

NOMENCLATURE (Continued)

κ_{11}^{i}	longitudinal curvature
κ_{12}^{i}	twisting curvature
κ_{22}^{i}	transverse curvature
σ	stress
$\sigma_{11,[\theta i]}^{LD}$	longitudinal stress in the ith delaminated ply
$\sigma_{11,[\theta i]}^{L}$	longitudinal stress in the ith laminated ply
σ_{L}^{D}	longitudinal stress in the delaminated region
σ_{FF}^{L}	far-field longitudinal stress
$\sigma_{\alpha\beta}^{[\theta i]}$	stress tensor in ply axes

CHAPTER 1

INTRODUCTION

Over the past twenty years, composites have found their way into many new industries. Their uses range from recreational; tennis racquets, skis, tent poles, and even sunglasses, to name a few, to the high technology industries like the aerospace industry. One of the great advantages of composite materials is their high specific stiffness and strength compared to metals. As a result, the major developments in composite materials have come from the aerospace industry where weight savings are at a premium.

With all of the advantages that composite materials offer, their usage has been limited. Part of the reason for this is that their behavior, particularly when damaged, has not been fully characterized. The many interactions and unknowns of a highly orthotropic material like a composite are complex and models which are capable of describing these interactions are limited in scope. As a result, composites have not been used to their fullest potential. Design engineers have instead often opted to use "quasi-isotropic" laminates which do not exploit the tremendous ability of these highly orthotropic composites to be tailored to a specific application. Thus, composites have been used by the aerospace industry mainly on secondary structural components such as flaps, tail sections,

and other selected structures.

As progress continues in the field of fracture in composites, predictions of strength and failure modes have improved greatly. Engineers have adapted methods used in describing the response of metals and have developed new techniques as well. This and other research has led to wider acceptance of the use of composite materials.

Composite materials are currently becoming a primary material in the construction of aircraft components. Trends in the aircraft industry to use composites in large structural load carrying members has made it important to consider their susceptibility to damage caused by an impact event. This type of damage can be caused during maintenance by dropped tools or parts or via in-service damage such as that caused by runway kick-up or bird strikes. Damage of this nature in metals will often cause dents providing warning that further damage like cracking may be present. In composite materials, however, damage may be internal, completely hidden from the inspector or operator's view.

Labor and Bhatia [1] conducted numerous impact tests on composite panels in order to characterize the damage sustained from such an event. They examined panel size, impact location, size and shape of impactor, panel thickness, type of edge supports, and variations in the mass and velocity of the impactor. Tests on graphite/epoxy panels of eight, sixteen, and thirty-two plies showed delamination as the dominant damage mode although matrix cracking was also present. Thinner panels

showed more delamination, especially near the panel midplane while the thicker ones showed less total delamination which occurred closer to the surface. Clearly these results have a profound effect on the aerospace industry. If the structure containing the delamination were a major aircraft component subject to tensile, compressive, and cyclic loads during service, the residual strength and life of the component could be dramatically affected.

This investigation will seek to provide some answers to the problem of delamination in composite materials. While a majority of the work accomplished has concentrated on the problems associated with delamination at the edges of panels, this study will examine the internal delamination problem which could be caused from an impact event. This is accomplished by implanting a release material into the laminate to cause an internal delamination. A review of the pertinent work which has been accomplished in the area of delamination is provided in Chapter 2. These include edge delaminations which arise as a result of tensile or fatigue loads and compression and fatigue of internal delaminations. The experimental program including manufacture, instrumentation, and testing is detailed in Chapter 3. The specimen as manufactured with the implants is then modeled in Chapter 4 to correlate and explain the experimental data. The experimental results are presented in Chapter 5 along with the response predicted by the analytical model. A discussion of the data and the accuracy of the model are provided in Chapter 6 along with the further implications

of this work. A summary in the form of conclusions and recommendations for further work is given in Chapter 7.

CHAPTER 2

SUMMARY OF PREVIOUS WORK

Delamination in composite materials often causes deterioration of laminate structural properties including strength, stiffness, reliability, and durability. Although delamination occurs initally as local damage, it can propogate rapidly causing catastrophic laminate failure. Numerous studies have been conducted in an effort to characterize delamination onset, growth, and fracture. These include research into the many aspects of the edge delamination problem and compression tests on specimens with delaminations embedded under different plies. A brief description of these problems as related to the effects of impact damage follows.

2.1 Free Edge Delamination Problem

The free edge delamination phenomenon has been examined for over a decade. The causes are the interlaminar tensile and shear stresses which are concentrated near the laminate free boundaries [2]. These stresses arise due to the mismatch in elastic constants from ply to ply [3]. Early analytical methods formulated to explain edge delamination and its characterisics concentrated on determination of the free-edge interlaminar stresses [4,5,6,7]. While a volume of promising

work continues in this area [8,9], research has recently turned to an alternate method of predicting delamination. Since delamination can be modeled as an interply crack, a fracture mechanics approach has been sought. This approach assumes that strain energy is released and converted to surface energy when delaminations form. The driving force for crack extension, G, is the strain energy available to be released per unit of newly created surface. Rybicki et al. [10] proved this to be a viable technique for describing the delamination process. This approach is used in the following three examples which associate the edge delamination problem to impact damage.

S.S. Wang [11] examined delamination growth from a transverse cut in a unidirectional laminate under static and cyclic loading. The cut modeled the damage which occurs when a sharp impactor contacts a composite panel. The unidirectional laminate was chosen since it is the simplest ply configuration. Thus the fundamental nature of delamination crack growth behavior could be studied. His results showed the delamination crack grew in a stable manner until a critical stress value, σ_c, was reached. He found σ_c to vary with laminate and geometric parameters, loading conditions, and enviroments. Delamination crack extension under cyclic loads was found to continue at an increasing rate until a critical number of cycles, N_c, for the specific cyclic loading condition.

Another source of delamination examined by several investigators [12,13,14,] are those which form at the tips of

longitudinal matrix cracks. These cracks were found to form during typical impact events [1]. The interlaminar stresses which arise in a ply interface when the crack tip is located there can cause local delaminations to form and grow. O'Brien [15] developed a simple equation for strain energy release rate and was able to predict the local delamination onset strains in $[\pm 25/90_n]_s$ laminates where the delaminations were located in the 90° plies. Additionally, the analysis predicted the trend of lower delamination onset strains associated with increased thickness of the 90° ply group.

The third example is a through-the-width delamination examined by several investigators. A.S.D. Wang and Slomiana [16] simulated this damage by embedding thin teflon strips, approximately 50 microns in thickness, in several laminates and subjected them to static tensile and fatigue loading. The strips measured 6.35 mm and 12.7 mm long and covered the full width of the specimens. They were located at the midplane of the laminates. A step load scheme was employed so delamination onset and growth could be monitored. After each step load, specimens were removed from the tester and examined using x-radiography for any damage occurring during that loading sequence. His results showed that the implants had some measurable adverse effects on the initiation of both transverse cracks and edge delamination. Both of these events occurred earlier; however the final failure strength of the laminates remained unaffected. X-radiographs showed that in both cases the free edge delamination growth was extremely stable so that

the influence of the implanted defect became insignificant as the load reached its ultimate. The tension-tension fatigue tests showed the presence of the implant precipitated early delamination leading to reduced life.

2.2 Internal Delamination Problem

Another type of delamination which can arise when an object impacts a composite part is an internal delamination. This may present a more dangerous condition since it is far more unlikely that this damage will be detected by an inspector. On the other hand, edge delamnation will always leave a clue since the initiation site must be a free edge. Research on this problem has concentrated on the effects of compressive failures.

In one of the most comprehensive works, Chai and Babcock [17] developed an analytical model to determine the compressive strength criticality of an elliptical interlaminar defect located near the surface. The elliptical delamination separated a thick isotropic plate from a thin orthotropic layer whose material axes were aligned with the ellipse axes. Conditions for growth initiation, or buckling, were found using the Rayleigh-Ritz method while the delamination growth was evaluated using the fracture mechanics approach of balancing the strain energy release rate and the energy required to create new surface area. They found that the parameters which govern the growth or arrest of the delamination are fracture

energy, disbond depth, and the elastic properties of the materials on either side of the delamination. Stable or unstable growth, parallel or normal to the loading axes, was dependent upon the degree of material anisotropy relative to the loading axes.

An experimental investigation into the compressive behavior of the internal delamination was conducted by Ramkumar [18]. He embedded both thru-the-width and circular internal delaminations at several locations near the surface of four, 64 ply specimens to simulate low velocity impact damage. Static compression tests showed that both implants were harmful when the delaminations were located under the surface ply of the $[0/45/90/-45]_{8s}$ specimens. The thru-the-width delamination caused a larger strength loss while the strength reduction for the specimen with a circular delamination was dependent upon the implant location. As the implant was moved toward the midplane, both failure strength and transverse deflection were reduced. The compression fatigue behavior showed the embedded flaw grew in a stable manner when it was located under a stiff (45° or 0°) ply and was accompanied by a large deflection of the flawed area. When the circular delamination was positioned farther away from the surface, flaw growth was sudden and unstable, much like the static compression failure modes.

A.S.D. Wang and Slomiana [16] also investigated the internal delamination problem and linked it with the free edge delamination phenomenon. They implanted a 6.35 mm circular disk within the interior of the laminate. Compression tests

revealed the delamination at the center had no effect on edge delamination, which occurred first. Once edge delamination started, however, the circular implant affected the growth behavior causing a lower failure load. Compression-compression fatique tests revealed specimens with implanted delaminations caused edge delamination in speciemens about 10% earlier reducing the life by about the same amount.

Other investigators have studied the internal delamination problem as well. These studies have centered around characterizing the compressive behavior where buckling of the delaminated "sublaminate" and subsequent delamination and growth are the primary concerns. On the other hand, tension studies have concentrated on examining the edge delamination problem. This study proposes to investigate the material effect which internal implanted delaminations have on the tensile response of a composite laminate, that is, without the local buckling which occurs in a compression test.

CHAPTER 3

THE EXPERIMENT

3.1 Material and Specimen Choice

The graphite/epoxy used in this investigation is Hercules AS4/3501-6. The material is furnished as a continuous roll of unidirectional tape with a nominal width of 305 mm. The epoxy system of the preimpregnated tape or "prepreg" is in a semi-cured state and hence stored in freezers at -18°C or below until used. The elastic properties of a unidirectional AS4/3501-6 ply are given in Table 3.1.

The specimen utilized in this investigation is a straight-edged coupon measuring 350 mm long by 71 mm wide. This is wider than the standard coupon used at TELAC [19]. The additional width is needed so that larger implanted delamination sizes can be used while still providing adequate distance between the implanted delamination edge and the coupon edge. Thus, any effects the coupon edge may have had on delamination initiation or growth were separated from those caused by the implant. Glass/epoxy loading tabs 76 mm long were bonded to the ends of the specimen with FM-123-2, a film adhesive from American Cyanimid. The loading tabs were 3M type 1002 with a lay-up of nine plies of alternating 0° and 90° plies. This provided the proper tab thickness to specimen thickness ratio recommended by the American Society for Testing and Matrials [20]. The final length of the gage, or test,

TABLE 3.1

ELASTIC PROPERTIES OF AS4/3501-6 GRAPHITE/EPOXY

E_L	147.2 GPa
E_T	9.65 GPa
G_{LT}	6.84 GPa
ν_{LT}	0.3

section of the specimen is thus 200 mm. The specimen and its dimensions are illustrated in Figure 3.1.

3.2 Laminate and Implant Specification Choices

Two laminates with different stacking sequences were chosen for this investigation: $[\pm 45/0]_s$ and $[0/\pm 45]_s$. Experiments by Lagace [21] on AS1/3501-6 have shown that laminates with these stacking sequences using lamination angles above 30° do not demonstrate a propensity to fail by delamination. The change in fiber from AS1 to AS4 should not change this characteristic significantly. Thus, the edge delamination and the implant problem are separated. The 45° lamination angle was also selected in part, for this reason but additionally due to the fact that 45° is a primary lamination angle used in composites within the aerospace industry. The $[\pm 45/0]_s$ laminate is the primary laminate investigated while the $[0/\pm 45]_s$ laminate is examined to determine the effect of a stacking sequence change.

To fully understand the effects the implanted delamination might have on the tensile strength and general behavior of the specimen, the implant size, shape, and thickness were varied. A circular shape was chosen because of its smooth exterior contour while a square shape provides sharp corners for contrast. The shapes were cut so the edge dimension of the square is the same as the diameter of the circle. This will be referred to as the implant width.

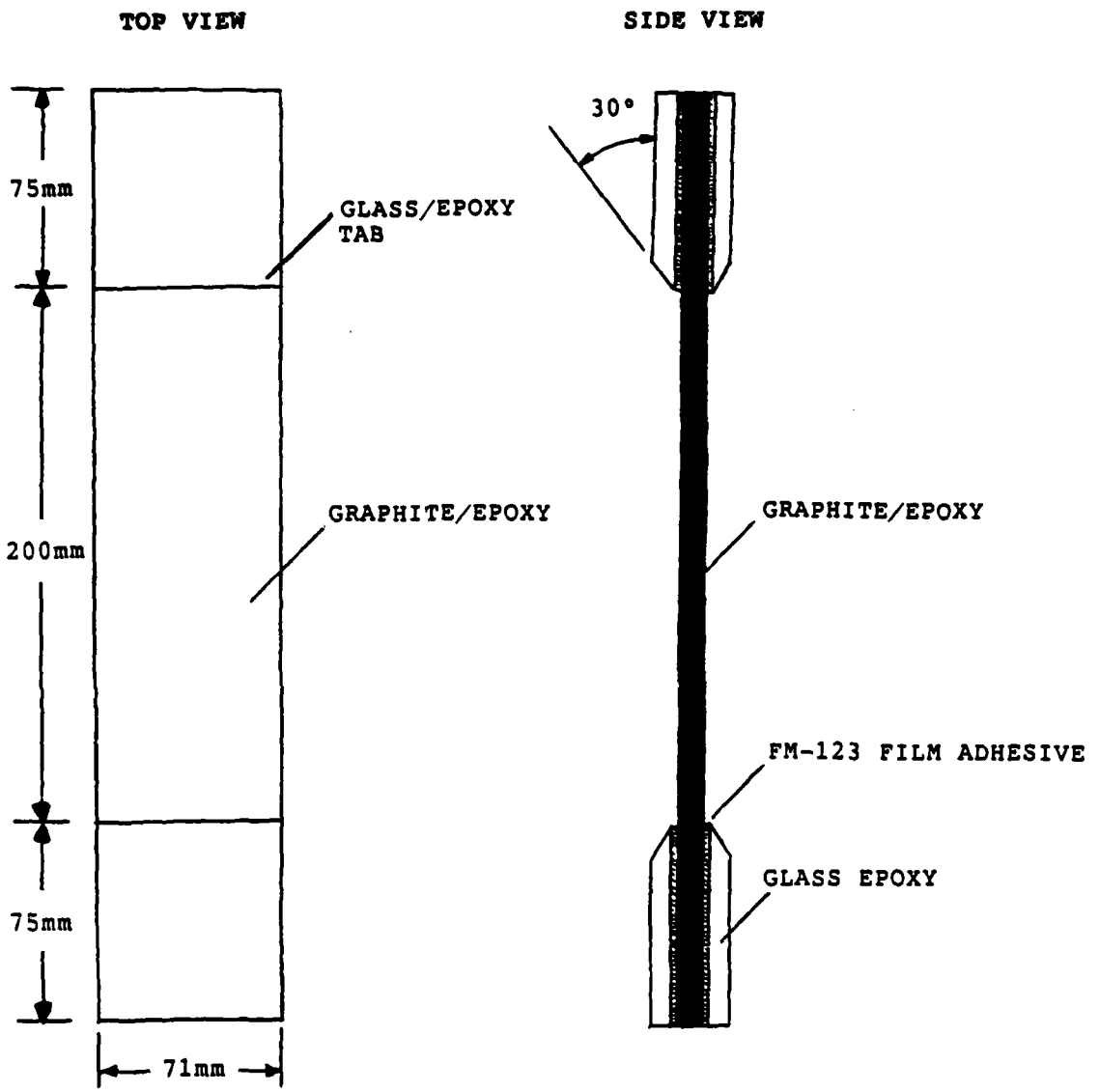

FIGURE 3.1 CONFIGURATION OF TEST SPECIMEN

Two implant widths were selected, 32 mm and 57 mm. The 32 mm wide implant gave a ratio of implant width to specimen width of approximately 0.5. The 57 mm wide implant was selected since it was the largest size that could be safely implanted in the specimen while still providing adequate margin from the specimen edge to avoid edge effects as well as to assure that the edges were well bonded given the limitations in accuracy of the manufacturing procedure. High interlaminar stresses exist at the free edges of coupon specimens and can cause delamination initiation there. Lagace and Kassapoglou [22] have shown these stresses decrease quickly away from the specimen edge and can be avoided by using this size implant.

In addition, two implant thicknesses were chosen to ascertain whether the thickness affects the results. These thicknesses were chosen based upon the material which was used to create the delamination. Teflon-Coated Glass Fabric, herein referred to as TCGF, was selected since it is used as a release material and will provide a clean, well defined delamination. Its thickness is 0.076 mm which is 56% of the nominal thickness of a cured graphite/epoxy ply. When five of these implants are stacked between the plies of a laminate, the specimen is no longer flat but has a large bulge at the implant site. Thus, Dupont FEP 50A general purpose teflon film was used as the second implant type. Its measured thickness is 0.0127 mm which is 10% of the nominal cured graphite/epoxy ply thickness of 0.134 mm. This implant results in a much less noticeable overall thickness change at the implant site.

Additionally, the implants were imbedded inside the laminate in four different configurations. A single implant located under the first ply was selected since studies by Labor and Bhatia [1] have shown that low velocity impacts can cause this type of delamination in thin composite panels. This single implant is then moved to a position under the second ply and then to the midply to determine if delamination location is a factor. When the implant is moved to this position, an oversized rectangular implant is used which is 57 mm wide but extends to within 13 mm from each loading tab. This large rectangular implant will serve to bound the single implant investigation. The last configuration chosen involves implanting a delamination at every ply interface. This not only simulates damage from a more severe impact event, but again provides a bound to this study. By changing implant size, shape, thickness, and location, a full compliment of tests were conducted on the $[\pm 45/0]_s$ laminates. In addition, size is varied in tests conducted on $[0/\pm 45]_s$ laminates to provide a comparison by stacking sequence. The entire test matrix indicating the number of specimens of each configuration is presented in Table 3.2.

3.3 Nomenclature

A shorthand notation was developed to aid in the identification of each individual specimen. The notation is a modification of the 3-bit TELAC code and has the following

TABLE 3.2

TEST MATRIX

CODE	LAYUP	DELAMINATION				NUMBER OF SPECIMENS
		SHAPE	NUMBER/LOCATION	SIZE [mm]	MATERIAL	
45A1-X	$[\pm 45/0]_s$	---	0/none	--	-	6*
C1-45A1-X1G		Circle	1/1st interface	32	G	5
S2-45A1-X2F		Square	1/2nd interface	57	F	6*
S3-45A1-XG		Rectangle	1/midplane	57x178	G	5
C4-45A1-X1F		Circle	5/all interfaces	32	F	5
S4-45A1-X1F		Square	5/all interfaces	32	F	5
S4-45A1-X2F		Square	5/all interfaces	57	F	6*
C4-45A1-X1G		Circle	5/all interfaces	32	G	10
S4-45A1-X1G		Square	5/all interfaces	32	G	5
S4-45A1-X2G		Square	5/all interfaces	57	G	15
45B1-X	$[0/\pm 45]_s$	---	---	--	-	5
S4-45B1-X1G		Square	5/all interfaces	32	G	5
S4-45B1-X2G		Square	5/all interfaces	57	G	5

X - Denotes Specimen Number
G - TCGF
F - Film
* - Denotes One Photoelastic Test Conducted

form:

Ql-θRm-npS

where the three parts are described as the prefix, the main body, and the suffix.

The main body of the notation describes the laminate and is of the form "θRm". The first part, "θ", represents the orientation of the angled plies in degress from the specimen longitudinal axis, or lamination angle. The "R" represents a letter denoting the location of any 0° plies. An "A" means the 0° plies are located inside the angled plies while a "B" means they are located on the outside of the angled plies. The "m" denotes the number of 0° plies in each half of the symmetric laminate. Thus, 45A1 represents a $[\pm 45/0]_s$ laminate and 45B1 a $[0/\pm 45]_s$ laminate.

A prefix was added to describe information regarding the implanted delamination shape and location. The prefix has the form "Ql". The "Q" represents a letter describing the implant shape. An "S" indicates a square shape while a "C" denotes a circular one. The "l" is a number representing the location of the implant within the six ply laminate. Since only four implant location configurations were used, this number ranges from one to four. A one denotes an implant under the first ply only; a two denotes the implant is located under the second ply only; a three denotes an implant located under the third ply only; and a four designates that implants are implanted between

all plies. These different configurations are identified in Figure 3.2.

The suffix describes the specimen number as well as the material from which the implant is made. This group has the form "npS". The "n" is the specimen number of the group while the "p" denotes the width of the implant. The width is 32 mm with p equal to 1 and is 57 mm with p equal to 2. The "S" is a letter denoting the implant material. A "G" means the implant is made from TCGF while an "F" means it is made from Teflon Film FEP 50A. The entire laminate shorthand code may look like: S4-45A1-12F. This indicates a 57 mm wide square film delamination is implanted in the first specimen of a $[\pm 45/0]_s$ laminate at each ply interface.

3.4 Manufacture of Specimens

The manufacture of all 83 specimens used in this investigation was done according to standard procedures developed at TELAC. A summary of these procedures follow.

The graphite/epoxy is supplied in rolls of semi-cured unidirectional preimpregnated tape or "prepreg" with a nominal width of 305 mm. To prevent curing of the matrix before layup, the prepreg is stored in freezers at a temperature below -18°C. One hour prior to manufacture, the roll was removed from the freezer and left in a sealed bag. This warm-up procedure prevents condensation from forming on the composite and helped to make the prepreg more pliable. The prepreg was

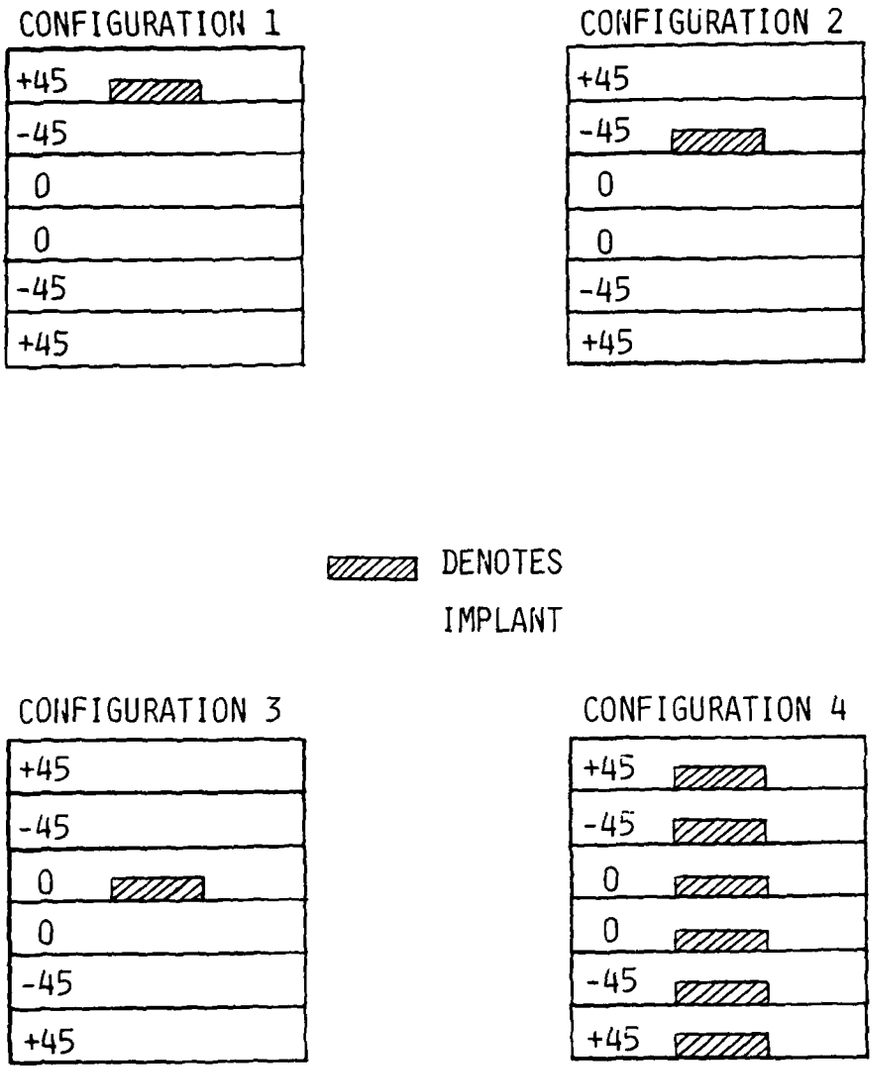

FIGURE 3.2 IMPLANT CONFIGURATIONS

cut and stacked into uncured laminates in an air conditioned "clean room". The air conditioning kept the temperature below 25°C and the relative humidity low. When handling the prepreg, surgical gloves were worn to avoid contamination by skin oil. The graphite was cut into shapes which could be placed together to form plies with dimensions of 305 mm by 350 mm. This was accomplished using Stanley razor knives and teflon covered templates which kept all cuts precise. When forming the +45° and -45° plies, the cuts were made to avoid fiber breaks in the ply. The edges of the two pieces which form this angled ply were placed together so the cuts were parallel to the fiber direction. In other words, only matrix joints were present within a laminae. After each ply is placed in the layup jig, the implants were positioned longitudinally using a ruler with gradations in millimeters and laterally with a custom made template containing scribe marks showing the exact implant position. Since the prepreg is tacky, the implants remained in place while the next ply is added to the unfinished laminate. Following layup, peel-ply was applied to both sides of the laminate. The peel-ply protected the laminate during the cure and also produced a textured finish to aid in bonding the loading tabs and strain gages.

A number of materials were used in preparing the layed up plate for cure. In addition to the peel-ply, nonporous and porous teflon, paper bleeder, and fiberglass air breather were utilized. This assembly was done on an aluminum caul plate which is large enough to cure six laminates at one time. Each

laminate is held in place by aluminium dams on two sides and by dams of corprene rubber (cork) on the other two sides. The corner of the aluminum dams provided a "good corner" which was used as a reference for the fiber orientations. With all cure materials in place, the plate was vacuum bagged with a high temperature nylon bagging material and vacumm tape. A schematic of the cure assembly is shown in Figure 3.3.

Curing the AS4/3501-6 graphite/epoxy is a two-stage process and is accomplished in a one meter diameter by 1.5 meter long autoclave. The autoclave pressure is raised to 0.59 MPa with an applied vacuum of 740 mm Hg. When the temperature reaches 117°C, the first stage or "flow stage" occurs. This temperature is held for one hour. The next stage of the cure is a two hour "set stage" at 177°C where most of the chemical crosslinking of the polymer chains in the epoxy occurs. To avoid thermally shocking the composite, all heat-up and cool-down rates were approximately 3°C per minute. The complete autoclave cure cycle is shown in Figure 3.4. All laminates were postcured in an oven at 177°C for eight hours after removal from the curing assembly.

When the peel-ply was removed from the cured laminates, the appearance of those containing implants was quite different from the laminates without implants which are referred to as "unflawed" laminates. Because of the finite thickness of the implanted delamination, the plies over the implants bulged out on one side of the laminate. The side which was against the caul plate is flat while the implants bulged out from the side

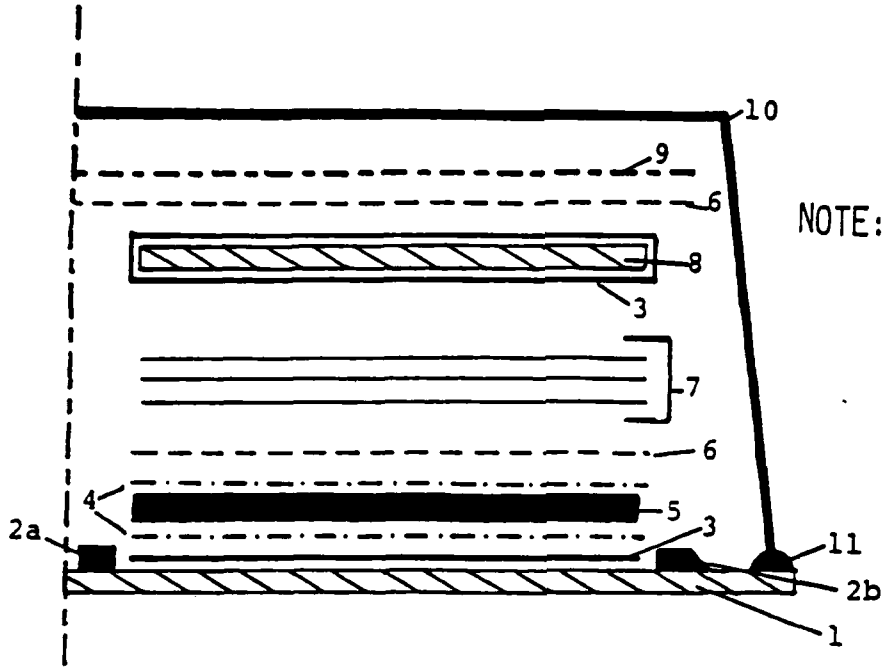

1. Aluminum Caul Plate, 3/8" thick MIC 6 aluminum with thin uniform coat of mold release 225 baked on
2a. Cork dam (Corprene), 1/8" x 1" with adhesive backing
b. Aluminum dam, 1/4" x 1", screwed down
3. Guaranteed non-porous teflon, TCGF-EHV .003, premium
4. Peel-ply #3921
5. Prepreg layup (laminate)
6. Porous teflon, TCGF .001-P porous
7. Paper bleeder (1 bleeder/2 plies of prepreg)
8. Aluminum Caul Plate, 1/4" thick MIC 6 aluminum with thin uniform coat of mold release 225 baked on
9. Air breather, #7781 fiberglass with volan finish
10. HS-6262 nylon vacuum bagging, 2 mils thick
11. Vacuum tape

FIGURE 3.3 STANDARD CURE ASSEMBLY

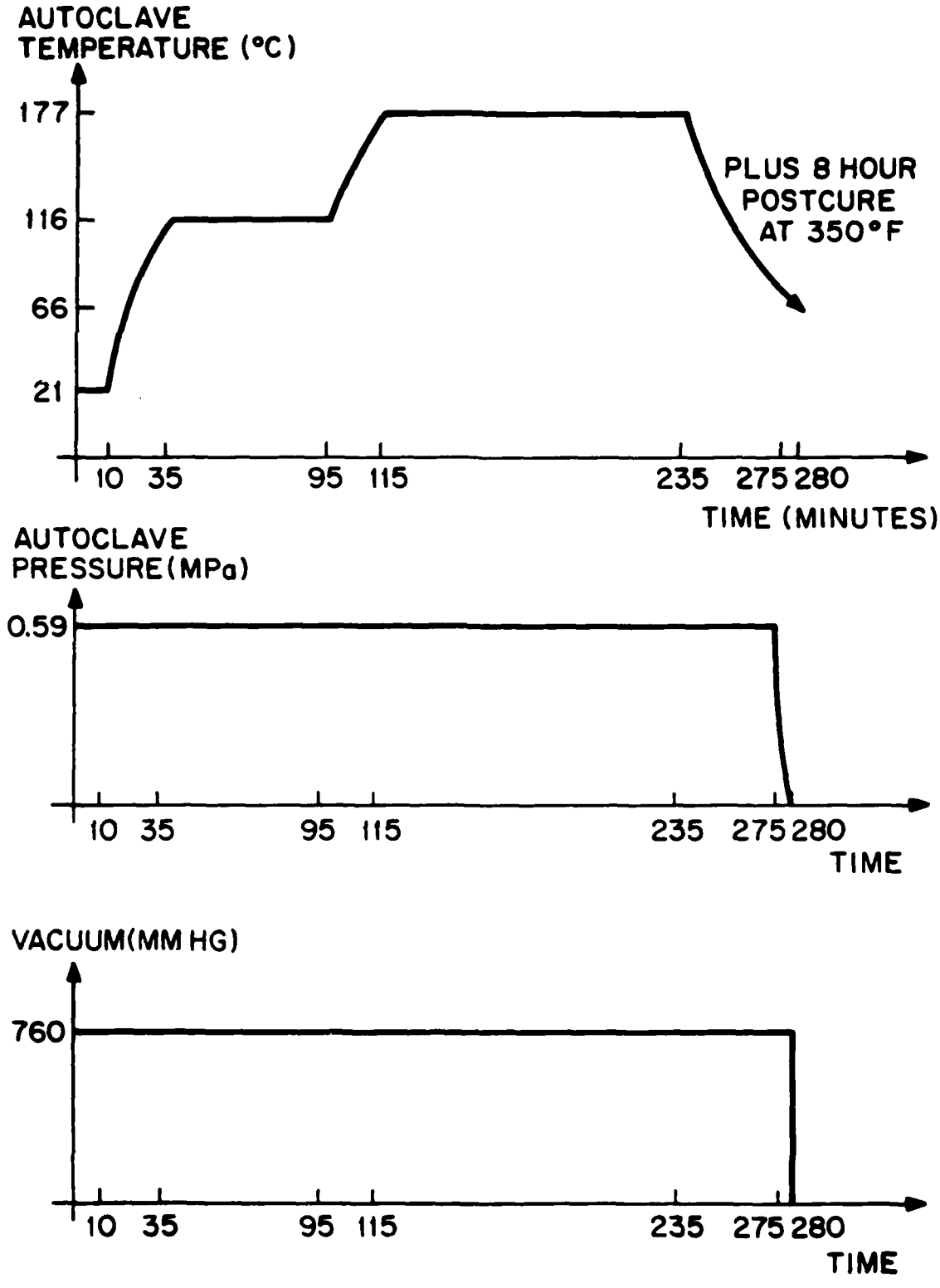

FIGURE 3.4 STANDARD CURE CYCLE FOR AS4/3501-6 GRAPHITE/EPOXY

covered by the three paper bleeder plies and the top plate. Because the top plate squeezed the laminate more at the implant site, the outer ply on laminates with implants at every ply interface showed a small dark black shiny area indicating a resin poor condition. In addition, the outer plies on these laminates often had one or more splits over the full length of the implant. These splits did not extend beyond the delaminated area. Laminates with a single implant under the second or third ply did not have these matrix splits. The photograph in Figure 3.5 shows these characteristics on a laminate implanted with TCGF at all ply interfaces.

All laminates were cut into four 71 mm by 350 mm specimens using a water-cooled diamond grit cutting wheel. This was accomplished on a milling machine with special attachments to ensure straight, parallel edges. Before the specimens were cut, approximately 8 mm was cut from the reference edge of the laminate and discarded. Since excess resin is bled from the laminate edges, removing this strip ensured the specimens cut from the edges of the plate did not contain an excess resin build-up. The positioning of the implants during layup takes into account this 8 mm strip on both sides of the laminate as well as the width of all cuts so that when each specimen is cut to 71 mm, the implants are positioned in the center.

The specimens were measured for width at three positions using a caliper and thickness at either nine or fifteen points using a micrometer. Specimens with 32 mm implants were measured at nine locations while those with 57 mm implants were

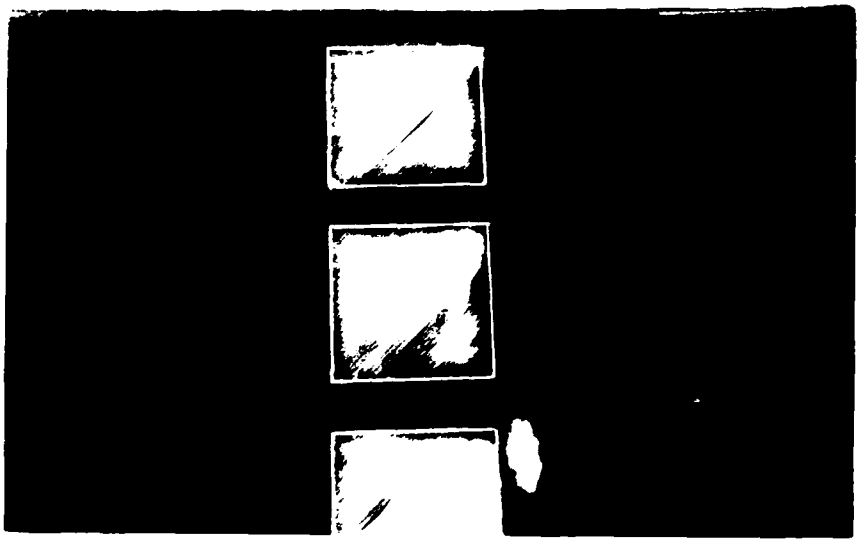

FIGURE 3.5 PHOTOGRAPH OF THE CURED LAMINATE SHOWING THE BULGE AND MATRIX SPLITTING AT THE IMPLANT LOCATION (WHITE CHALK USED AT IMPLANT LOCATION TO EMPHASIZE FEATURES)

measured at fifteen different points. The exact location of the measurement points are given in Figure 3.6. The average values for both thickness and width are provided in the data tables in the appendix. The thickness measurements were taken as a quality control check. Application of the peel-ply causes dimpling of the laminate surface which distorts the thickness measurements. Thus, a nominal thickness of 0.804 mm was used in all stress calculations. This is calculated from the manufacturer's nominal per ply thickness of 0.134 mm. The average thickness of the laminate sections away from implant locations is 0.857 mm. The average for points implanted with Dupont FEP 50A teflon film is 0.894 mm while for points implanted with TCGF is 1.123 mm. All coefficients of variation were approximately 2%. The thickness measurements taken at the film implant sites were an average of 0.027 mm greater than the nominal laminate thickness plus the thickness of five layers of film while the measurements taken over TCGF implants were an average of 0.062 mm thinner than the nominal laminate thickness plus the thickness of five layers of TCGF. This indicates that within experimental tolerances, the thickness of the implant region is equal to the nominal thickness of the plies plus the thickness of the implant(s). This would imply that the implant did not affect the curing of the composite in the implant region.

Measurements taken adjacent to the implant, particularly when TCGF was used, yielded thicknesses greater than nominal. This could be expected since this region represents a

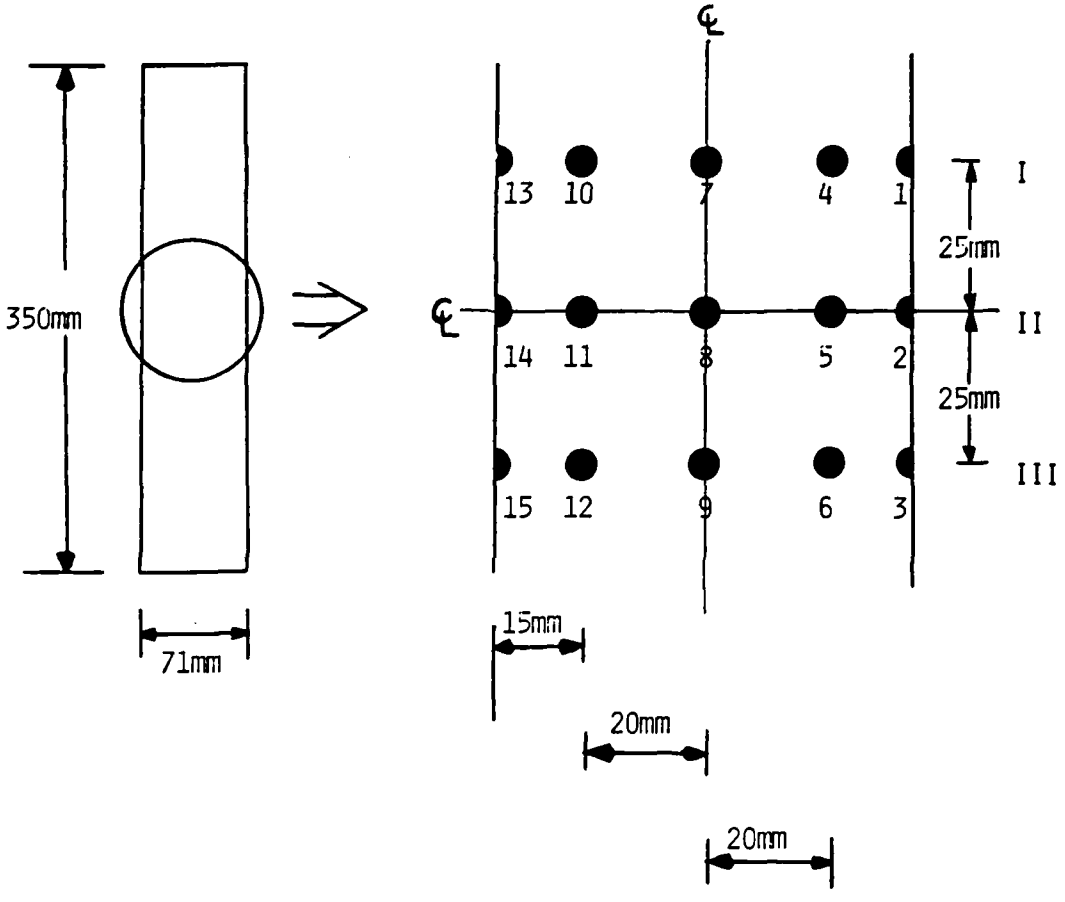

FIGURE 3.6 LOCATIONS ON SPECIMEN OF THICKNESS AND WIDTH MEASUREMENTS

transition region where the total laminate thickness decreases dramatically. Several specimens which were implanted with both materials used to produce a delamination were cut across the width and examined under a microscope. Figures 3.7 - 3.8 show the transition region between laminated and delaminated plies. The area adjacent to the TCGF implants show a number of large voids because the laminate thickness changes so abruptly. The film implants are so thin that the transition region looks similar to the remainder of the cross section.

The glass/epoxy loading tabs, described in Section 3.1, were bonded to the graphite/epoxy strips with an adhesive film, FM-123-2, supplied by American Cyanimid. The adhesive was applied directly to the tab which was then carefully aligned and applied to the coupon. The film, which is stored at -18°C, becomes very tacky at room temperature and thus holds the tab in place on the coupon until curing. The specimens were placed on an aluminum caul plate and covered with porous TCGF before placing steel top plates on each specimen. Nonporous TCGF and then fiberglass air breather were placed on top of the plates and the entire assembly vacuum bagged. The film adhesive was cured for two hours at 107°C with an applied vacuum and an autoclave pressure of 0.07 MPa. This provided an absolute pressure of 0.35 MPa on the bonding surface.

3.5 Instrumentation of Specimens

Strain gages were attached to all but three specimens to

FIGURE 3.7 PHOTOGRAPH (15X) OF TRANSITION REGION BETWEEN LAMINTED AND DELAMINATED PLIES WITH TGCF IMPLANTS

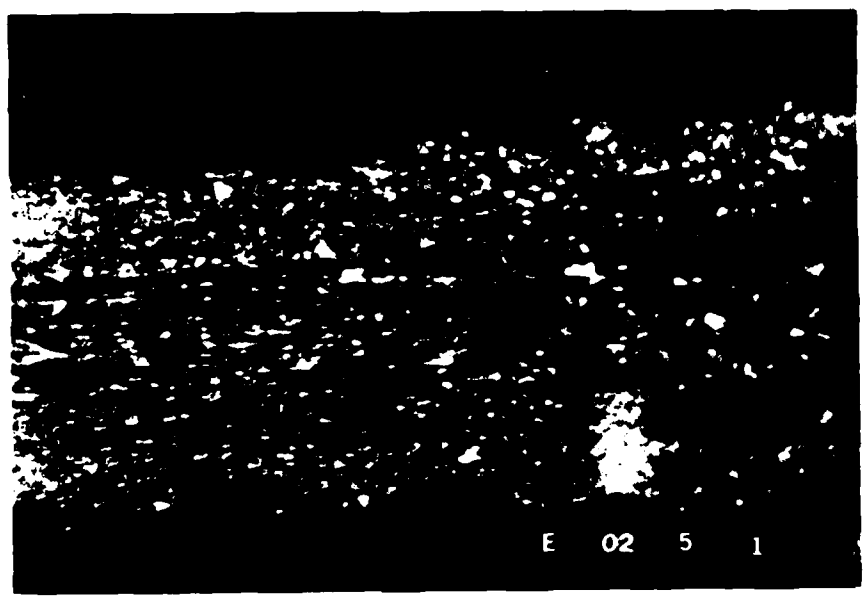

FIGURE 3.8 PHOTOGRAPH (15X) OF TRANSITION REGION BETWEEN LAMINATED AND DELAMINATED PLIES WITH FILM IMPLANTS

monitor longitudinal strain during testing. These three specimens were bonded with photoelastic coating, a procedure which will be explained later. The gages used were type EA-06-125AD-120 with a gage factor of 2.04 and an accuracy of ±0.5% and type EA-06-031DE-120 with a gage factor of 2.01 and accuracy ±1.0%. The gages were bonded onto the specimen with M-Bond 200 adhesive. During initial tests, gages were placed in five positions on the specimen. These included a gage centered at the top edge of the implant, one in the center of the specimen over the implant, one on either side of the implant and centered at the right implant edge, and a far-field gage located one-fourth of the width from the right specimen edge and one-fourth of the distance of the specimen's test section from the lower loading tab. These positions are depicted in Figure 3.9 along with the gage type used at each location. All of the gages, except for the far-field one, were no longer used after the initial tests since the information they provided was of limited significance. Later, a second gage was added to ten specimens containing 32 mm square implants. These were placed in line with the far-field gage and centered to the right of the implant. They were added to determine if the strain at the center of the specimen differed from that measured at the far-field position. Strain gages were placed in multiple locations on different specimens but all specimens had at least one gage type EA-06-125AD-120 mounted to monitor far-field strain in order to obtain data to

determine longitudinal modulus. Figure 3.9 provides a complete depiction showing all strain gage positions. Additionally, the data tables indicate how each specimen is gaged for testing.

Photoelastic coatings were applied to these $[\pm 45/0]_s$ specimens: one with no implants, one with a single 57 mm square film implant under the second ply, and one with 57 mm square film implants at all ply interfaces. The purpose of this test is to obtain a full-field stress distribution of the specimen and "see" if there were any abnormal stress gradients around the implant. Specimens with film implants were chosen because of problems associated with mounting the coating over the large bulge on specimens containing TCGF implants. The unflawed specimen was tested to provide a baseline for the results.

The surfaces were prepared by scrubbing lightly with cheesecloth before the PC-1 adhesive, which was mixed with ten parts PCH-1 hardener for every part of adhesive, was applied to the specimen. The PS-1C photoelastic coating measuring 1.0 mm thick was cut, using scissors, to 71 mm by 180 mm. The coating was applied to both sides of each specimen to ensure uniform reinforcing effects and thus no bending. The adhesive was allowed to cure for twelve hours at room temperature before testing.

3.6 Testing Procedures

All testing was conducted under monotonic tensile loading

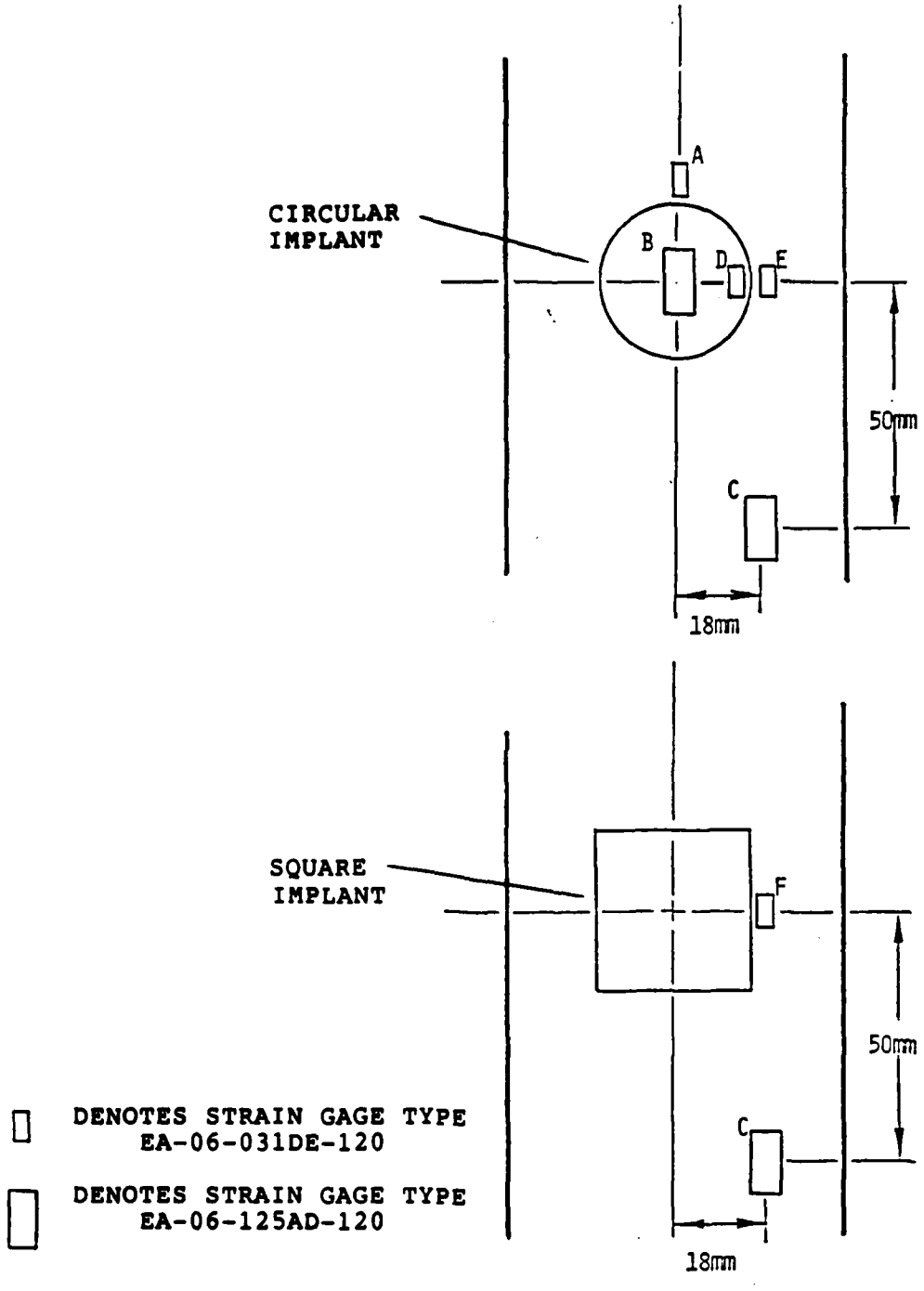

LETTER DENOTES GAGE POSITION

FIGURE 3.9 LOCATIONS OF STRAIN GAGES ON SPECIMENS

performed using a MTS 810 Material Test System equipped with hydraulic grips. A stroke rate of 1.09 mm/minute was used. For a specimen with a 200 mm test section, this translates to a strain rate of approximately 5500 microstrain per minute.

After the specimen was aligned properly in the upper grip using a machinist's square, the grip was closed and the strain gages attached to Vishay conditioners. This free hanging position is defined as the zero load position. The gages were calibrated before the lower tab was gripped. Each gage was first "balanced" so zero strain registered in this zero load position, then the proper resistor was connected in parallel with each strain gage to calibrate the system. The PDP/1134 computer was utilized to store data from the conditioners through analog-to-digital devices.

The data aquisition program was started just prior to the application of the load by the testing machine. All tests were conducted to failure. During the test, the specimens were inspected visually for signs of cracking or matrix splitting and monitored for sounds indicating splitting or ply failure. When sounds were detected, marks were placed at the corresponding point in the data file using a feature offered by the data aquisition software. At failure, the fracture load and stroke were recorded and a photograph was taken of the specimen while it was still mounted in the grips.

Testing of the specimens with photoelatic coatings were similar to the tests described previously except that the tests were not conducted monotonically to failure. Each specimen was

loaded at 2250 N increments up to 20,000 N which produces the maximum strain allowable in the coating. In order to determine the strain at any point, both normal and oblique-incidence fringe orders were read. Normal incidence, N_n, readings are taken by turning on the light source of the Vishay Model 031 Reflection Polariscope. The light passes through a polarizer/quarter-wave plate and strikes the coating at a normal incidence. Light which reflects back passes through the analyzer filter. A compensator attached to this filter allows identification of the proper fringe order and strain can be read directly on the Model 532 Digital Strain Indicator by zero-balancing the compensator by turning the attachment knob until a black fringe appears at the test point. Oblique incidence, N_θ, readings are taken in a similar fashion using an adapter which brings the light from the polariscope at an angle to the normal. Longitudinal strain is calculated using the equation:

$$\varepsilon_L = \left(1.5N_\theta - N_n \right) C_{PS} \qquad (3.1)$$

where C_{PS} is a plane stress correction factor applied since the photoelastic coatings reinforce the stiffness of the specimen [23]. The value of C_{PS} for all the tests conducted is 1.099. The points on each specimen where the strain readings were taken are shown in Figure 3.10.

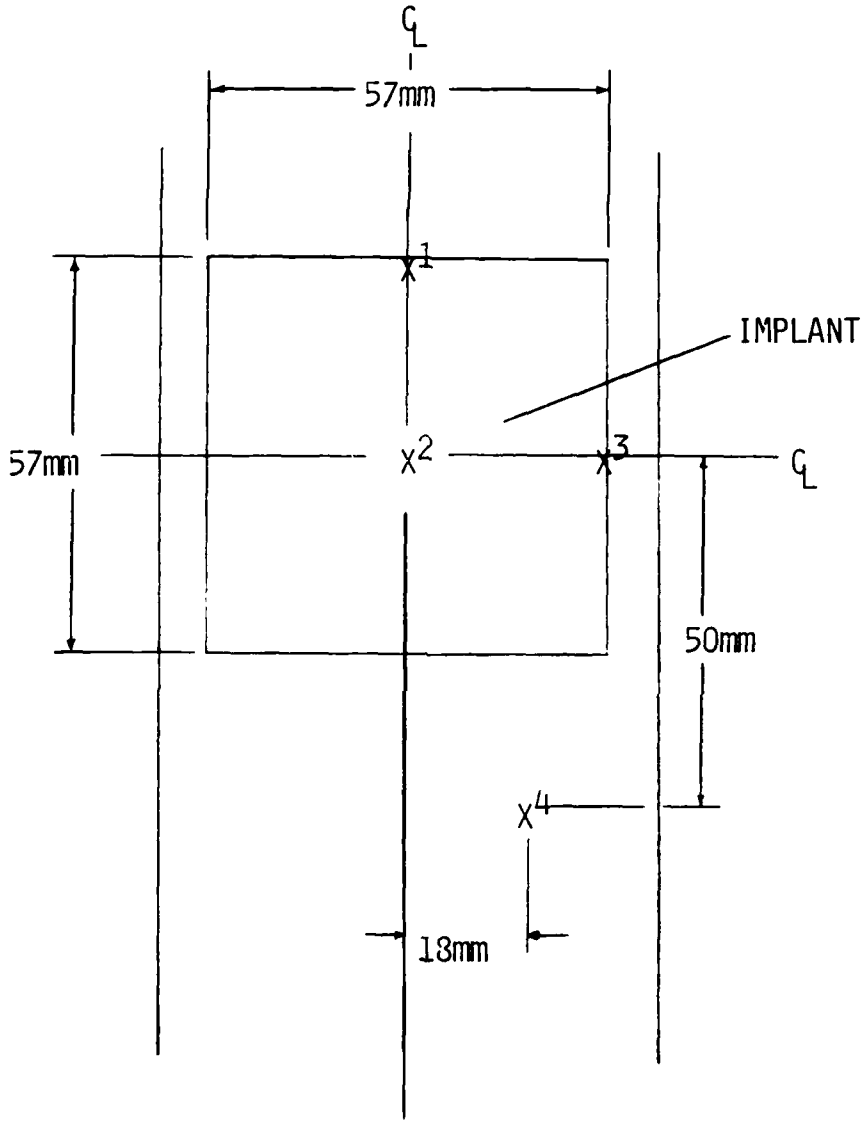

FIGURE 3.10 LOCATIONS ON THE SPECIMEN WHERE STRAIN READINGS WERE TAKEN DURING PHOTOELASTIC TESTS

3.7 Data Reduction

Following each testing period, the data was stored on floppy disks to form a permanent record. The data was analyzed on computer software written at TELAC [24]. This analysis consisted of editing out points in the data file which were recorded before the test started and after it ended. Thickness and width measurements were added to the data file so that load could be converted to stress. The slope of all the stress and strain data was computed using a program called LIN6. This program uses an algorithm to determine best fit linear regions of a data set. The modulus at the far-field position and the failure stress were calculated using this program. Finally, a graph was drawn on the pen plotter showing the stress-strain behavior at all gage positions, as well as the marks which were placed in the data file when noises were heard.

CHAPTER 4

ANALYTICAL METHODOLOGY

4.1 Problem Formulation

To adequately predict the response of the specimen with implanted delaminations, a quasi-two-dimensional model is formulated which incorporates the primary characteristics of the specimen as manufactured. The characteristics of concern are the bulging out of the plies at the implant site and the subsequent splitting of the outer plies on either side of the specimen. It should be noted that this bulge only occurs on one side of the specimen while the other side of the specimen is flat as explained in Section 3.4. Thus, the laminate's plane of symmetry at the implant site is not the midplane of the rest of the laminate. To determine the state of stress in the specimen during loading and thus, ultimately, predict failure, a model of the implant region is made. A depiction of the modeled region of the specimen is given in Figure 4.1

4.2 Assumptions

A number of assumptions are made on the model shown in Figure 4.1. One, each ply in the laminate can be viewed as macroscopically homogeneous. Thus, individual properties of both fiber and matrix are "smeared". This is the normal assumption in determining ply stresses in composite laminates. Two, "classical laminated plate theory" (CLPT) can be applied

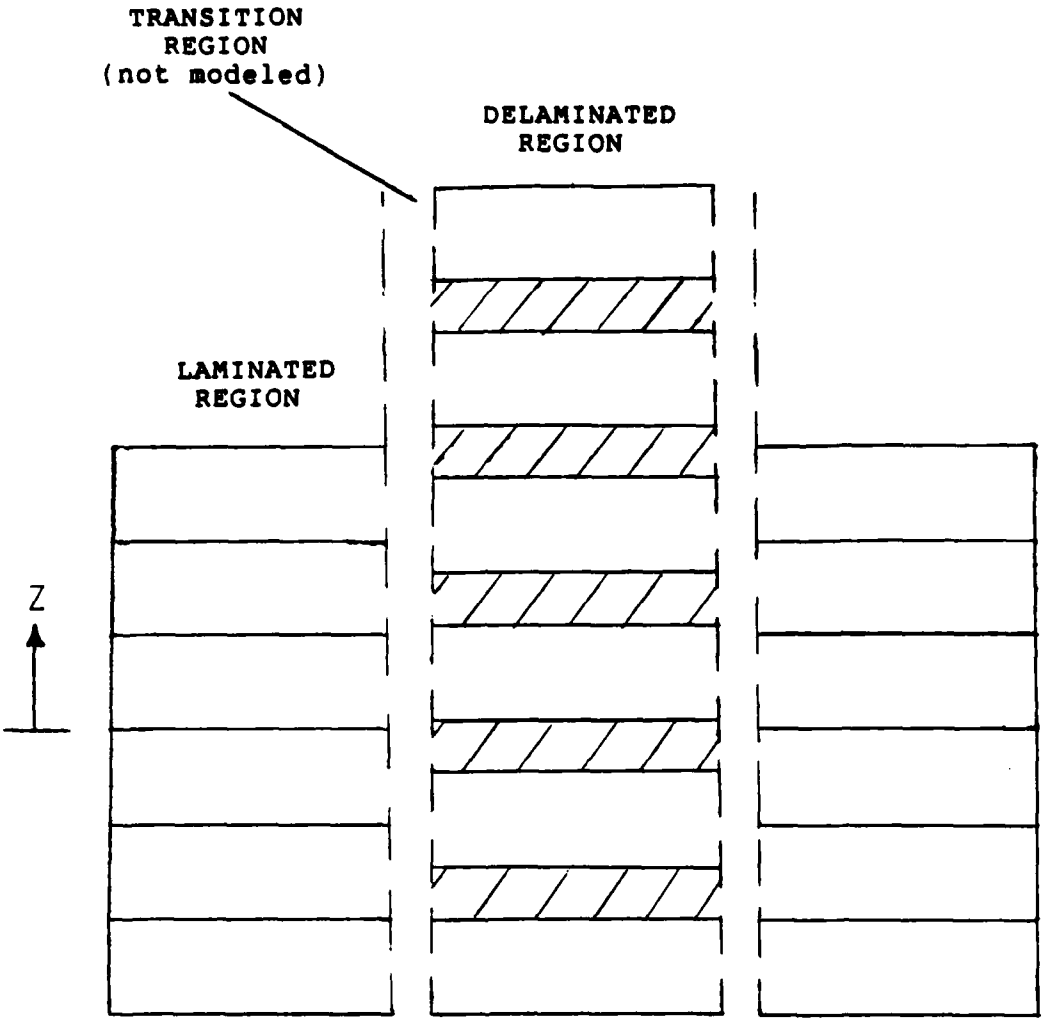

FIGURE 4.1 DEPICTION OF THE MODELED REGION ON THE SPECIMEN

in the delaminated region. Three, the implant is a perfect delamination and thus carries no load and does not act to transfer load from ply to ply. Four, no distinction is made between the circular and square implants since the "worse case" width is considered as the critical factor. Five, the transition region between laminated and delaminated regions is "perfect" and "immediate" so that stress concentrations do not arise and perfect and immediate load transfer occurs. Six, longitudinal strain varies linearly through the thickness. This condition ensures curvature compatibility between plies in the implant region. Since the implant region is constrained on all boundaries by the laminated plies, the delaminated plies are forced to bend together. Thus, twisting of the laminate is also ruled out. Seven, transverse strain in the delaminated region is constant through the thickness and width and is the same as that outside the delaminated region. This ensures displacement compatibility at the sides of the delaminated region. Since bending in the transverse direction is small, it is assumed to be negligible. This model thus assures that within the implant/delaminated region, stress and strain do not change in the x_2 direction. Finally, the shear strain in the delaminated region is assumed to be zero, as it is outside the implant region, since the edges of this region are constrained on all boundaries by the laminated plies. It is important to note that these strains are referred to laminate axes.

4.3 Governing Equations

The restrictions of force balance require that every section be under force and moment equilibrium. The forces which act on the modeled area are shown in Figure 4.2. Examination of these forces yields the following force equilibrium equations:

$$\sum_{i=1}^{n} \sigma_{11,[\theta i]}^{LD} \, t_{ply}^{[\theta i]} = \sum_{i=1}^{n} \sigma_{11,[\theta i]}^{L} \, t_{ply}^{[\theta i]} = \sigma_{FF}^{L} \, h \qquad (4.1)$$

$$\sum_{i=1}^{n} \sigma_{22,[\theta i]}^{L} \, t_{ply}^{[\theta i]} = 0 \qquad (4.2)$$

where σ_{FF}^{L} is the far-field stress in the specimen, and h is the laminate thickness. The force equilibrium equation for the shear stress is not needed since it represents a redundant equation. Moment equilibrium must also be satisfied. Since there is no applied moment:

$$\sum_{i=1}^{n} \int_{z_{il}}^{z_{iu}} \sigma_{11,[\theta i]}^{L} \, t_{ply}^{[\theta i]} \, z dz = 0 \qquad (4.3)$$

where z is measured from the midplane of the laminated region of the specimen and z_{iu} and z_{il} are the distances from this

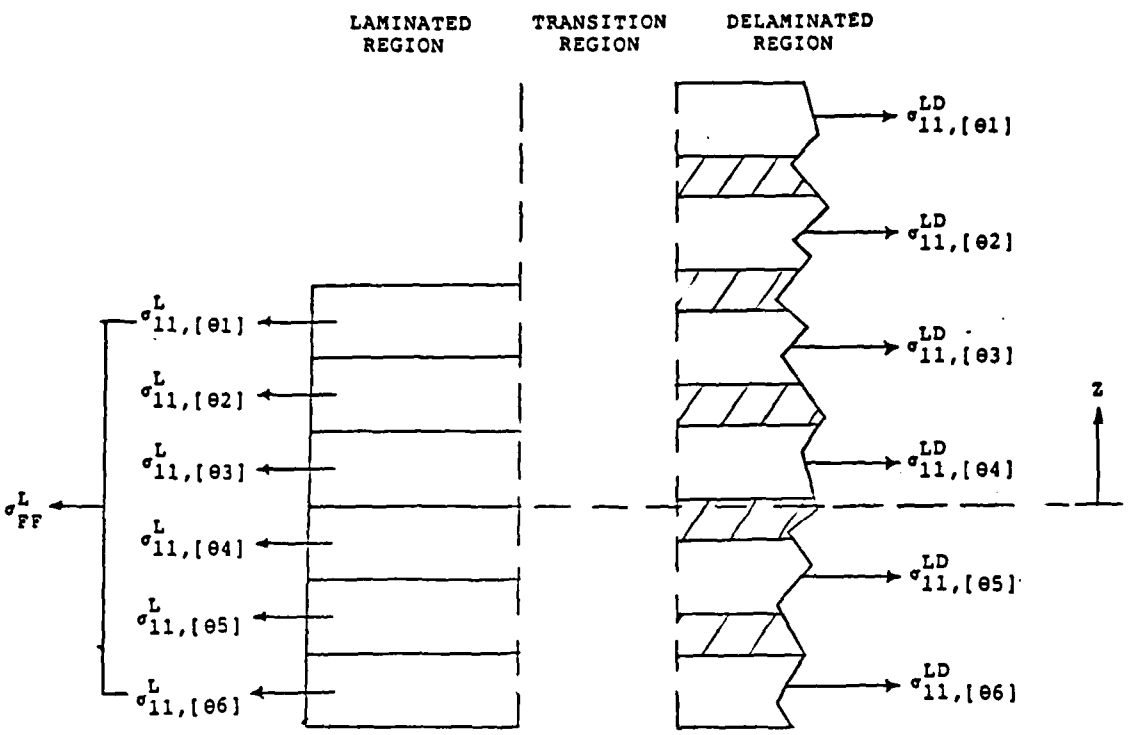

FIGURE 4.2 STRESSES WHICH ACT ON THE MODELED REGION

midplane to the upper and lower surfaces of the ith ply. The moment equilibrium equations in the transverse and twisting cases also represent redundant equations. The final equation needed to solve for the stresses in the delaminated plies comes from the curvature compatibility condition:

$$\varepsilon_{11}^{i} = \kappa_{11} z^{i} + \varepsilon_{11}^{\circ} \tag{4.4}$$

where κ_{11} is the specimen curvature, z^{i} is measured to any point on the i th ply, and ε_{11}° is the strain at the plane where z is equal to zero. Since κ_{11} and κ_{12} are assumed to be zero, we have that ε_{22} is equal to ε_{22}° and ε_{12} is equal to 0 at any z location. These governing equations will permit the determination of $\sigma_{11,[\theta i]}^{L}$, $\sigma_{22,[\theta i]}^{L}$, and $\sigma_{12,[\theta i]}^{L}$, in the delaminated region.

4.4 Calculation of Stresses

Determination of the response of the delaminated region to tensile loading can be accomplished by examining stresses in individual delaminated plies. These plies act like springs in parallel. Since load can not be transferred from ply to ply, load introduction can only come from outside the delaminated area through the laminated plies. For the individual delaminated ply:

$$\sigma^{L}_{11,[\theta i]} = \left[E^{[\theta i]}_{1111}\ \varepsilon^{i}_{11} + E^{[\theta i]}_{1122}\ \varepsilon^{i}_{22} \right] t^{[\theta i]}_{ply} \qquad (4.5a)$$

$$\sigma^{L}_{22,[\theta i]} = \left[E^{[\theta i]}_{1122}\ \varepsilon^{i}_{11} + E^{[\theta i]}_{2222}\ \varepsilon^{i}_{22} \right] t^{[\theta i]}_{ply} \qquad (4.5b)$$

$$\sigma^{L}_{12,[\theta i]} = \left[E^{[\theta i]}_{1112}\ \varepsilon^{i}_{11} + E^{[\theta i]}_{2212}\ \varepsilon^{i}_{22} \right] t^{[\theta i]}_{ply} \qquad (4.5c)$$

Substituting equation 4.4 into 4.5a and b yields:

$$\sum_{i=1}^{n} \sigma^{L}_{11,[\theta i]}\ t^{[\theta i]}_{ply} = \left[\varepsilon^{\circ}_{11} \sum E^{[\theta i]}_{1111} + \kappa_{11} \sum E^{[\theta i]}_{1111}\ z^{i} + \varepsilon^{\circ}_{22} \sum E^{[\theta i]}_{1122} \right] t^{[\theta i]}_{ply} = \sigma^{L}_{FF}\ h \qquad (4.6)$$

$$\sum_{i=1}^{n} \sigma^{L}_{22,[\theta i]}\ t^{[\theta i]}_{ply} = \left[\varepsilon^{\circ}_{11} \sum E^{[\theta i]}_{1122} + \kappa_{11} \sum E^{[\theta i]}_{1122}\ z^{i} + \varepsilon^{\circ}_{22} \sum E^{[\theta i]}_{2222} \right] t^{[\theta i]}_{ply} = 0 \qquad (4.7)$$

In the same fashion, equations 4.4 and 4.5a can be substituted into 4.3 giving the expression in terms of in-plane strain.

$$\varepsilon_{11}^{\circ}\sum_{i=1}^{n}\int_{z_{il}}^{z_{iu}} E_{1111}^{[\theta i]}\, z\,dz + \kappa_{11}\sum_{i=1}^{n}\int_{z_{il}}^{z_{iu}} E_{1111}^{[\theta i]}\, z^2 dz$$

$$+ \varepsilon_{22}^{\circ}\sum_{i=1}^{n}\int_{z_{il}}^{z_{iu}} E_{1122}^{[\theta i]}\, z\,dz = 0 \qquad (4.8)$$

These equations can be rewritten in matrix form as:

$$\begin{bmatrix} \Sigma E_{1111}^{[\theta i]} & \Sigma E_{1111}^{[\theta i]} & \Sigma E_{1122}^{[\theta i]}\, z^i \\ \Sigma E_{1122}^{[\theta i]} & \Sigma E_{1122}^{[\theta i]} & \Sigma E_{2222}^{[\theta i]}\, z^i \\ \Sigma\int E_{1111}^{[\theta i]}\, zdz & \Sigma\int E_{1111}^{[\theta i]}\, zdz & \Sigma\int E_{1122}^{[\theta i]}\, z^2 dz \end{bmatrix} \begin{Bmatrix} \varepsilon_{11}^{\circ} \\ \varepsilon_{22}^{\circ} \\ \kappa_{11} \end{Bmatrix} = \begin{Bmatrix} N_{11}^{\circ} \\ 0 \\ 0 \end{Bmatrix} \qquad (4.9)$$

This matrix equation has the form of:

$$\begin{bmatrix} A_{1111}^{eff} & A_{1122}^{eff} & B_{1111}^{eff} \\ A_{1122}^{eff} & A_{2222}^{eff} & B_{1122}^{eff} \\ B_{1111}^{eff} & B_{1122}^{eff} & D_{1111}^{eff} \end{bmatrix} \begin{Bmatrix} \varepsilon_{11}^{\circ} \\ \varepsilon_{22}^{\circ} \\ \kappa_{11} \end{Bmatrix} = \begin{Bmatrix} N_{11}^{\circ} \\ N_{22}^{\circ} \\ M_{11} \end{Bmatrix} \qquad (4.10)$$

where the superscript "eff" denotes that the elements are effective laminate constants.

To solve equation 4.9 for ε_{11}°, ε_{22}°, and κ_{11}, values are needed for $E_{\alpha\beta\sigma\gamma}^{[\theta i]}$, z^i, σ_{FF}^{L} and $t_{ply}^{[\theta i]}$. The two-dimensional

elasticity tensor $E^{[\theta i]}_{\alpha\beta\sigma\gamma}$ is formed by using the unidirectional ply properties listed in Table 3.1. Since the outer plies have numerous splits at the implant site, $E^{[\theta 1]}_{\alpha\beta\sigma\gamma}$ and $E^{[\theta 6]}_{\alpha\beta\sigma\gamma}$ are set equal to zero at the outset. Although these plies are still capable of carrying some load along the fibers, setting the appropriate stiffness equal to zero will be conservative and help to bound the problem.

The measurement of z^i for each ply depends only upon the implant used to cause a delamination. This is because the different implant materials have different thicknesses. Figure 4.3 shows two cross sections of delaminated specimens implanted with TCGF and film with their associated z^i values.

Once ε°_{11}, ε°_{22}, and κ_{11} are found from Equation 4.9, these values can be substituted into equation 4.5 to give values for $\sigma_{\alpha\beta,[\theta i]}$. These stresses represent the new stress distribution in the delaminated region, as referred to laminate axes, due to the presence of the implants.

4.5 Failure Criteria

The Maximum Stress Criterion [25] is used to find the order and magnitude of ply failure. The allowable stress values are:

$$-2356 \text{ MPa} \leq \sigma^{[\theta i]}_{11} \leq 2356 \text{ MPa}$$

$$-220 \text{ MPa} \leq \sigma^{[\theta i]}_{22} \leq 49.4 \text{ MPa}$$

$$-105 \text{ MPa} \leq \sigma^{[\theta i]}_{12} \leq 105 \text{ MPa}$$

The maximum stress in the ply, where z^i is a maximum, is used

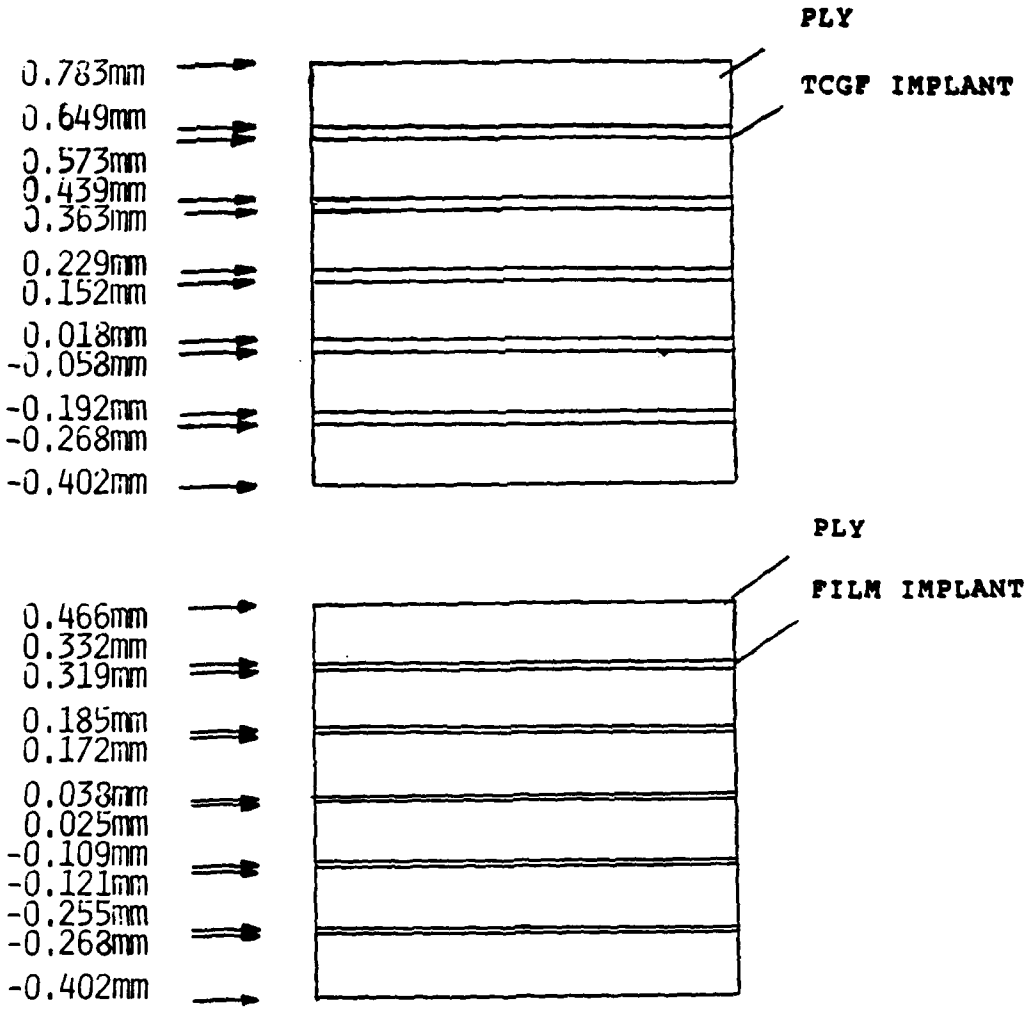

FIGURE 4.3 z^i VALUES FOR TCGF IMPLANTS (TOP) AND FILM IMPLANTS (BOTTOM)

for this purpose. These ply stresses in laminate axes must be rotated in to ply axes to apply the failure criterion. By scaling the applied stress, σ^{L}_{FF}, the proper ply and its failure stress can be found. In addition, the strain at failure is calculated using:

$$\varepsilon^{\circ}_{11} = E^{D}_{L}\ \sigma^{D}_{failure} \tag{4.11}$$

where the superscript D designates the delaminated region. The stiffness, E^{D}_{L}, is merely:

$$E^{D}_{L} = \sum E^{D}_{1111} - \left[\frac{\left(\sum E^{D}_{1122}\right)^{2}}{\sum E^{D}_{2222}} \right] \tag{4.12}$$

where the subscript L indicates the longitudinal direction.

4.6 Width Effects

To account for differences in the width of the delaminated area, a rule of mixtures approach is utilized. This approach takes a "weighted average" of laminate longitudinal stiffness in both delaminated and laminated regions based upon the width of each region as a function of total specimen width.

When the specimen is subjected to a given loading during testing, the longitudinal strain across the width of the specimen is uniform. Therefore, the longitudinal strain in

both the laminated and delaminated regions must be equal. Thus:

$$\varepsilon_L^{specimen} = \left[\varepsilon_L^L = \frac{\sigma_L^L}{E_L^L} \right]^{laminated\ region} = \left[\varepsilon_L^D = \frac{\sigma_L^D}{E_L^D} \right]^{delaminated\ region} \qquad (4.13)$$

where the subscripts D and L represent conditions in the delaminated and laminated regions respectively. However, the stresses are not uniform in these regions since the modulus will not always be the same depending upon the configuration and the number of failed plies. This is illustrated in Figure 4.4. Taking the weighted averages of the stresses in each region yields:

$$\sigma_L^D W^D + \sigma_L^L (W - W^D) = \sigma_L W \qquad (4.14)$$

where values without superscripts refer to the entire specimen. Substituting 4.13 into this equation gives:

$$\sigma_L = \frac{\varepsilon_L}{W} \left[E_L^D W^D + (W - W^D) E_L^L \right] \qquad (4.15)$$

or rewriting:

$$\sigma_L = \frac{\varepsilon_L}{W} \left[W^D (E_L^D - E_L^L) + W E_L^L \right] \qquad (4.16)$$

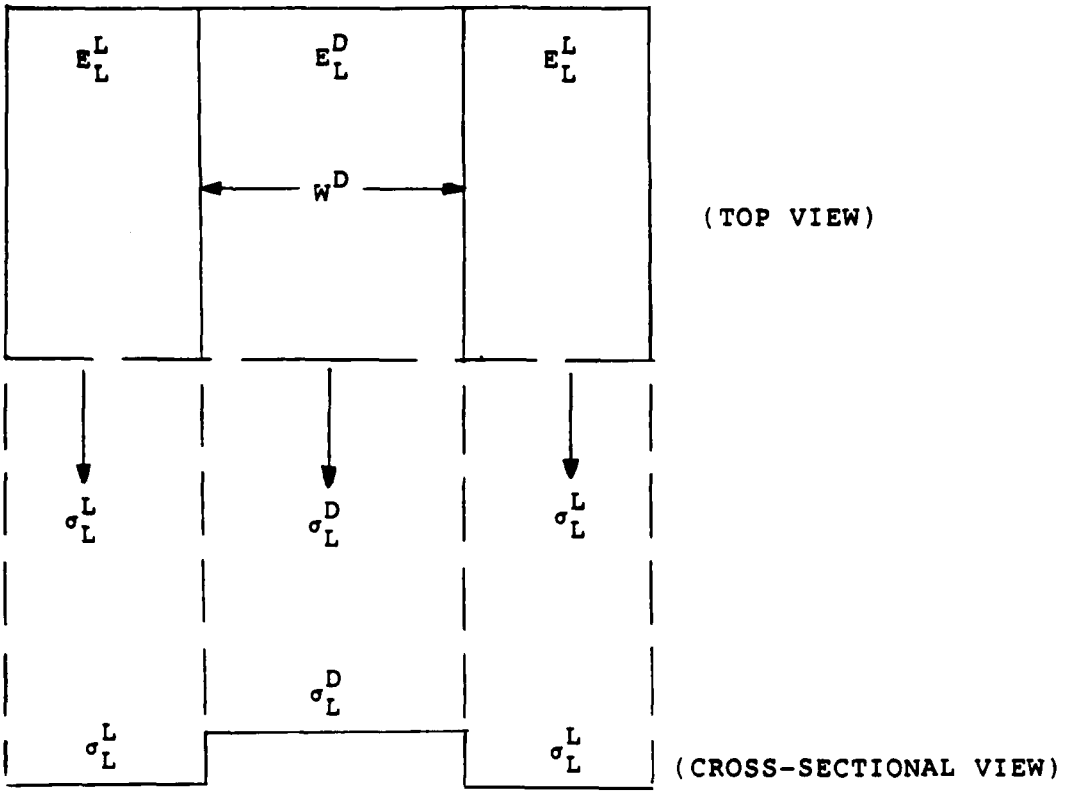

FIGURE 4.4 ILLUSTRATION OF GENERIC STRESS DISTRIBUTION ACROSS THE SPECIMEN

Both E_L^L and E_L^D represent the modulus in the respective regions. The value of E_L^L is found by analyzing the laminated region. To determine the strain, the equation:

$$\sigma_L^D = \varepsilon_L \, E_L^D \tag{4.17}$$

is used in which both E_D^L and σ_L^D have been determined by following the procedures stated in the previous section.

While this rule of mixtures approach neglects curvature compatibility between laminated and delaminated regions and does not address problems such as how the curvature changes along the width, it does represents a straightforward method of determining the change in laminate stiffness so that stresses for different implant sizes can be found.

4.7 Solution Procedure

Determining the ultimate failure stress of a specimen implanted with a specific width delamination is a straightforward procedure as outlined in the flowchart in Figure 4.5. The state of stress in the delaminated region is determined as explained in Section 4.4 with the consideration of width effects described in Section 4.6. Ply failure is calculated using a Maximum Stress Criterion as described in Section 4.5. This is applied separately to the laminated and delaminated regions. The "failed ply" has its $E_{\alpha\beta\sigma\gamma}^{[\theta i]}$ set equal to zero. If plies remain unbroken, the procedure is repeated

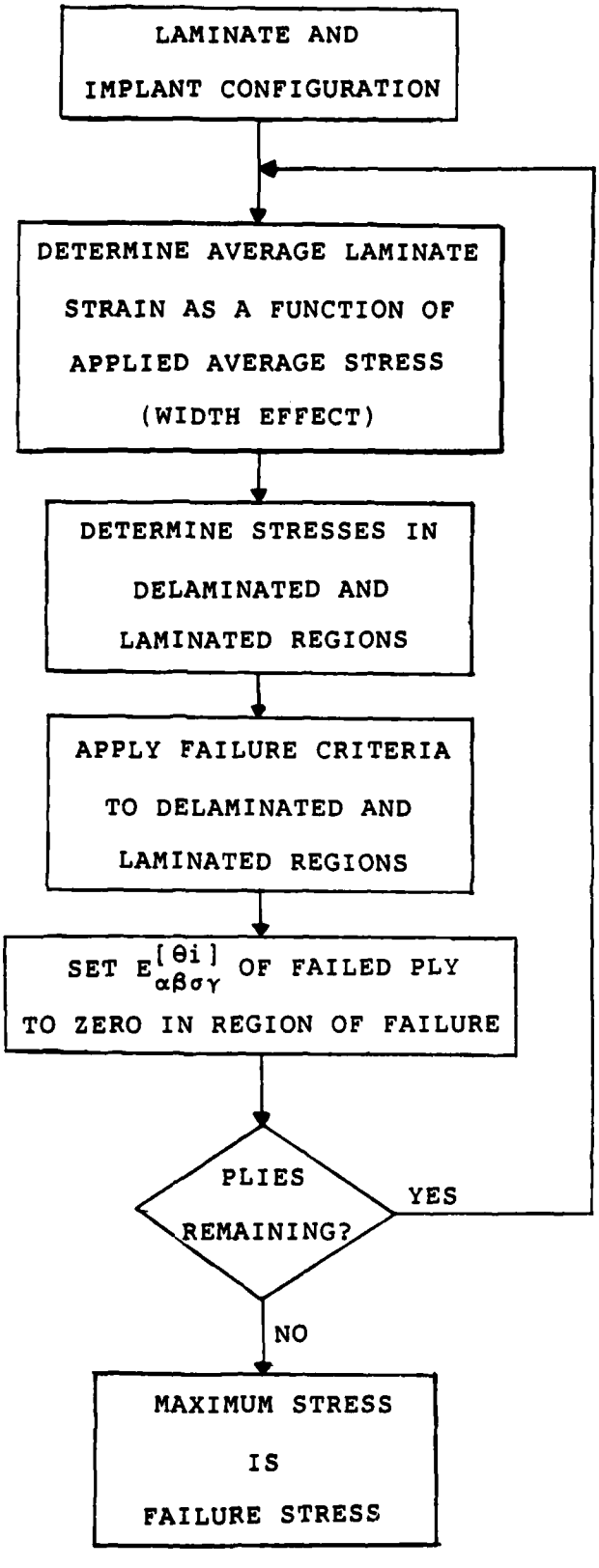

FIGURE 4.5 FLOWCHART OF SOLUTION PROCEDURE

until all plies have failed. The highest ply failure stress calculated is the ultimate fracture stress of the specimen.

CHAPTER 5

RESULTS

5.1 Far-field Stress-strain Behavior

The far-field stress-strain behavior of the various specimen types will be discussed in this section. All stress calculations were computed using load data from the testing machine, measured width, and a nominal ply thickness of 0.134 mm. This nominal value gives a specimen thickness of 0.804 mm. Actual specimen thicknesses varied slightly from this value depending upon distance from the implant site. Average thicknesses for each specimen are reported in the Data Tables.

For simplicity, specimens will be grouped according to stacking sequence and type of implant. Audible sounds detected during each test as well as their time of occurrence will be described. These audible sounds or pops provide information as to when damage may occur and may explain changes in the stress-strain behavior.

A number of terms are used to describe the various types of stress-strain behavior observed. These are illustrated in generic sketches of these typical stress-strain behaviors. The first type is linear which means the strain increases at a constant rate as load increases as illustrated in Figure 5.1. Softening describes a gradual decrease in tangent modulus with increasing load as shown in Figure 5.2. The stress where the

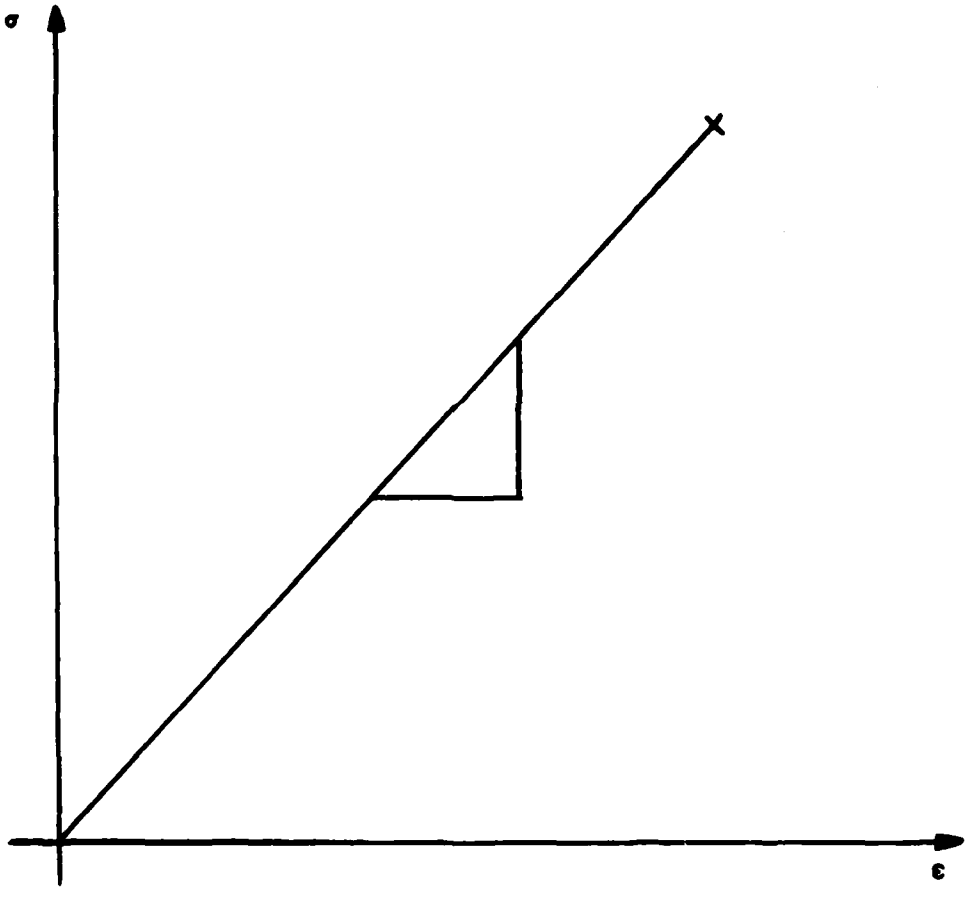

FIGURE 5.1 STRESS-STRAIN PLOT SHOWING LINEAR-TO-FAILURE BEHAVIOR

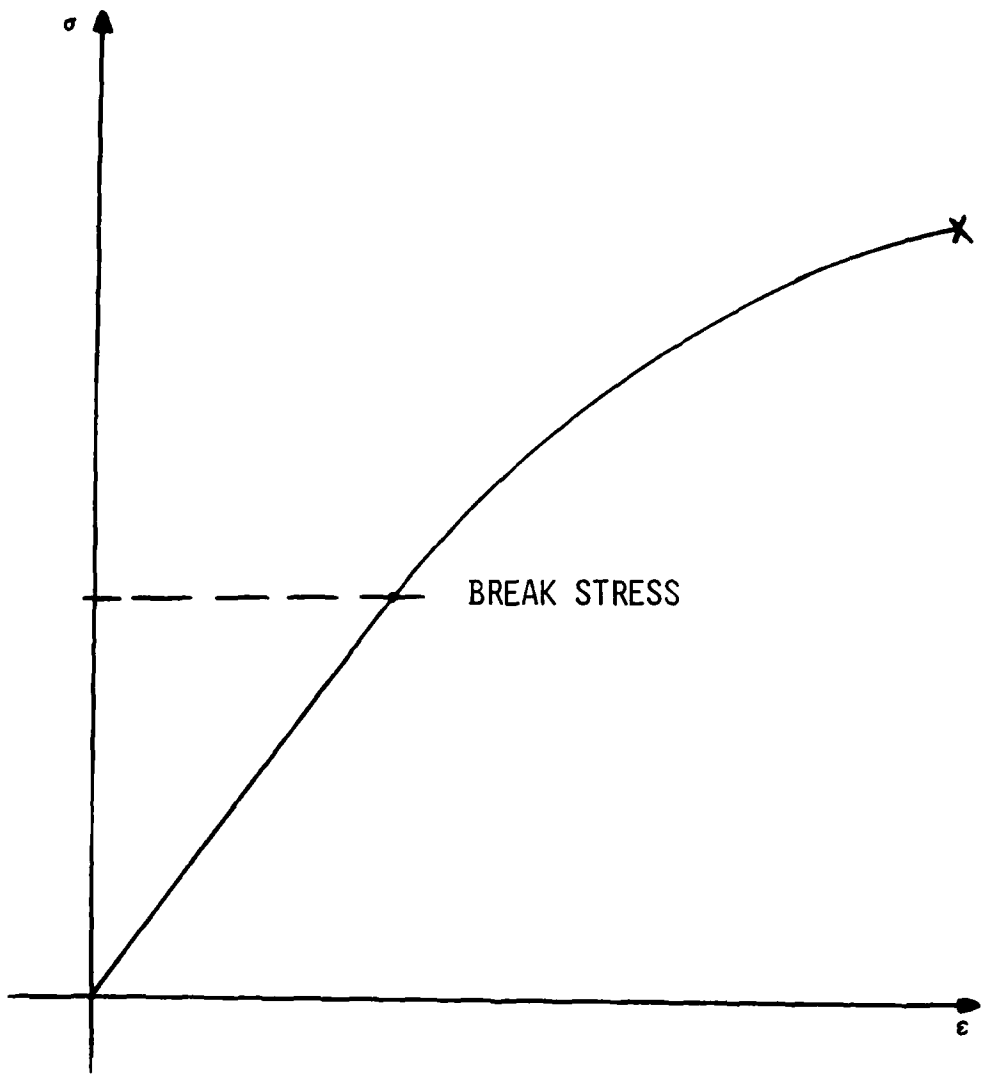

FIGURE 5.2 SKETCH OF STRESS-STRAIN PLOT SHOWING A REDUCTION IN TANGENT MODULUS ("SOFTENING")

modulus becomes nonlinear, also indicated in Figure 5.2, is called the break stress [26]. Discontinuity describes two conditions which cause nonlinearities in the stress-strain behavior. These are strain discontinuities, wherein strain increases at a constant load as illustrated in Figure 5.3, and reversal points, where both strain and load decrease for a short period of time as shown in Figure 5.4. Load drop describes a condition where the load decreases at either a constant or increasing strain value. Their load drop behavior is illustrated in Figure 5.5 and is not to be confused with the reversal point. In addition, the stress-strain behavior of all the specimen types is catagorized in accordance with the types described above, in Tables 5.1 and 5.2. These are discussed in detail below.

5.1.1 [±45/0]s Specimens

To provide a means of comparison, the behavior of each specimen type will be compared to the behavior of the unflawed specimens in order to provide information on the effect of the implants. A summary of the results are provided in Table 5.1. The unflawed specimens showed a softening stress-strain behavior as indicated in a typical plot in Figure 5.6. Audible pops did not occur until after the break stress value of 230 MPa and usually not until about 500 MPa. Three or four loud pops were heard from this point until failure.

The specimens containing one 32 mm circular TCGF implant

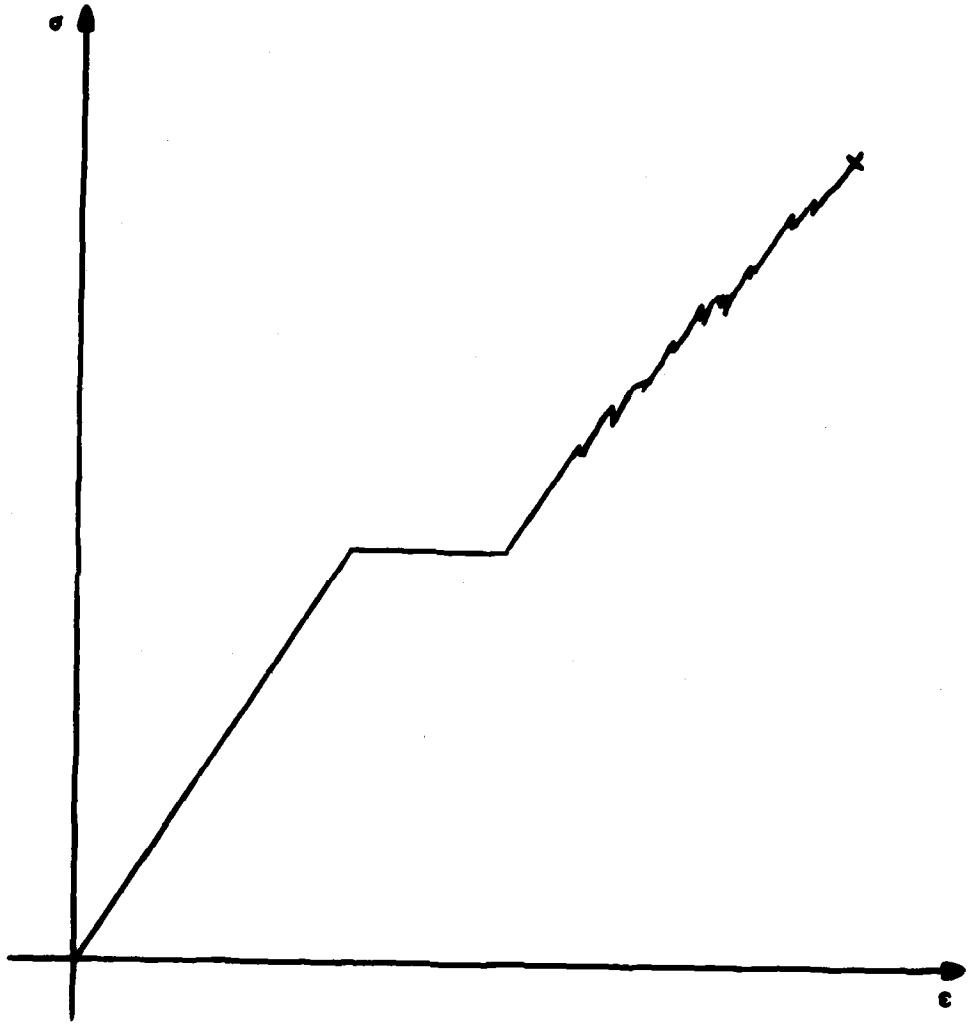

FIGURE 5.3 SKETCH OF STRESS-STRAIN PLOT SHOWING STRAIN DISCONTINUITY POINTS

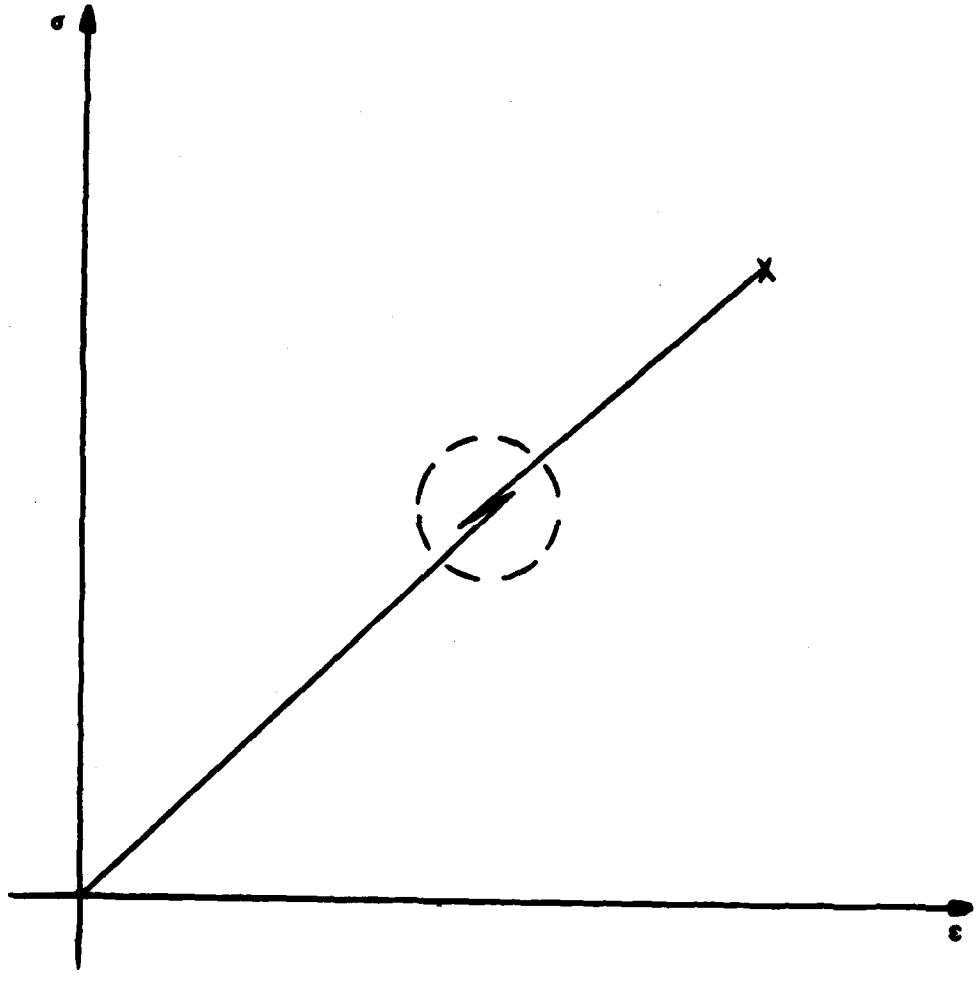

FIGURE 5.4 SKETCH OF STRESS-STRAIN PLOT SHOWING A REVERSAL POINT

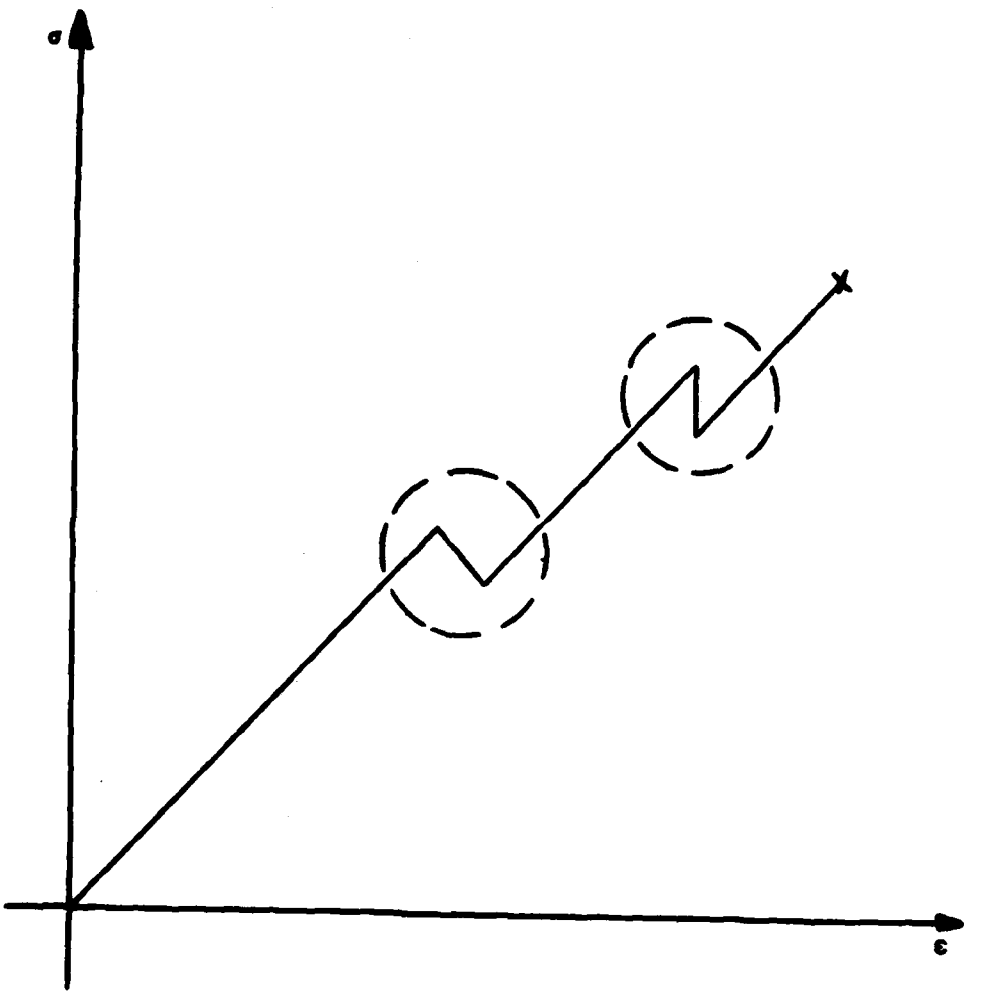

FIGURE 5.5 SKETCH OF STRESS-STRAIN PLOT SHOWING LOAD DROPS

TABLE 5.1

SUMMARY OF STRESS-STRAIN BEHAVIOR FOR $[\pm 45/0]_s$ SPECIMENS

SPECIMEN	BEHAVIOR PATTERN
UNFLAWED	SOFTENING
C1-45A1-X1G	DISCONTINUITIES
S3-45A1-XG	NOT RECORDED
C4-45A1-X1G	DISCONTINUITIES
S4-45A1-X1G	DISCONTINUITIES
S4-45A1-X2G	DISCONTINUITIES
S2-45A1-X2F	SOFTENING
C4-45A1-X1F	DISCONTINUITIES
S4-45A1-X1F	DISCONTINUITIES
S4-45A1-X2F	DISCONTINUITIES

TABLE 5.2

SUMMARY OF STRESS-STRAIN BEHAVIOR FOR $[0/\pm45]_s$ SPECIMENS

SPECIMEN	BEHAVIOR PATTERN
UNFLAWED	DISCONTINUITIES
S4-45B1-X1G	DISCONTINUITIES
S4-45B1-X2G	DISCONTINUITIES

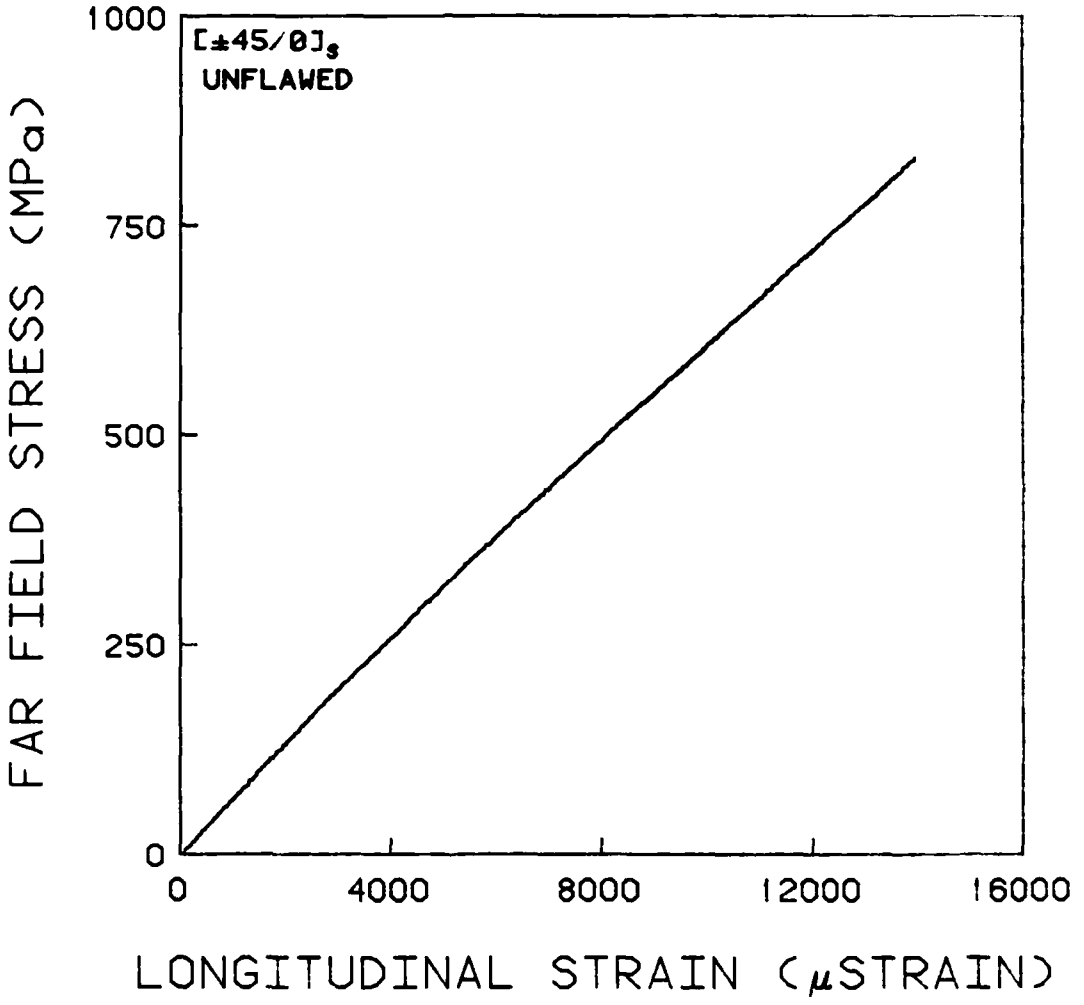

FIGURE 5.6 TYPICAL STRESS-STRAIN PLOT FOR A [±45/0]s UNFLAWED SPECIMEN

under the first ply had numerous strain discontinuities and reversal points occuring between 460 MPa and 650 MPa. A typical plot is shown in Figure 5.7. Audible pops generally started at approximately 250 MPa and occurred at regular intervals until failure. The other specimens with one implant contained a large 57 mm by 178 mm rectangle at the midplane. Their far-field stress-strain behavior was not recorded as explained in Section 3.5, but the stress-strain behavior recorded from a gage mounted in the center in the specimens show either a softening or a linear pattern. The only stress-strain irregularity which occurred was a reversal point in one specimen at 730 MPa.

All of the specimens implanted with the 32 mm delaminations at each interface responded fairly consistently regardless of implant shape and thickness. Their stress-strain pattern is characterized by discontinuities as shown for a typical case in Figure 5.8. The first audible pops occurred at approximately 200 MPa but stopped about midway to failure. In addition, softer cracking noises were heard throughout the entire range of testing. These were attributed to splitting of the plies over the implant area which were visually observed to correlate with these softer cracking sounds. A picture of these splits on a specimen during a test is shown in Figure 5.9. Strain discontinuities and reversal points occured on a number of the specimens with the circular implants at about 600 MPa. In each instance, the specimen failed within 50 MPa. Three of the five specimens with square implants displayed this

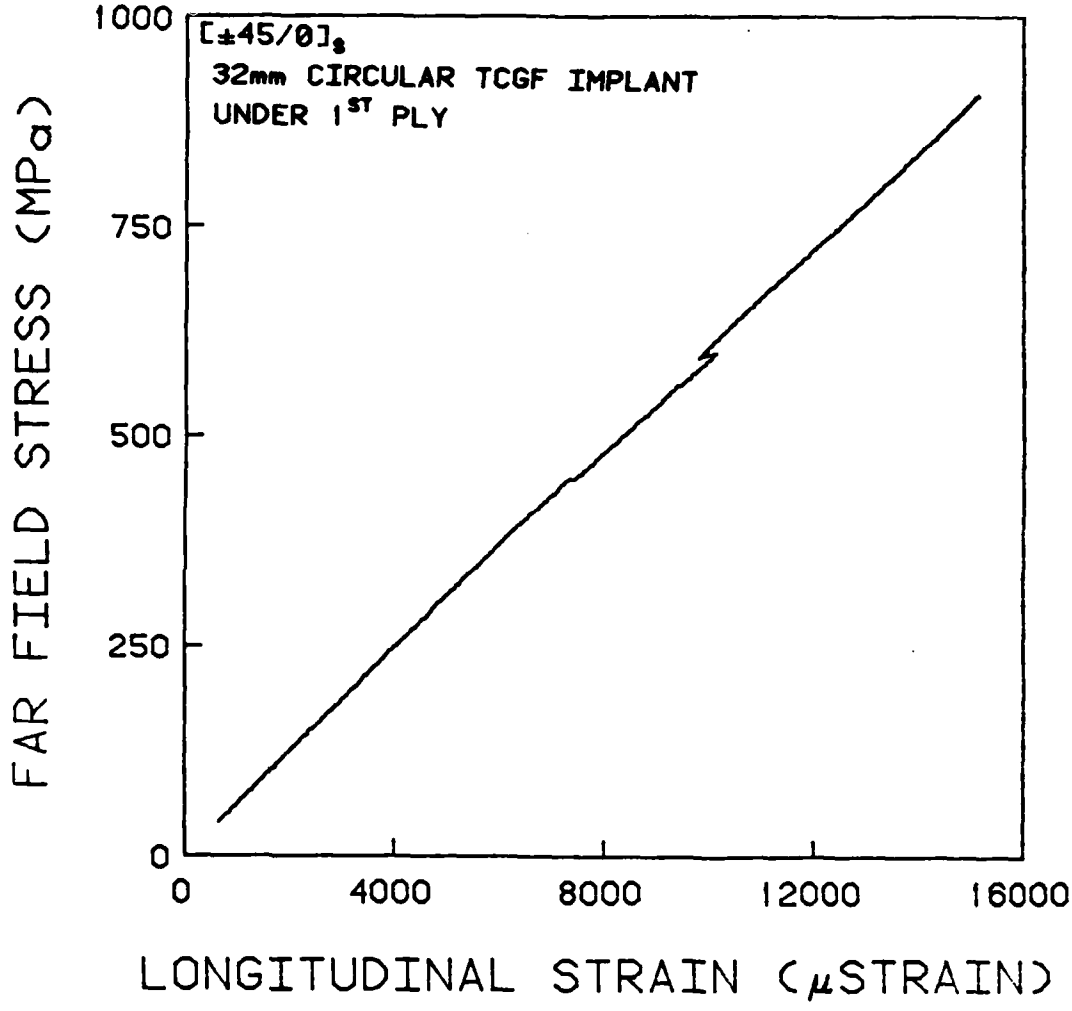

FIGURE 5.7 TYPICAL STRESS-STRAIN PLOT FOR A [±45/0]s SPECIMEN WITH A 32mm CIRCULAR IMPLANT AT THE FIRST PLY INTERFACE

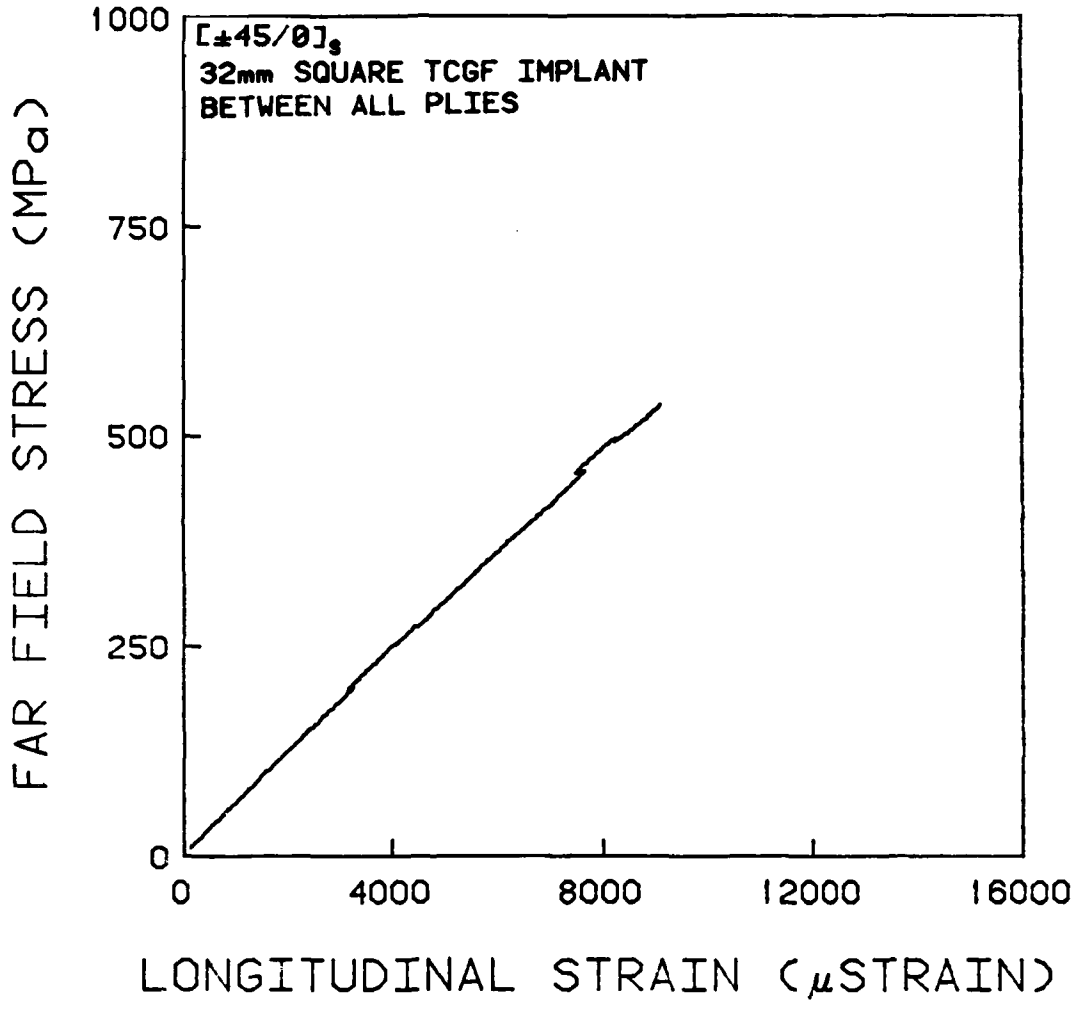

FIGURE 5.8 TYPICAL STRESS-STRAIN PLOT FOR A [±45/0]s SPECIMEN WITH 32mm IMPLANTS AT EACH PLY INTERFACE

Figure 5.9 A LOADED [±45/0]s SPECIMEN WITH A 32mm SQUARE IMPLANT AT EACH PLY INTERFACE, SHOWING MATRIX SPLITTING

pattern occurring at 450 MPa with failure generally occurring within 100 MPa of the applied stress.

The fifteen specimens with 57 mm TCGF implants were manufactured and tested in three different groups. Their stress-strain behavior is generally characterized by discontinuities. Audible pops start at about 170 MPa, as was the case with the smaller implant size, with two or three more occurring until 400 MPa. The softer cracking noises were heard throughout the entire range of loading as plies over the implant continued to split. Three of the stress-strain plots from the first group of five specimens exhibited reversal points at about 675 MPa and failure occurred almost immediately afterwards in each case. The reversal points also occured at about 400 MPa on four of the stress-strain curves. The reversal points for the second and third groups of five specimens occurred earlier, however, with two at 270 MPa, two at 400 MPa, and four at about 500 MPa. Several of the specimens in these groups did not have discontinuities although they fractured at very low stress values which were close to the point where the discontinuities occurred on the others. Loud audible pops occurred at the same stress value as these reversal points in all cases but one. A typical plot of the stress-strain behavior is shown in Figure 5.10. The stress-strain behavior of the specimens implanted with the 57 mm film squares at each interface were like the first five specimens implanted with TCGF. All were characterized by discontinuities which occurred at the same stress level as

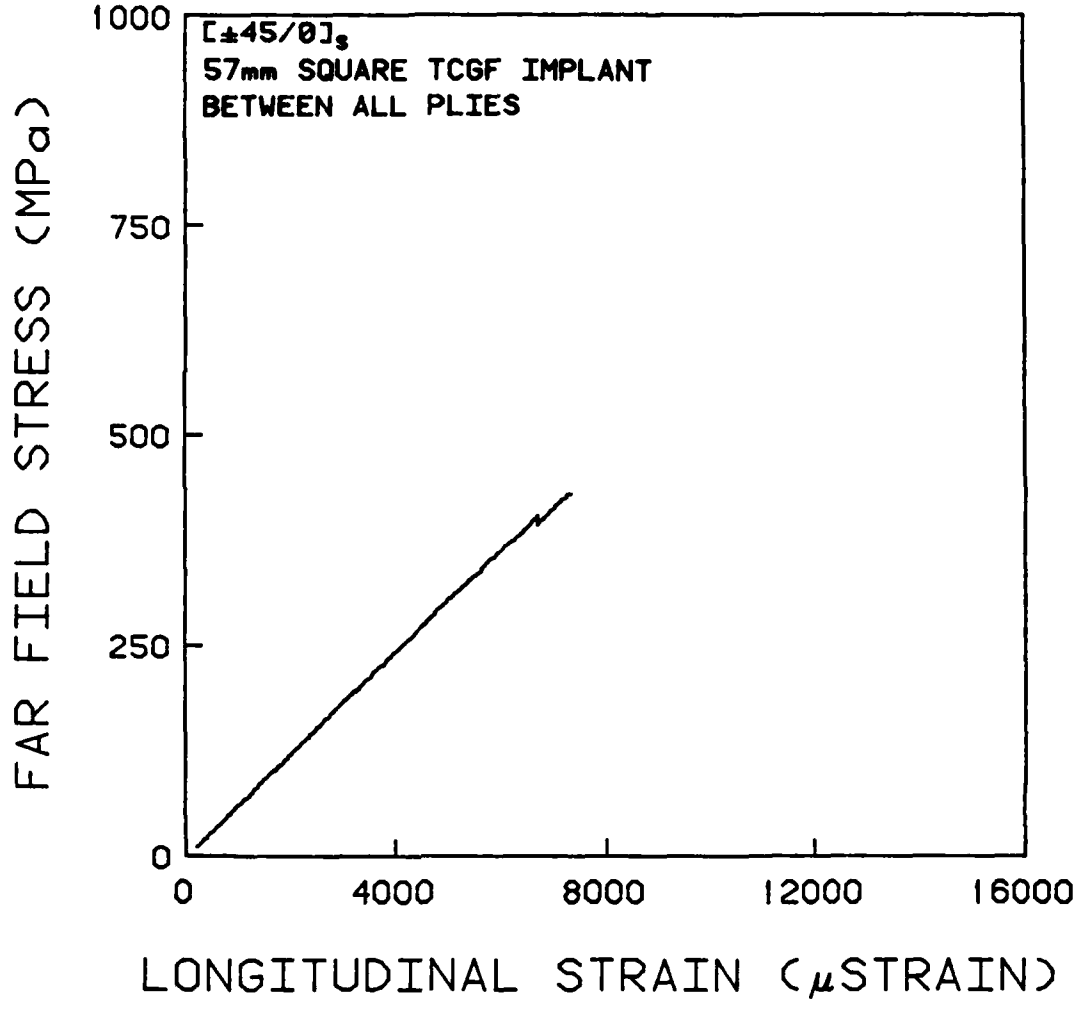

FIGURE 5.10 TYPICAL STRESS-STRAIN PLOT FOR A [±45/0]s SPECIMEN WITH 57mm TCGF IMPLANTS AT EACH PLY INTERFACE

these specimens.

The final specimens containing film implants had 57 mm film squares under the second ply only. Each displayed the softening stress-strain pattern with a break stress of 290 MPa as can be seen in Figure 5.11. About four regularly spaced audible pops were detected starting at 180 MPa and continuing until 520 MPa. None of the softer cracking noises occurred in these specimens and no splitting was noted before fracture as well.

5.1.2 [0/±45]s Specimens

The stress-strain behavior of these specimens are catagorized in Table 5.2. More specific details follow. The stress-strain behavior of the unflawed specimens are characterized by discontinuities as shown in Figure 5.12. Many strain discontinuities, usually on the order of 50-100 microstrain, were present after 400 MPa. One specimen, however, exhibited a strain discontinuity of 500 microstrain but not until a stress of 650 MPa. Audible pops were observed from 180 MPa until about 550 MPa and preceded the strain discontinuities.

The stress-strain behavior of the specimens implanted with 32 mm squares was also characterized by discontinuities but also included load drops as shown in Figure 5.13. Audible pops were detected in the range of 200 MPa to 600 MPa. Many of these pops coincided with both the strain discontinuities and

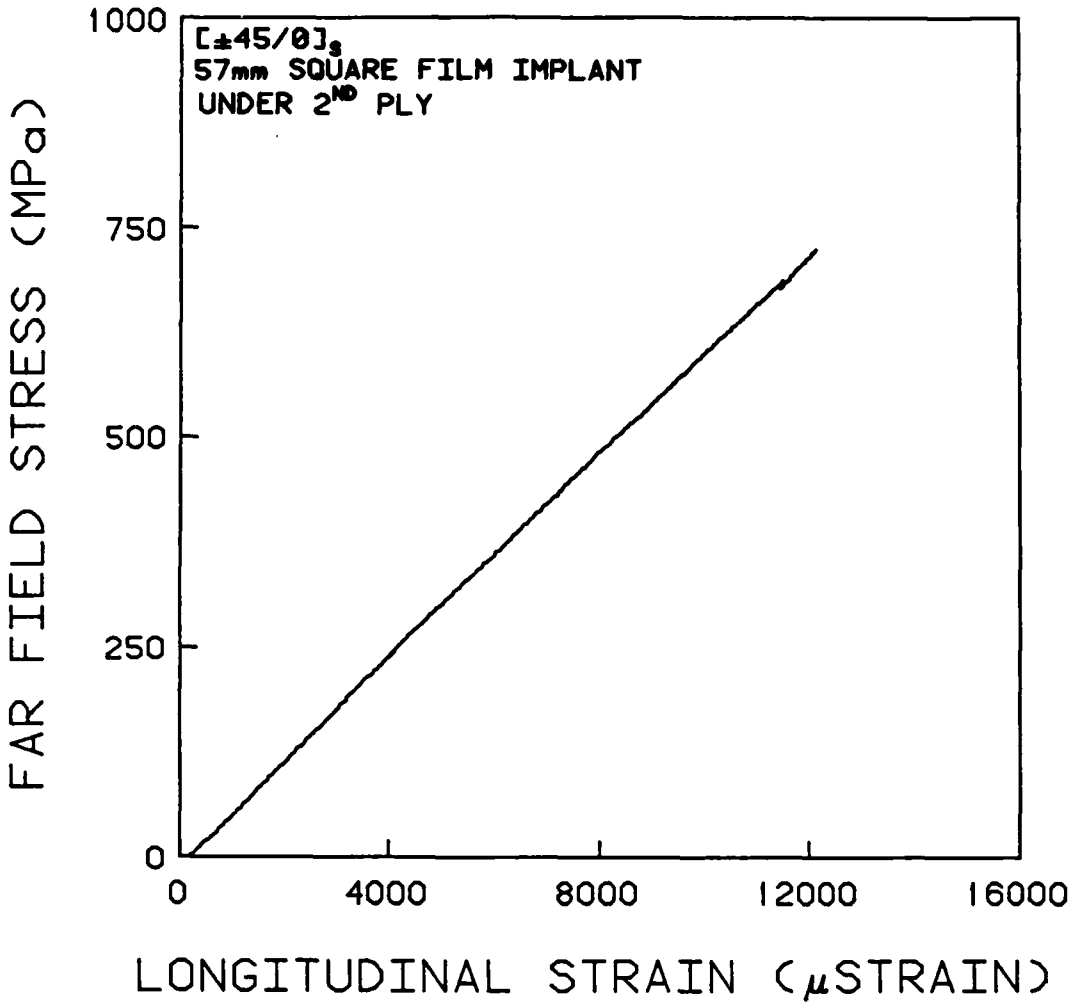

FIGURE 5.11 TYPICAL STRESS-STRAIN PLOT FOR A [±45/0]s SPECIMEN WITH 57mm FILM IMPLANTS AT EACH PLY INTERFACE

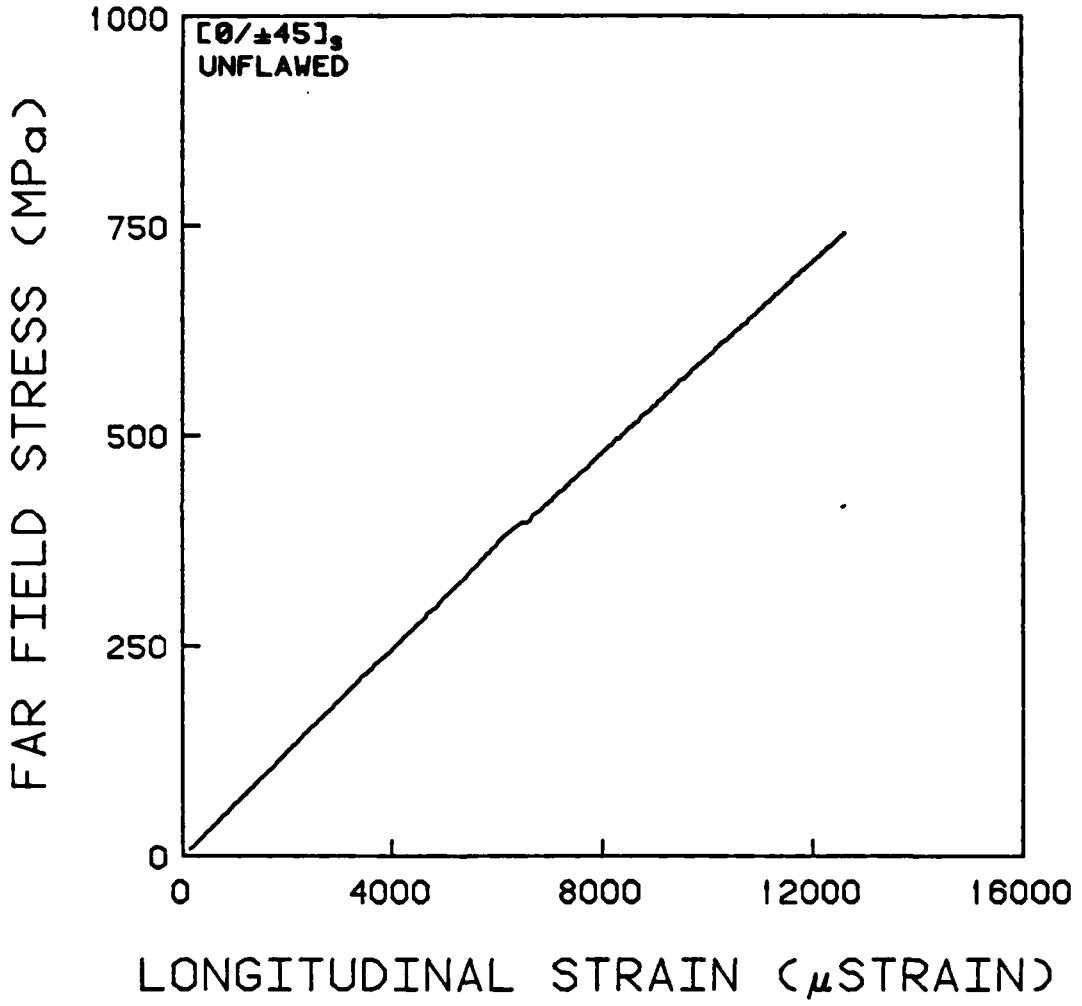

FIGURE 5.12 TYPICAL STRESS-STRAIN PLOT FOR A [0/±45]s UNFLAWED SPECIMEN

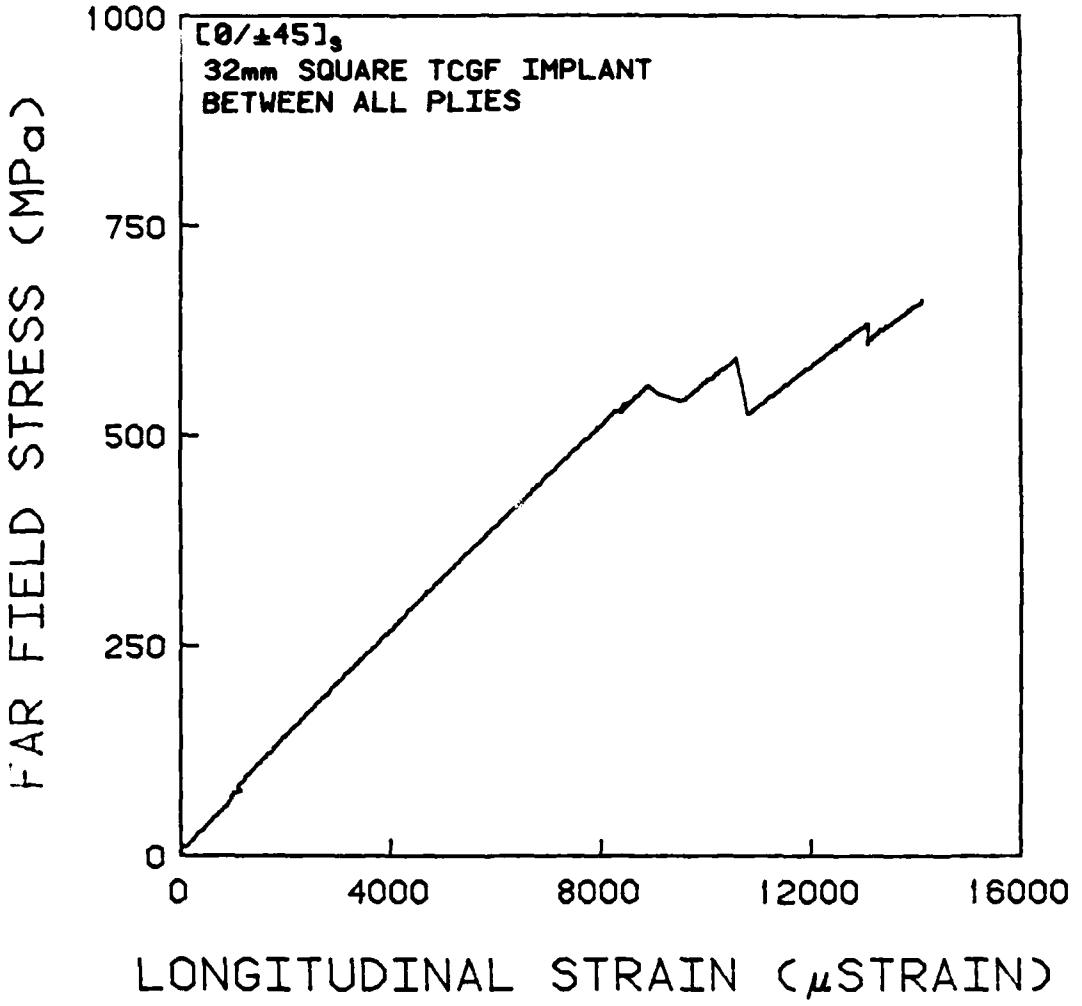

FIGURE 5.13 TYPICAL STRESS-STRAIN PLOT FOR A [0/±45]s SPECIMEN WITH 32mm TCGF IMPLANTS AT EACH PLY INTERFACE

load drops. Strain discontinuities were generally small but load drops ranged from 10 MPa to 70 MPa. Matrix cracking was very evident on these specimens as was the case for most of the specimens with implants. On one occasion, a large number of the 0° plies over the implant separated from the specimen. At the same instant this occurred, the load dropped. In contrast to this behavior, the specimens having the 57 mm implants displayed fewer strain discontinuities and only two minor load drops at 450 MPa. Audible pops coincided with these load drops and occurred in the range of 200 MPa to 450 MPa as can be seen in Figure 5.14. Substantial matrix cracking was also present.

5.1.3 Longitudinal Moduli

The far-field (i.e., away from the implant) stress-strain data was used to determine longitudinal modulus. This is defined as the slope of the initial linear portion of the stress-strain curve as determined by the LIN6 program described in Section 3.7. However, this was not done for the S3-45A1-XG specimens since the implant was so large that a gage could not be placed anywhere except over the delaminated region. The average moduli for each specimen type are summarized in Tables 5.3 and 5.4. Comparing modulus calculations shows that it is independent of implant size, shape, thickness, or number of implants. In fact, the average modulus for all specimens is 60.9 GPa with a coefficient of vartiation of only 4.0%. The values for individual specimens are reported in the Data

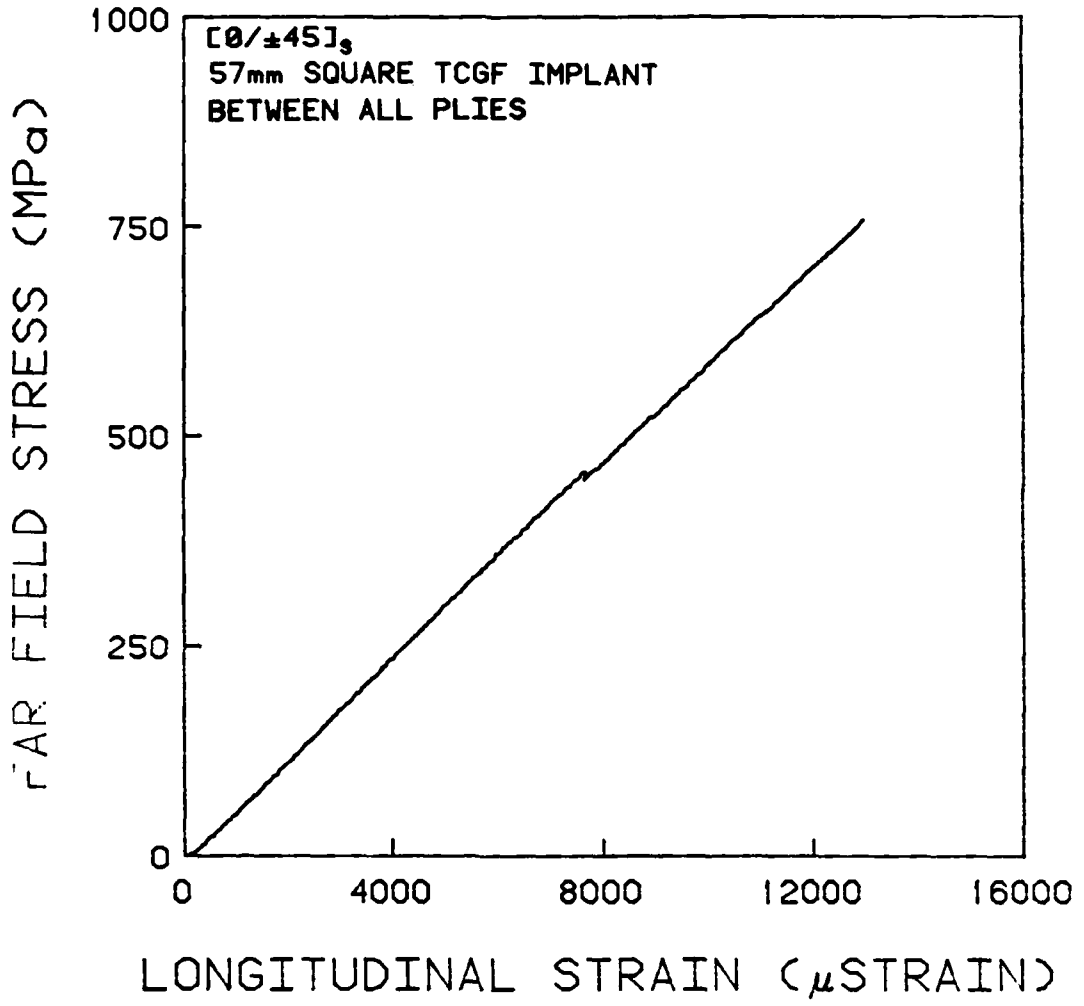

FIGURE 5.14 TYPICAL STRESS-STRAIN PLOT FOR A [0/±45]s SPECIMEN WITH 57mm TCGF IMPLANTS AT EACH PLY INTERFACE

TABLE 5.3

SUMMARY OF LONGITUDINAL MODULI FOR $[\pm 45/0]_s$ SPECIMENS

SPECIMEN TYPE	LONGITUDINAL MODULUS [GPa]	C.V.
45A1-X	62.6	6.7%
C1-45A1-X1G	61.1	2.8%
S2-45A1-X2F	60.0	3.6%
S3-45A1-XG	58.8	2.5%
C4-45A1-X1F	59.1	7.0%
S4-45A1-X1F	61.0	1.7%
S4-45A1-X2F	59.8	5.7%
C4-45A1-X1G	60.0	4.3%
S4-45A1-X1G	60.0	2.9%
S4-45A1-X2G	62.5	2.3%
AVERAGE	60.9	

TABLE 5.4

SUMMARY OF LONGITUDINAL MODULI FOR $[0/\pm45]_s$ SPECIMENS

SPECIMEN TYPE	LONGITUDINAL *MODULUS [GPa]*	C.V.
45B1-X	61.6	1.7%
S4-45B1-X1G	60.7	2.2%
S4-45A1-X2G	61.4	3.6%
AVERAGE	61.2	

Tables. A theoretical value for modulus was computed using lamination theory and the data of Table 3.1. This value is 63.3 GPa for both stacking sequences.

5.2 Stress-Strain Behavior at Other Locations

In an attempt to characterize the behavior of the implanted delamination(s), strain gages were placed over delaminated plies and in close proximity to the implant on a number of specimens as described in Section 3.5. The exact location of these gages was illustrated in Figure 3.5.

The strain readings from the gage placed at the center of the implant region tended to show the most erratic behavior of all the gages. A typical case is shown in Figure 5.15. Often at very low stress levels, strain discontinuities appeared, probably due to splits forming around and under the gage. Some specimens displayed linear regions which paralleled the far-field curve, but large nonlinearities were more common. In most cases a split would render this gage inoperative early in the test. The gage placed over the implant just inside the right edge displayed much the same behavior. No consistent behavioral patterns could be noted, however, between the readings from this gage and those mounted on the implant center.

The strain gages placed just above the implant and beyond its edge and those to the right of the implant edge generally gave readings similar to those from the far-field gage. No

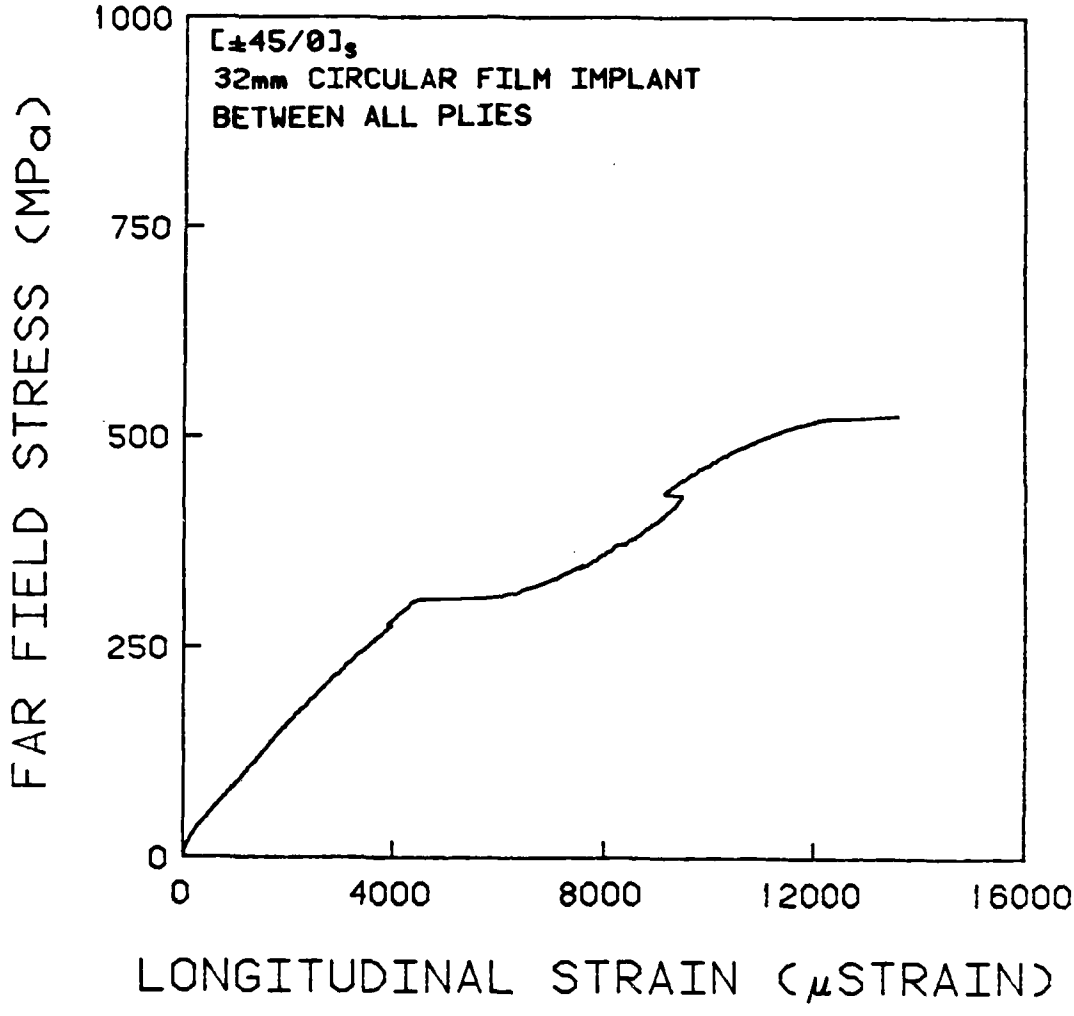

FIGURE 5.15 TYPICAL BEHAVIOR OF STRAIN GAGE PLACED ON THE DELAMINATED PLIES

AD-A171 329 THE EFFECTS OF IMPLANTED DELAMINATIONS ON THE TENSILE STRENGTH OF GRAPHITE/EPOXY LAMINATES(U) AIR FORCE INST OF TECH WRIGHT-PATTERSON AFB OH L M ROBICHAUX 1986 2/2

UNCLASSIFIED AFIT/CI/NR-86-130T F/G 11/4 NL

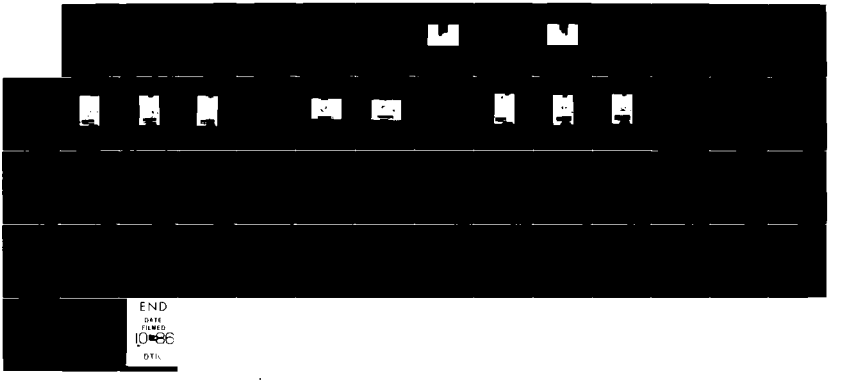

END

DATE FILMED

10-86

DTIC

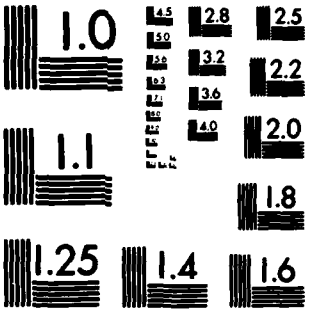

distinct pattern could be noted, however, as to whether the strain was consistently higher or lower than the far-field readings. The behavior was generally linear but large discontinuities were displayed at times. Many times these discontinuities were not perceived by the far-field gage. A typical plot for all these gages is shown for specimen C4-45A1-X1G in Figure 5.16. This behavior was independent of implant type or configuration.

Two different types of specimens had an additional strain gage mounted to the right of the implant and in line with the far-field gage in addition to the far-field gage as shown in Figure 3.5. The stress-strain behavior at these locations was nearly identical to that recorded at the far-field location. Modulus readings were within 3% of far-field and each showed the same characteristic behavioral patterns. These strain readings on $[\pm 45/0]_s$ specimens with 32 mm square film implants, however, were always slightly higher than far-field, while strain readings on $[0/\pm 45]_s$ specimens with 32 mm square TCGF implants were slightly lower in all but one case. In addition, the stress-strain behavior at these sites showed strain-discontinuities where none were present at the far-field position. A typical stress-strain plot is shown for a $[\pm 45/0]_s$ specimen in Figure 5.17 and for a $[0/\pm 45]_s$ specimen in Figure 5.18.

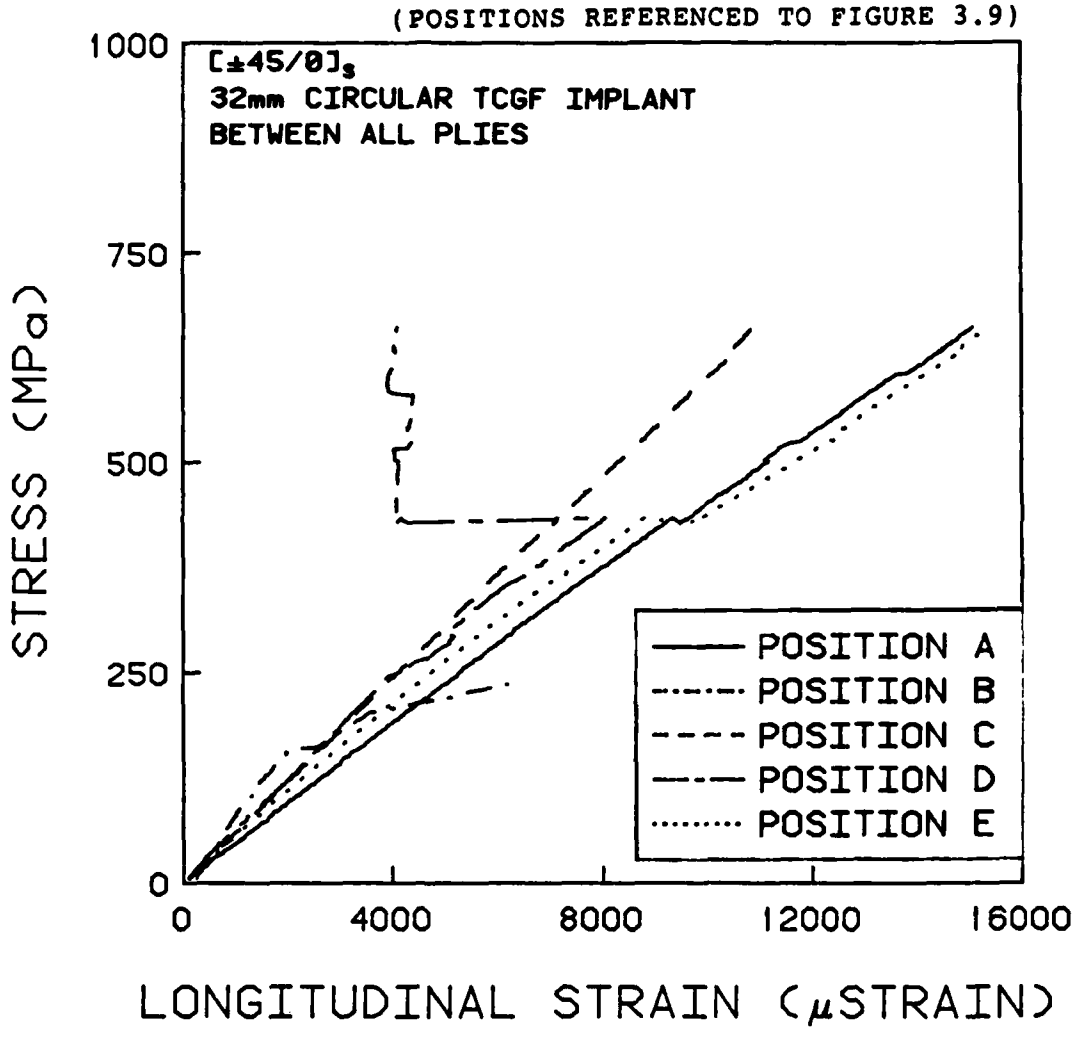

FIGURE 5.16 TYPICAL STRESS-STRAIN BEHAVIOR FROM STRAIN GAGES LOCATED ON AND AROUND THE IMPLANT

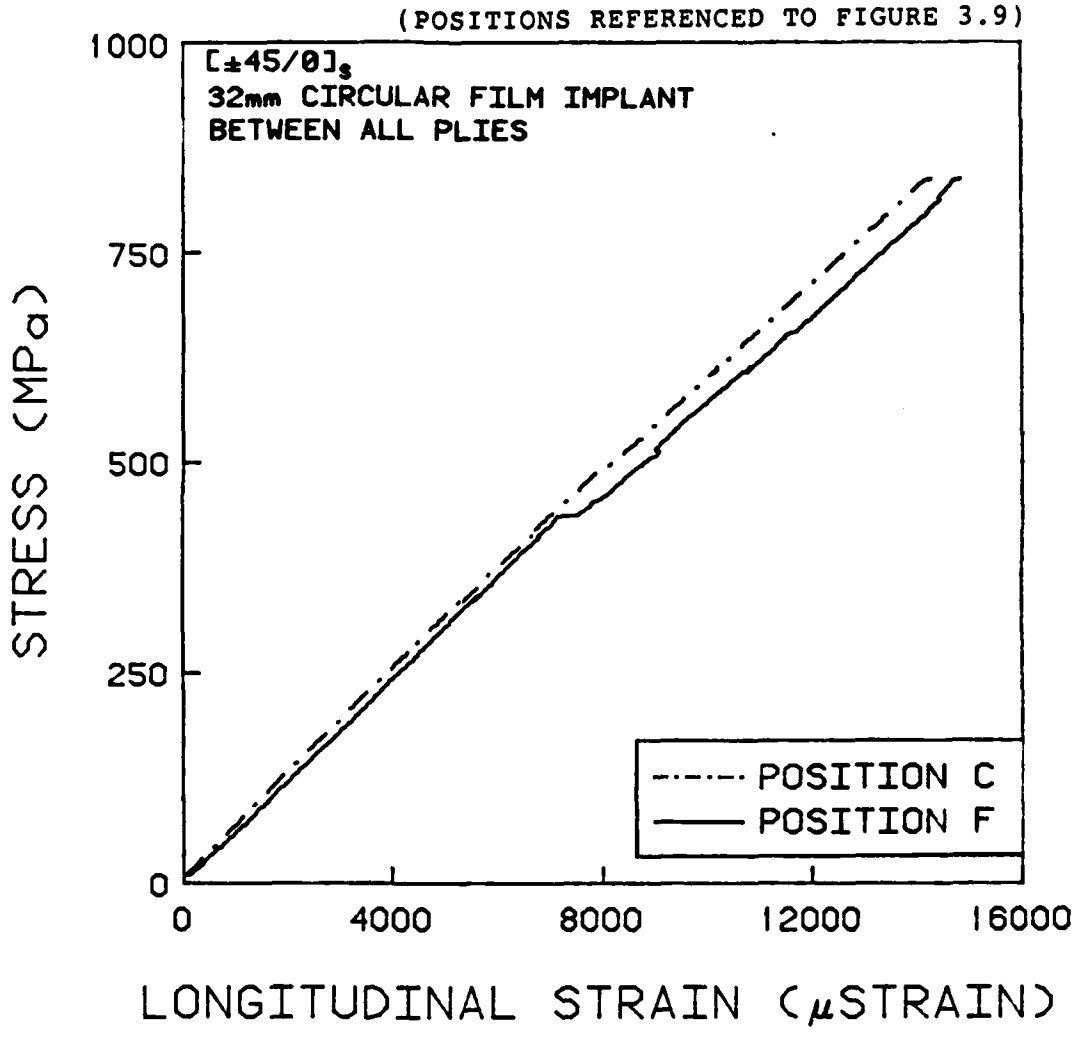

FIGURE 5.17 TYPICAL STRESS-STRAIN BEHAVIOR OF $[\pm 45/0]_S$ SPECIMENS CONTAINING TWO STRAIN GAGES

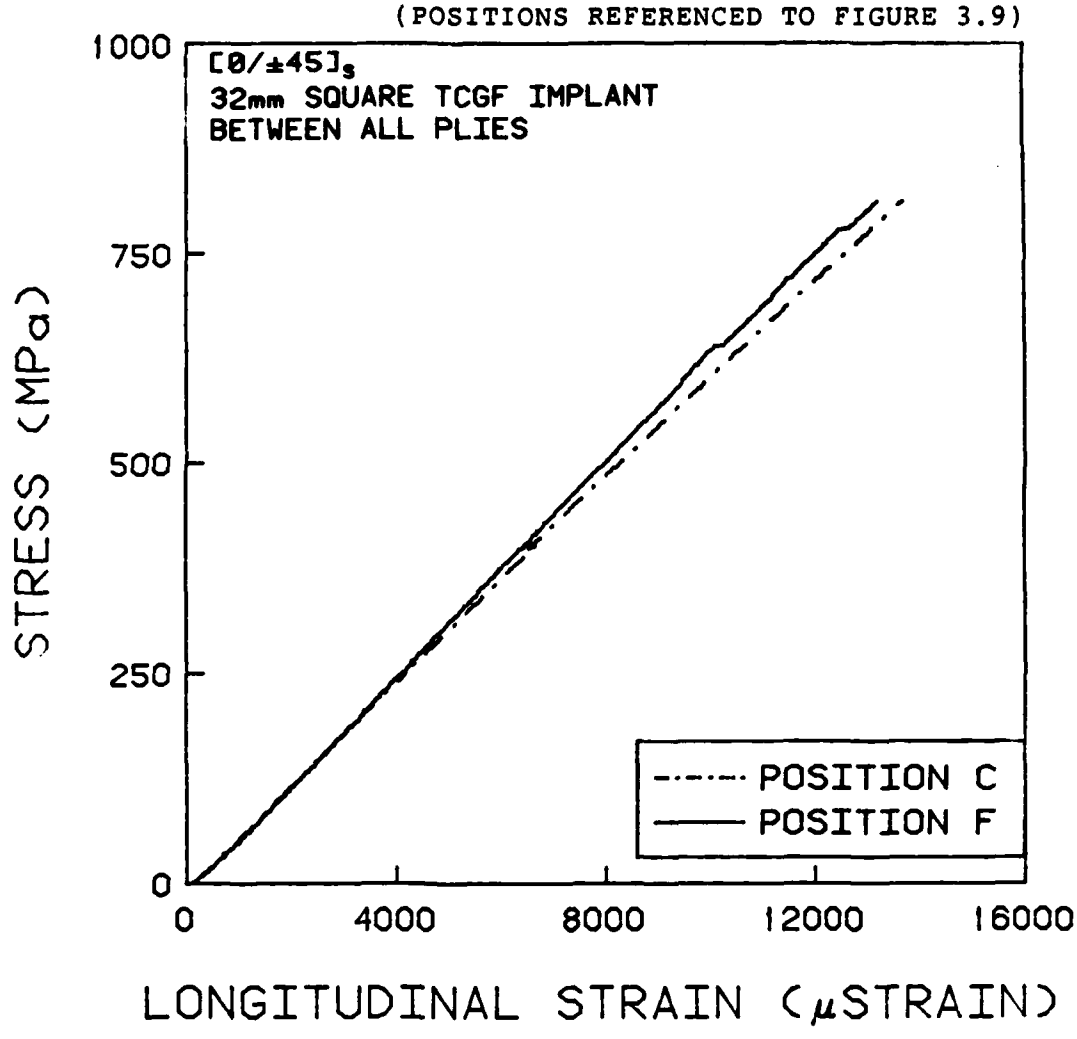

FIGURE 5.18 TYPICAL STRESS-STRAIN BEHAVIOR OF [0/±45]s SPECIMENS CONTAINING TWO STRAIN GAGES

5.3 Photoelastic Test Results

As discussed in Section 3.6, testing of specimens with photoelastic coatings was not to failure. The slope of the stress-strain curve was computed using a linear regression on the data points up to 200 MPa. This is where the first audible pops were noted and the plot became nonlinear. The slope was determined for each of the locations shown in Figure 3.6. The modulus of the unflawed specimen was measured at 53.4 GPa. This is approximately 15% lower than the average value for specimens instrumented with strain gages. This, however, can be useful in comparing the moduli of the other specimens tested. The slope determinations for the specimen implanted with 57 mm film delamination under the second ply were all within 5 MPa averaging 54.4 MPa. The value in the implant center was the highest. The tester was unable to visually detect the presence of the implant until the specimen was unloaded. At 4400 N the implant could be seen with crisp detail. There were no signs of delamination growth but a number of dark 45° lines covered the implant site as shown in Figure 5.19. These may have been splits which formed during load application.

Strain readings at the four locations on the specimen implanted with 57 mm film delaminations between every ply were more diverse. This is because the appearance of dark 45° lines over the implant area made identification of the proper fringe almost impossible. The fringe was not a distinct line and

FIGURE 5.19 PHOTOELASTIC PHOTOGRAPH OF THE [±45/0]s SPECIMEN WITH A FILM INPLANT IN THE SECOND PLY INTERFACE AT A 4400 N LOAD

moved erratically when it came near these 45° lines. The lowest slope recorded was directly over the implant, which was calculated to be 38.4 GPa. The highest reading of 62.3 GPa was on the top of the implant, while the far-field modulus was 53.8 GPa, and the slope at the right implant edge was 62.1 GPa. The existence of the splits in the implant region, as indicated by the lines in the photoelastic coating, most likely render the strain readings in the implant region less meaningful in this context since they are more indicative of very local effects due to the presence of the splits. From the time of initial loading, the implant could be clearly seen through the coating. Again, no odd behavorial patterns were noticed exept the dark 45° lines over the implant. These lines are shown in Figure 5.20 for an applied load of 8900 N.

5.4 Fracture Stresses

Specimens made in this investigation fall into two broad groups according to stacking sequence. Within these two groups, implant size, shape, and thickness were varied. A summary of the mean fracture stresses with a breakdown by stacking sequence are given in Tables 5.5 and 5.6. The results for individual specimens are given in the Data Tables. The coefficients of variation noted are typical for fracture stresses of multidirectional composite laminates.

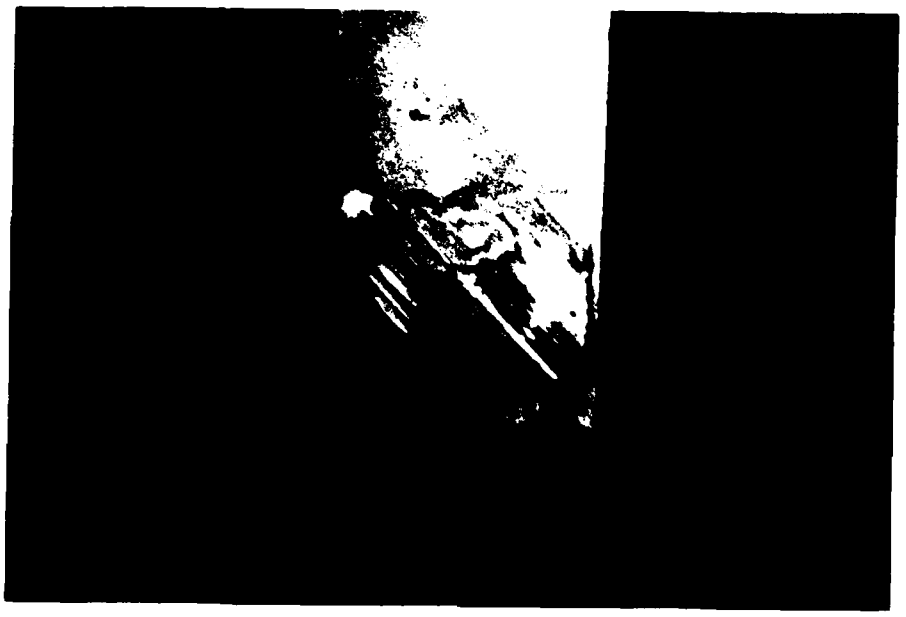

FIGURE 5.20 PHOTOELASTIC PHOTOGRAPH OF THE [±45/0]s SPECIMEN WITH 57mm FILM IMPLANTS AT ALL INTERFACES AT AN 8900 N LOAD

TABLE 5.5

AVERAGE FRACTURE STRESSES FOR $[\pm 45/0]_s$ SPECIMENS

IMPLANT TYPE	IMPLANT SIZE	IMPLANT CONFIG.	NUMBER TESTED	σ_f [MPa]	C.V.
-	-	-	6*	826	9.7%
G(TCGF)	32 mm	C1	5	853	4.1%
Film	57 mm	S2	6*	825	5.0%
G(TCGF)	57 mm x 178 mm	S3	5	784	8.3%
Film	32 mm	C4	5	782	7.0%
Film	32 mm	S4	5	820	3.9%
Film	57 mm	S4	6*	704	9.7%
G(TCGF)	32 mm	C4	10	619	7.9%
G(TCGF)	32 mm	S4	5	599	12.1%
G(TCGF)**	57 mm	S4	5	722	5.1%
G(TCGF)**	57 mm	S4	10	481	15.0%

* Indicates one specimen from this group was tested using a photoelastic coating.

** Three groups of five specimens were tested using the implants listed. Additional specimens were tested because of large differences in the fracture stress by groups.

TABLE 5.6

AVERAGE FRACTURE STRESSES FOR $[0/\pm45]_s$ SPECIMENS

IMPLANT TYPE	IMPLANT SIZE	IMPLANT CONFIG.	NUMBER TESTED	σ_f [MPa]	C.V.
-	-	-	5	795	6.2%
G(TCGF)	32 mm	S4	5	713	13.8%
G(TCGF)	57 mm	S4	5	712	13.4%

5.4.1 [±45/0]s Specimens

Test results show that fracture stress is dependent upon number of implants, implant thickness, and implant width. All specimens with one implanted delamination showed no significant reduction in fracture stress compared to the unflawed specimens. Thus, the fracture stress was independent of implant size, shape, or thickness for these specimens. This is not true for specimens implanted with delaminations at every ply interface. While those with 32 mm film implants showed no significant loss in strength regardless of shape, specimens with 57 mm film implants failed 15% lower than the unflawed ones. Specimens with TCGF implants showed the largest reduction in fracture stress. The specimens with 32 mm TCGF implants at each interface failed at stresses 26% lower than in the unflawed cases, regardless of shape. The specimens with 57 mm implants failed at an average stress which is 32% lower than the unflawed case. However, these specimens were manufactured and tested in three groups of five specimens and the fracture stress between the first group and the last two groups were markedly different. The first five specimens failed at an average stress of 704 MPa while the average for the latter two gruops is 481 MPa. These differences will be discussed later.

5.4.2 [0/±45]s Specimen

Unflawed specimens of this stacking sequence were made so

a direct comparison could be made to flawed specimens. The mean unflawed failure stress of 795 MPa was close to the value obtained for the $[\pm 45/0]_s$ stacking sequence. Specimens containing 32 mm and 57 mm implants failed at virtually the same value; 713 MPa for the former and 712 MPa for the latter. Coefficients of variation for both were 13%.

5.5 Fracture Modes

This section includes a brief description of the fracture mode for each specimen type. The description is based upon postmortem visual examinations. Photographs of typical facture modes are included in Figures 5.21 through 5.28. Because of strong similarities in the fracture mode of specimens with TCGF and film implants, the specimens will be grouped by stacking sequence.

5.5.1 [±45/0]s Specimens

Fracture in these specimens is not a function of implant type but rather, number of implants. Where equal number of implants are present, implant size affects the fracture mode. Fracture in the unflawed specimens was in-plane with fairly "clean" cracks. That is, cracks were not accompanied by delamination and matrix cracking and splitting was not predominant. Cracks either occurred at 45° angles on either side of the center of the test section or at a 90° angle to the longitudinal axis and through the specimen center. Generally,

fracture left the specimen in two or three pieces. Their failure is shown in Figure 5.21.

All specimens containing a delamination at a single interface exhibited the same fracture pattern with damage centered around the implant area with some secondary fracture occurring in the vicinity of the loading tabs. A unique characteristic of this group's fracture is the presence of small longitudinal cracks in the center of the specimen. These cracks are approximately 25 mm long and extend from the implant edge. Failure is, again, primarily in-plane but there is a large amount of splitting with some delamination of the plies at the implant area. The characteristic failure pattern of these specimens is shown in Figure 5.22.

All specimens having 32 mm implants between every ply, regardless of thickness or shape, had similar fractures. A typical specimen fracture mode is shown in Figure 5.23. The longitudinal cracks extending from the implant which appeared on the single implant specimens were highly developed. These cracks grew to about 75 mm and usually terminated by combining with 90° cracks which spread to the specimen edge. This cracking pattern was evidently produced by the same mechanism which caused the sides of most specimens to collapse toward the center resulting in an "hour-glass" shaped specimen. Even when the specimen sides remained intact, the long longitudinal cracks were present. Many times these types of specimens had large pieces of laminate separate from the specimen during failure. Usually, the 45° plies which covered the implant were

FIGURE 5.21 TYPICAL FRACTURE MODE FOR A [±45/0]s UNFLAWED SPECIMEN

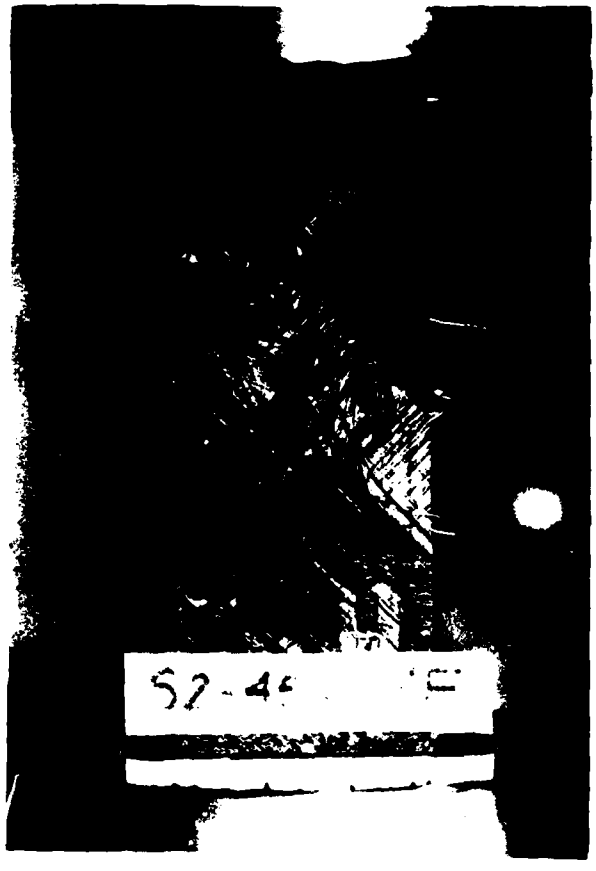

FIGURE 5.22 TYPICAL FRACTURE MODE FOR A [±45/0]s SPECIMEN WITH ONE IMPLANT

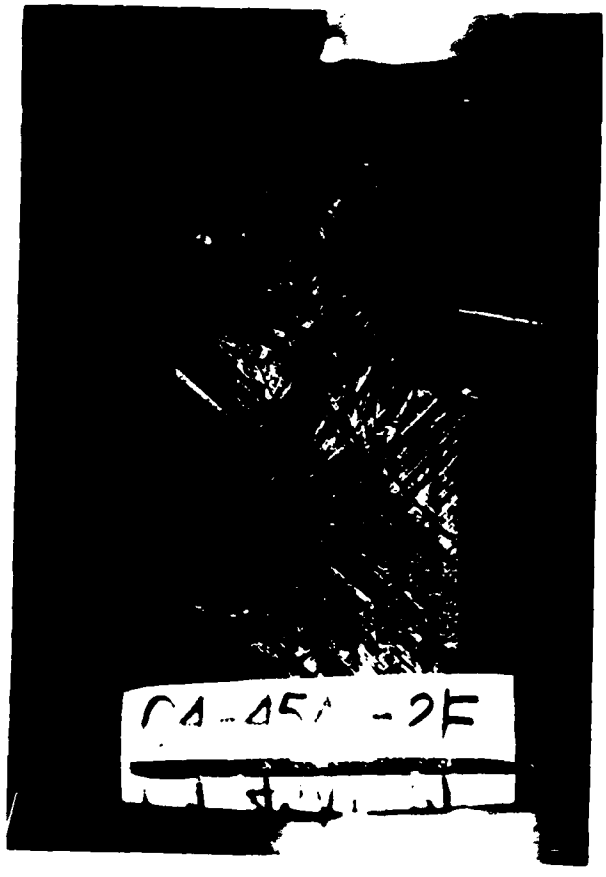

FIGURE 5.23 TYPICAL FRACTURE MODE FOR A [±45/0]s SPECIMEN WITH 32mm IMPLANTS AT ALL PLY INTERFACES

completely delaminated from the specimen while the remaining plies showed massive splitting and shredding.

The specimens with the 57 mm implants between all plies were the only ones with two distinct fracture modes. The specimens with the film implants and the first batch of five specimens made containing the TCGF implants, which had the higher failure stresses, showed identical fracture patterns. These specimens had the most destructive failures with all of the plies in the implant region delaminated, split apart, and shredded. Damage is restricted to this area but basically nothing is left of this area. Again, some longitudinal cracks can be seen extending away from the center toward the loading tab. Failure is primarily out-of-plane. The fracture of a specimen in this group is shown in Figure 5.24.

The last fracture pattern observed was seen in the last two groups of specimens implanted with the 57 mm TCGF squares and is shown in Figure 5.25. Unlike the other specimens with the same implant, very little damage is evident. Usually only the outer plies are delaminated from the implant region; the other plies are all intact. Small 90° cracks connect the implant edge and the specimen edge at the implant corners. On most specimens, the -45°/0°/0°/-45° group of plies are still laminated and intact on either side of the implant. Fracture is in-plane with no secondary damage noticed away from the implant.

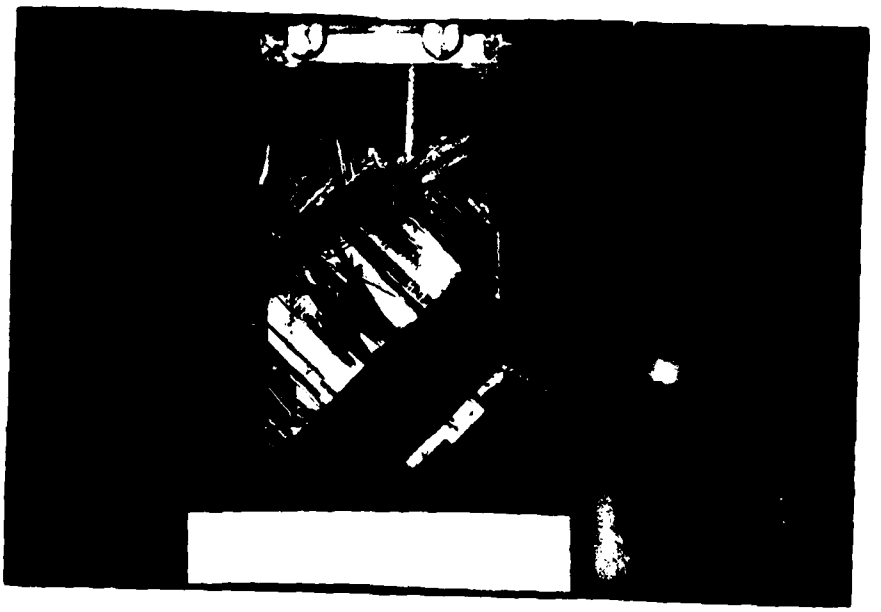

FIGURE 5.24 TYPICAL FRACTURE MODE FOR A [±45/0]s SPECIMEN FROM THE FIST BATCH WHICH HAD 57mm TCGF IMPLANTS AT EACH PLY INTERFACE

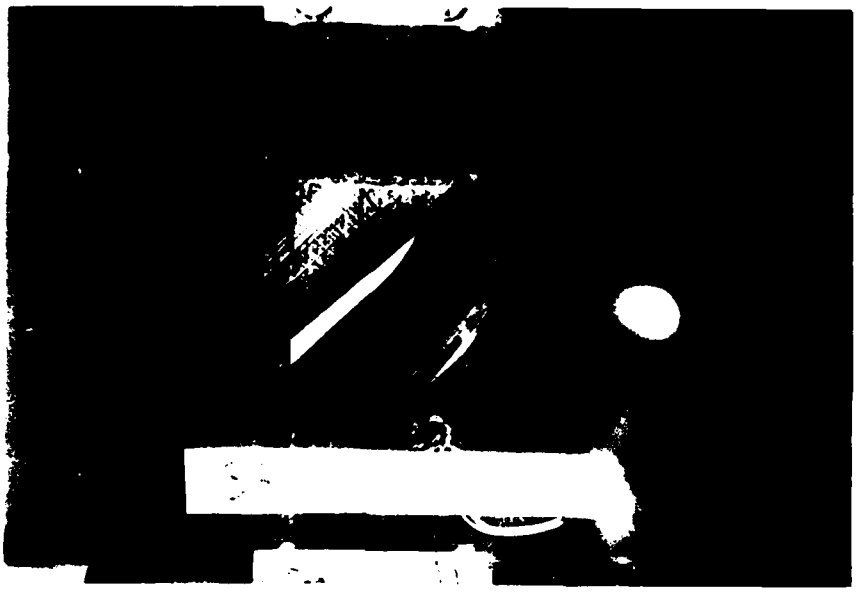

FIGURE 5.25 TYPICAL FRACTURE MODE FOR A [±45/0]s SPECIMEN FROM THE THIRD BATCH WHICH HAD 57mm TCGF IMPLANTS AT EACH PLY INTERFACE

5.5.2 [0/±45]s Specimens

The fracture mode of the unflawed specimens were generally along 45° lines on either side of the specimen center as can be seen in Figure 5.26. These two cracks which traversed the width of the specimen were "dirty," meaning the 0° fibers along the cracks were pulled out and fractured when the specimen was torn in two pieces. Some secondary damage was also present near the loading tabs.

The specimens implanted with the 32 mm TCGF squares showed none of the characteristics of the unflawed specimens. Cracks extended from every corner of the implant in 90° and 0° lines. All of the outer 0° plies were broken off of the area covering the implant with much splitting and delamination extending away from the center. The fracture pattern can clearly be seen in Figure 5.27. Specimens implanted with 57 mm squares showed generally the same characteristics with less cracking. However, more 0° plies were delaminated from the implant area. This might be expected since the implant area is much larger. The specimens are generally intact with a few cracks extending away from the center of the specimen. With the exception of the delamination, most damage is in-plane as can be seen in Figure 5.28.

5.6 Analytical Results

In this section, typical results for the analysis described in Chapter 4 are presented. These predictions serve

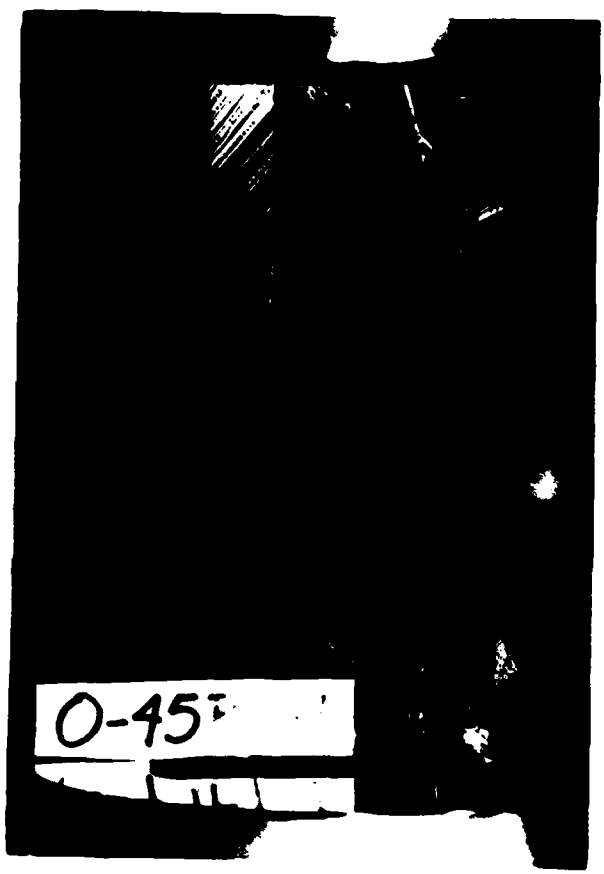

FIGURE 5.26 TYPICAL FRACTURE MODE FOR A [0/±45]s UNFLAWED SPECIMEN

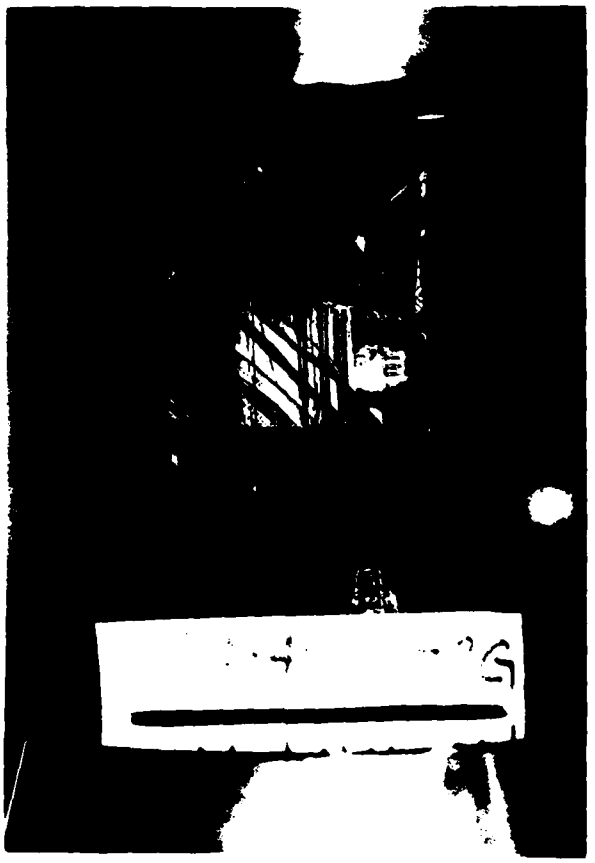

FIGURE 5.27 TYPICAL FRACTURE MODE FOR A [0/±45]s SPECIMEN WITH 32mm TCGF IMPLANTS AT EACH PLY INTERFACE

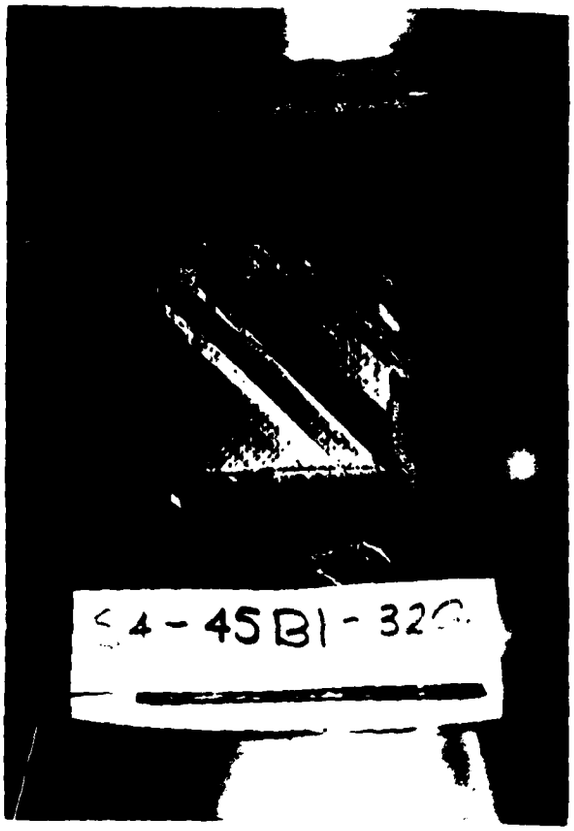

FIGURE 5.28 TYPICAL FRACTURE MODE FOR A $[0/\pm45]_s$ SPECIMEN WITH 57mm TCGF IMPLANTS AT EACH PLY INTERFACE

as a lower bound for the fracture of specimens containing the various implants discussed previously due to the conservative assumption used in post ply failure analysis (see Section 6.1). These results will be divided into the effects of implant thickness, number of implants, and implant width on ultimate fracture stress.

Changing the implant thickness causes a large difference in specimen fracture strength. The predicted strength as a function of implant thickness for the case of a 32 mm wide implant at each interface of a $[\pm 45/0]_s$ laminate is shown in Figure 5.29. Fracture stress is very sensitive to a change in implant thichness in the range fron zero to 3 mm and relatively insensitive to changes in thicknesses above 6 mm.

The dependence of fracture stress on the number of implants is shown in Figure 5.30. The case presented here is a 32 mm wide TCGF implant (thickness equal to 0.0762 mm) in a $[\pm 45/0]_s$ laminate. The first implant is located under the surface ply opposite the flat side of the specimen. Consecutive implants are then added to the interface just below the current implant location. Results show that the single implant does not affect the fracture stress. However, each additional implant after the first causes a reduction in strength.

Finally, a comparison is made to determine the influence of implant width. The baseline case of a film implant (thickness of 0.0127 mm) at each ply interface of a $[\pm 45/0]_s$ laminate is considered. The rule of mixtures approach,

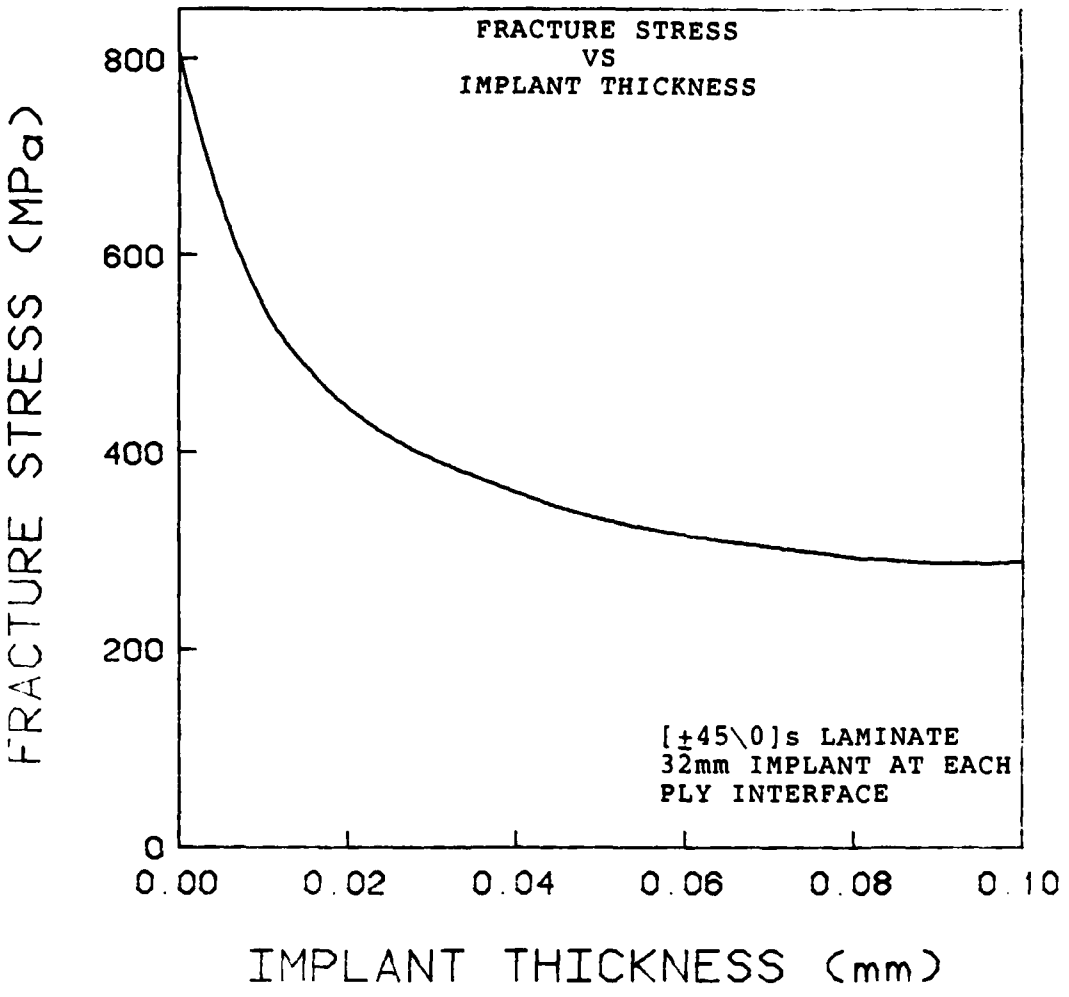

FIGURE 5.29 PLOT OF THE PREDICTED FRACTURE STRESS VERSUS IMPLANT THICKNESS FOR A [±45/0]s SPECIMEN WITH A 32mm IMPLANT AT EACH INTERFACE

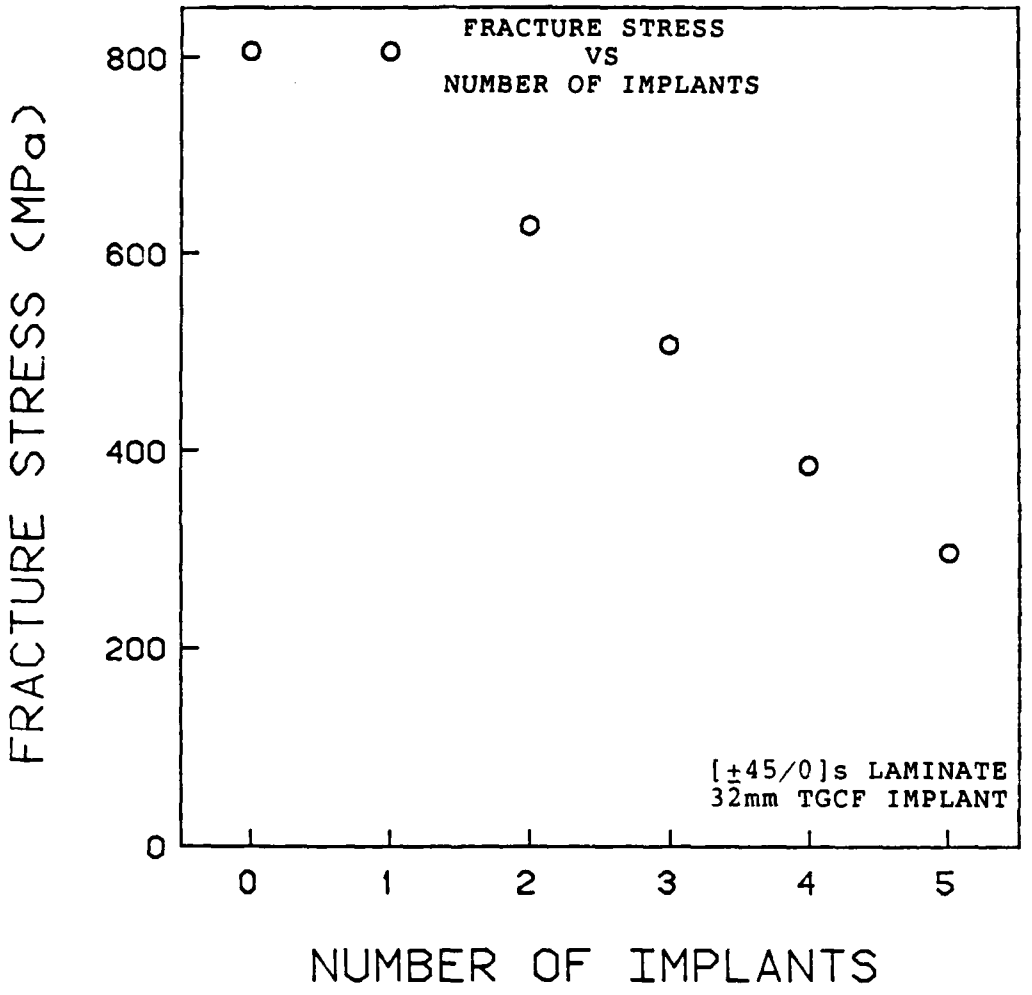

FIGURE 5.30 PLOT OF THE PREDICTED FRACTURE STRESS VERSUS NUMBER OF IMPLANTS FOR A [±45/0]s SPECIMEN WITH A 32mm TGCF IMPLANT

described in Section 4.6, provides a drastic change in fracture strength for widths up to 15 mm as illustrated in Figure 5.31. After this, the decrease in strength tapers off and declines at a constant rate up to a width equal to that of a specimen.

The calculations presented in this section do not specifically relate to the configurations tested in this investigation. Rather, they are intended to show the general trends in fracture stresses which the model predicts as various configurations are considered.

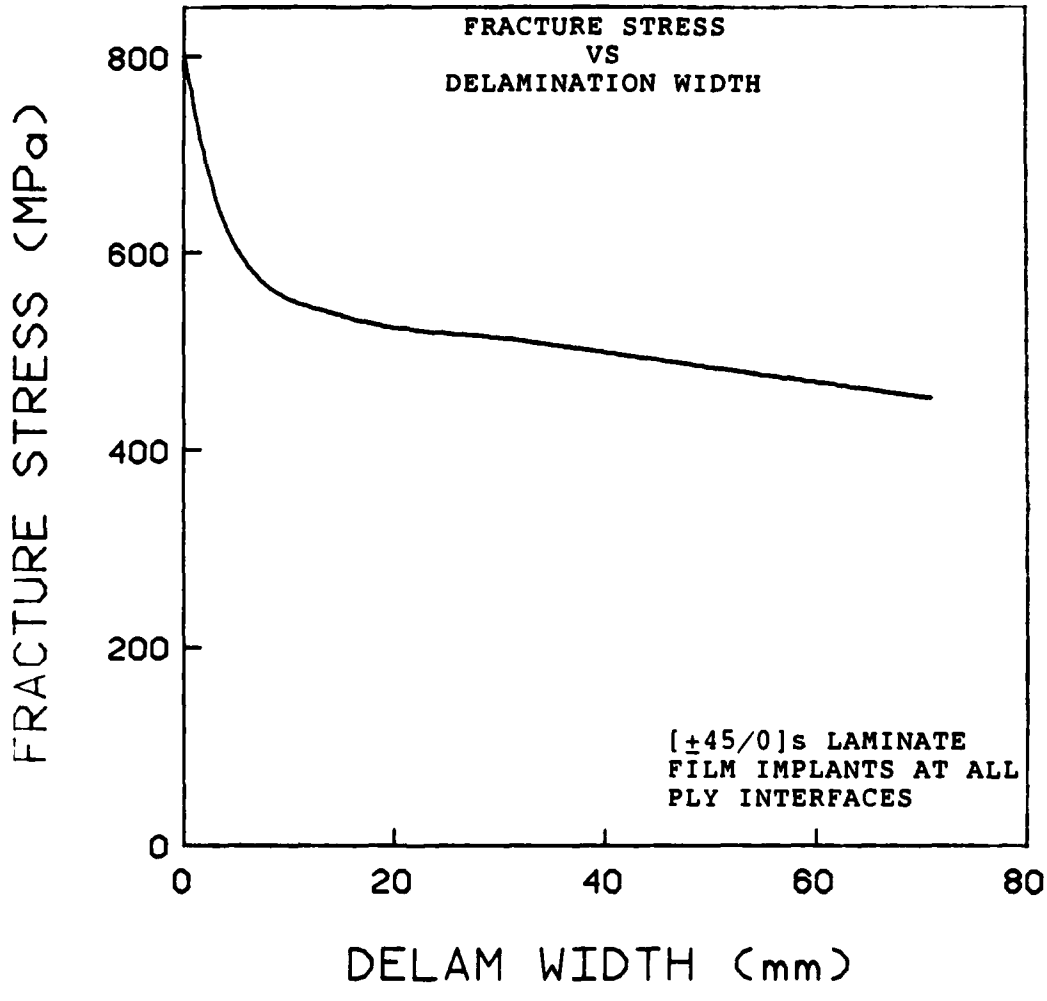

FIGURE 5.31 PLOT OF PREDICTED FRACTURE STRESS VERSUS IMPLANT WIDTH FOR A [±45/0]s SPECIMEN WITH FILM IMPLANTS AT ALL INTERFACES

CHAPTER 6

DISCUSSION

This chapter contains a discussion of the experimental and analytical results reported in Chapter 5. The effects of implant thickness, number, location, and width are discussed.

6.1 Implant Thickness Effects

The difference in the fracture stress between specimens implanted with TCGF and those with film is clearly evident in Table 5.5. This same trend is shown by the analytical model. Examining the stress-strain behavior in light of these facts may provide some insight.

The stress-strain behavior of the unflawed specimens show a softening which becomes obvious at around 270 MPa. After this, the modulus gradually decreases until failure. The failure criterion predicts a first ply failure for this specimen at 587 MPa. However, the 0° plies are still able to carry load and as a result, ultimate failure occurs much later. In actuality, the $\pm 45°$ plies will not completely fail at 587 MPa but will sustain a considerable amount of damage until the specimen fails. The point at which damage starts occurring in the $\pm 45°$ plies is probably prior to the predicted first ply failure stress. The audible pops detected during the

test confirm this as they start at 275 MPa and then continue to failure. This may indicate that the damage to these plies also continues until final fracture. Any damage which does occur, however, does not create any visual observable phenomenon on the specimen.

In contrast to this, the stress-strain behavior of the specimens implanted with either TCGF or film at every ply interface were linear up to the unflawed break stress and then contained numerous discontinuities. As an example, the specimens implanted with a 32 mm TCGF delamination at every ply interface contained both strain discontinuities and reversal points in the ranges from 335 MPa to 480 MPa and then from 550 MPa to 640 MPa. After these discontinuities in the stress-strain curve, the modulus changed. In addition, new splits formed over the implant region shortly after the load was applied and continued until failure. These splits were restricted to the area covering the implant. In the implant region, these plies are unconstrained once they are not bonded to the neighboring plies. Flaggs and Kural [27] showed that the strength of such plies are much lower than their "in situ" strength (i.e. when they are contained in a laminate and thus constrained by neighboring plies). When these plies are in a laminated section and matrix cracks do form within them, the load can be transferred around the crack into the neighboring plies through the bondline. Within the implant region, there is no such three-dimensional load transfer mechanism. Thus, cracks which form continue until they are arrested by the

laminated plies where the load can be redistributed. These observations indicate that the damage is more severe for these specimens with implants than for the unflawed ones as the analytical model indicates.

Additionally, the laminate's plane of symmetry is different at the implant site than at the remainder of the specimen, and as a result, a bending moment is introduced. This causes the specimen to bend so that the flat side is in tension, as illustrated in Figure 6.1, and significantly changes the order and time of ply failure.

The failure model described in Section 4.7, where the properties of the failed ply are set to zero, results in a very conservative estimate of the final failure stress. In order to provide a better estimate of the stress levels where ply failure occurs, the failure model can be modified so that plies which fail due to transverse tension, transverse compression, or shear do not have all their load carrying properties reduced to zero. In other words, in these cases the failure mode is matrix dominated. It is very likely that the fibers are intact and can still carry load. To model this, all elastic moduli in that ply except the component in the fiber direction, $E_{1111}^{[\theta_i]}$ are set to zero. The entire analysis, as outlined in Figure 4.5, was redone and the new predictions with this post ply failure model are very close to the experimentally determined ultimate fracture stress. Additionally, this results in a new order of ply failure.

It should be noted that since the outer plies already have

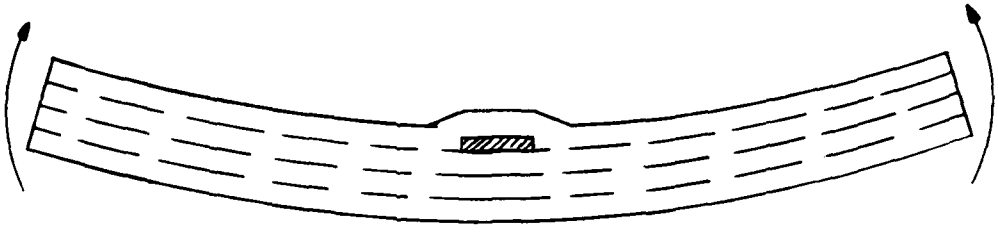

FLAT SIDE OF SPECIMEN

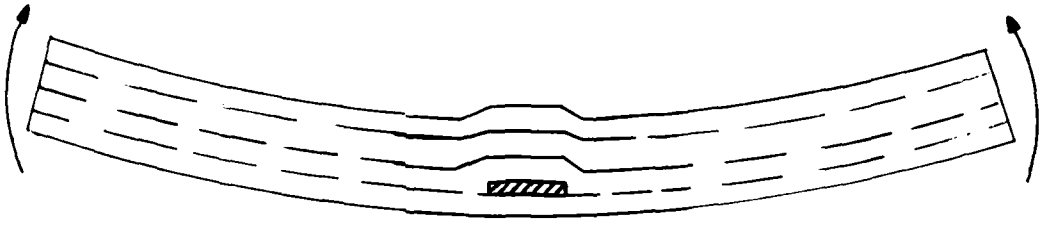

FLAT SIDE OF SPECIMEN

FIGURE 6.1 ILLUSTRATION OF INDUCED BENDING MOMENT FROM AN IMPLANT LOCATED UNDER A SURFACE PLY

matrix cracks before loading, their ply properties will be degraded, as explained above, at the outset. "First ply failure" in this context thus does not refer to the failure of these plies, but subsequent plies after loading begins. Checking the new first ply failure, the modified model predicts that the -45° ply on the flat (or bottom) side of the laminate will fail at 340 MPa followed by failure of the -45° ply on the opposite side of the specimen just prior to ultimate failure. This correlates well with the observed large discontinuities in the stress-strain behavior of these specimens. Now, only the 0° plies remain. Because bending is present in the specimen, the two 0° plies do not carry the same amount of load. This causes one of the 0° plies to fail at a lower load than for the unflawed case. When failure occurs in either of the 0° plies, the other is forced to carry all of the load for the entire specimen. Since this load could not be carried by two plies, certainly one ply will not be able to carry the load. As a result, the entire specimen fractures. Thus, the implants change the stress distribution in the plies to such a degree that one of the primary load bearing plies is forced to carry more than its normal share of the load (as referenced to the unflawed case). This leads to an earlier failure whenever the specimen is implanted with delaminations at every ply interface.

The same characteristics can be seen with the film implants. However, since the implant thickness is smaller, the bending moment is smaller. This leads to less of a distortion

of the "normal" loading distribution in the plies. The modified model predicts a first ply failure of the 45° ply on the bottom side of the laminate at 488 MPa followed shortly thereafter by failure of the other -45° ply on the opposite side of the laminate. Since the 0° plies are loaded more evenly, ultimate fracture does not occur until 750 MPa.

It should be noted that the practice of only degrading the matrix properties on the failed ply if a matrix failure is predicted is not totally accurate as shown by Chou, Orringer, and Rainey [28]. While it is true that fibers remain intact on the laminate after the predicted ply failure stress, the amount of load the ply is able to carry, particularly when bending is present, cannot be accurately determined. Thus, the modified model only provides a rough estimate of the actual response of the laminate. On the other hand, degrading all ply properties following a predicted ply failure, while not precise, provides a limiting condition whereby it is highly unlikely that fracture will occur below. This explains why the predictions made by that model are much lower than the experimental results.

Based upon these facts, it is easy to see why the model using the conservative approach predicts a fracture stress for the specimens with the 32 mm wide film implants at 511 MPa. In practice, this particular implant thickness may be very close to the thickness needed so that no significant stress redistribution or bending moments are produced within the laminate. Both the circular and square 32 mm film implant

shapes failed at approximately the unflawed fracture stress. This not only implies an implant geometry independence, but more significantly, that if the specimen truly contained delaminations at every ply interface, it would not affect the tensile strength. The model predicted a fracture stress of 805 MPa for specimens implanted with delaminations of "zero" thickness. Even the film implants measuring 57 mm wide failed close to the unflawed value. Although the average fracture stress in this case is slightly lower than the mean unflawed fracture stress, all values lie very close to the lowest fracture stresses recorded for an unflawed specimen.

6.2 Effects of the Number and Location of Implants

In this investigation, specimens embedded with either one or five implants located at different ply interfaces were examined. All specimens containing only one implant failed near the unflawed specimen strength independent of implant thickness, size, or shape or location. The analytical model predicts this same effect and provides insight into why this happens.

Since the implants can cause a redistribution of the stresses in the laminate, strength will depend upon the magnitude of the stresses which are redistributed into the primary load carrying plies. An implant located under the surface ply of the $[\pm 45/0]_s$ stacking sequence used in this investigation results in the +45° ply bending out over the

implant area with some splits forming. However, the loss of this ply does not cause a large stress redistribution in the laminate as long as the implant thickness is not too large, so as to cause a larger bending moment.

However, if the single implant were located on the bottom side of the laminate as shown in Figure 6.1, all of the other plies would bend around the implant causing an unequal loading in the 0° plies and thus a large stress redistribution. If the implant is located on the side of the laminate which bulges out, only the top +45° ply will be forced to bend around the implant while the others remain in a straight position just as they would in an unflawed laminate. In this case since the +45° ply fails early, the effect of the implant is neutralized and the laminate responds as if the implant were not present. When the implant is located on the bottom, however, the stress redistribution will cause one of the primary load bearing plies to carry more than its share of the load, resulting in a lower fracture stress. This is substantiated by the model which predicts fracture at 674 MPa when the implant is on this side of the laminate and 805 MPa for the opposite case. Although single implants were not tested in the $[0/\pm45]_s$ stacking sequence, a strength reduction may be expected if the implant thickness was greater than the thickness of the film implants, since a major load carrying ply, a 0° ply, would be forced to bend around the implant.

Of course, the same argument can be extended to the case where more than one implant is present in a laminate. Since

more implants are present, even further bending and resultant stress redistribution occur. This will cause a primary load carrying ply to carry more than its share of load and thus fail even earlier. This effect of embedding consecutive implants in the interface below the current implant was calculated from the model and shown in Figure 5.30. Reductions in strength are noted for specimens with more than one implant. The experimental data is thus in agreement with these conclusions.

Specimens embedded with a film implant under the second ply show no reduction in fracture stress. Because the implant does not fully isolate any single ply, matrix crack growth is hindered since load can be transferred around any crack and into the neighboring plies. Thus, the "in situ" strength of the plies is not significantly affected. It should be noted that in this case, no splits were visually observed in the implant region either before or during loading. In addition, since the single implant is so thin, it does not force any of the plies to bend significantly around the implant. In either case, the stress distribution in the ply is not significantly affected. The stress-strain behavior of these specimens reinforce these conclusions since the stress-strain behavior is nearly identical to that for the unflawed specimens.

For the specimens with one TCGF implant under the surface ply, the implant was located on the bottom side of the laminate in all cases but one. The stress-strain behavior of the specimens with the implant on the the bottom side was somewhat similar to the behavior of those containing implants at all ply

intefaces. Both were characterized by numerous discontinuities although they occurred later on the singly implanted specimens. Even though the location of the implant near the bottom of the laminate causes the five plies to bend around the implant, the implant thickness is not large enough to significantly affect the stress distribution in the plies. This is not only because the moment is small but also because the "in situ" strength of only the 45° ply is affected. Cracking in the remainder of the laminate is minimal since load can be transferred around any matrix cracks. In addition, the 45° ply will fail first, negating the effect of the implant so that the remaining section will soon look like the unflawed specimen. This happens whether the implant is located on the top or the bottom. Thus, the behavior will be similar for these two cases.

Specimens containing the large rectangular TCGF implant at the midply will not have a large stress redistribution in the laminate either. Since there is only one implant and it is located at the midply, only one of the primary load bearing plies is forced to bend around the implant. Thus, only this ply and the two above it are affected by this single implant. Also, since the implant is located at the midply, none of the plies are isolated by the implant. That is, all plies are constrained at least on one surface by the neighboring ply bonded to it. Thus splitting cannot easily occur and the effective "in situ" strength of the ply increases. Therefore, the specimen fails near the unflawed fracture stress. As noted

in Chapter 3, these specimens did not have a far-field gage to measure modulus. The gage mounted in the center of the implant did provide, however, a stress-strain plot which did not contain any discontinuities. This indicates that no large splits formed as in the case where a ply was unrestrained due to being isolated by the implant.

The only other specimens which did not have the discontinuities were those with a single film square implanted under the second ply. In both cases, the outer plies did not contain any matrix cracks since the implant was not directly below the surface. Additionally, matrix cracking did not appear during the test as would be expected since load can be transferred to other plies as soon as a crack formed. This implies that at least some of the discontinuities which characterize the stress-strain behavior of all other specimens must be related to the formation of matrix splits. Matrix cracking, however, occurs throughout the entire test so the discontinuities must either be related to the intensity of the cracking or to another phenomenon caused by or related to this cracking.

6.3 Width Effects

Most of the specimens tested with two different widths showed that the larger width failed at a lower stress level. The one exception is the first batch of five specimens implanted with 57 mm wide implants. These five failed at an

average of 722 MPa with a coefficient of variation of 5.1%. These findings seemed contradictory to the results of the tests conducted on the film implants where the specimens with larger implants failed 13% lower than those with the 32 mm wide implants. To validate the results of the tests with 57 mm TCGF implants, a second batch of five specimens were manufactured and tested. The mean fracture stress of these specimens were 519 MPa with a coefficient of variation of 13.7%. The tests were repeated once more with five new specimens and the results were similar to the second batch of tests.

A large effort was made to determine why the first five specimens showed this uncharacteristically high fracture stress. As stated previously, the fracture modes and stresses for these specimens were very similar to the specimens with film implants. This led to a belief that these TCGF implants were not the same thickness as the other TCGF implants. Micrometer measurements showed that the TCGF from all fifteen specimens were the same thickness, however. In addition, checks were made on the implant width, alignment, the stacking sequence of all laminates, and the material. All factors were the same on all fifteen laminates although the prepreg used on the final batch came from a different roll than that used on the first two batches. Since the higher fracture stresses of the first batch is attributed to more than scatter, the difference remains unexplained. Only the data from the similar two batches are included in the average fracture stress of the specimens with 57 mm wide implants, however. It should be

noted that if the data from the first batch is included, the mean fracture stress of these fifteen specimens is still 60 MPa lower than the specimens implanted with the 32 mm wide TCGF implants.

The rule of mixtures approach used to estimate the effects of the change in implant width does not provide adequate results. It depends upon the modulus of both laminated and delaminated regions prior to a delaminated ply failure. The determination of ply failures in each region is accomplished independently of the behavior of the other region. Thus the $\pm 45^{\circ}$ plies will always fail at 587 MPa in the laminated region. This is not truly the case, however. Since the implants cause the bending moment in the specimen, the order of ply failure in both regions will be influenced greatly. The magnitude of the bending moment will be affected by the width of the implant as well. If the implant spans the entire width of the specimen, then the bending moment would be the greatest. If the implant is within the borders of the specimen, then the laminated area between the implant edge and the specimen edge will increase the bending stiffness of the specimen. Thus, the smaller the implant, the greater the bending stiffness. Since bending is responsible for such an unequal loading in the plies, then specimens with smaller implants will have a more equal loading so that fracture stress will be greater and vice versa. The "quasi-two-dimensional" model makes no provision for this restriction of bending due to the constraint of the laminated region. Thus, the model will

be conservative.

Finally, the rule of mixtures does not account for the fact that the implants isolate the plies making load transfer within this region impossible. As a result, once matrix splitting begins, the splits extend completely across the implant region greatly reducing the strength of the ply and causing the load to be redistributed to other plies contributing to their earlier failure. Thus, larger implants will lead to an even lower fracture strength since a greater portion of the specimen has reduced load carrying capability.

6.4 Implications

The effects that an implant/delamination can have on a composite part can be very significant. While it is unlikely that implants would be intentionally embedded in a part, there are many situations which can arise in manufacture or service which can simulate these conditions. The most obvious might be an inclusion which becomes embedded in a composite during manufacture. For a single inclusion, its criticality will depend upon its thickness, size, and location. The experimental test results from this study show that a thickness of 0.076 mm did not affect the strength of the laminate. As discussed earlier, since the implant is located under a ply which does not carry a substantial part of the load and then fails first anyway, the implant does not adversely affect the distribution of stress in the laminate. This would not be the

case for a $[0/\pm45]_s$ laminate, however. Now the primary load bearing plies are on the outside and isolated from neighboring plies. The combination of bending forces in this ply as well as substantial matrix cracking will vastly degrade the ability of the ply to carry load. Early failure of this ply will then lead to a premature fracture of the laminate. This is substantiated by the model as well. Thus, the inclusion location can be detrimental depending upon the composite layup. If the primary load bearing plies are located on the outside, then splits could easily form in this ply and spread over the width of the inclusion. This happens since this ply is isolated from other plies and load cannot be transferred to neighboring plies. The reduced strength of this primary load carrying ply would cause early failure of the part. Under these circumstances, it would be beneficial to "bury" the load carrying plies so that it is better constrained by neighboring plies thus restricting splitting and increasing the "in situ" strength of the ply. If this is not possible, then the addition of "sacrificial" plies on the outside may be an option to protect principal load carrying plies from this problem.

Another likely situation can result from an impact. Since an impact can cause delamination between plies, this delamination can divide the part into unsymmetric sublaminates. These sublaminates will now deflect and separate because of residual thermal stresses. This separation will act as an "effective" implant. It may be worse if several delaminations exist. In this case, the laminate will have

several "effective" implants which can cause significant stress redistributions due to bending as well as gross matrix cracking due to the inability of a single delaminated ply to transfer load to neighboring intact plies. All of these effects will combine to reduce the strength of the part.

The thickness of the internal implant can have an even greater effect in compression. This is of interest in service, but particularly to researchers who simulate delamination via some sort of implant. These implants will produce a bending moment in compression just as they did in tension and thus a redistribution of stress. This bending can exacerbate the problem of local sublaminate buckling at the delaminated area and may cause the delaminated plies to buckle sooner than expected. Thus, care must be taken in using implants to simulate in-service damage.

CHAPTER 7

CONCLUSIONS AND RECOMMENDATIONS

An investigation was performed to examine the tensile behavior of specimens with implanted delaminations. Experiments were conducted to study the effects of implant thickness, number, location, shape, and width. In addition, an analytical model of the implant area was developed to gain insight into the mechanisms relating to fracture. The following conclusions are made based upon this work:

1. Internal implanted delaminations can significantly affect the strength of a laminate subjected to tensile loads. However, the strength reduction is dependent upon implant thickness, number, location, and width.

2. Implant thickness affects a laminate by producing a bending moment in the specimen which causes the plies to bend around the implant. These change the stress distribution within the plies. Increasing the implant thickness, creates more bending and thus a greater redistribution of the stress.

3. The analytical model shows the trends in the experimental data well, especially when the modified post ply failure

procedures are followed.

4. Implant width affects a laminate in two ways. Larger widths reduce the bending stiffness of the laminate and increases the area available where matrix cracks can form. Both of these factors have a deleterious effect on the laminate.

5. The rule of mixtures approach is inadequate in estimating the affects due to implant width.

6. Multiple implants which isolate a ply from the neighboring plies inhibit load transfer from the ply. As a result, cracks which form will span the implant area quickly and cause a strength reduction in the ply.

7. To protect the primary load bearing plies from becoming isolated from neighboring plies by a delamination due to events such as impact, it is better to "bury" them within the laminate. This will better assure that the three-dimensional load transfer mechanism due to the bond between plies will not be destroyed so that large splits do not grow in primary load bearing plies.

In order to gain additional insight into the implanted delamination problem and advance the work conducted in this investigation, the following work is recommended:

1. The analytical model be improved by matching the bending stiffness of the laminated and delaminated regions. This will provide a more accurate determination of ply failure as well as fracture strength.

2. More accurately define the effects which the number of implants have on the fracture strength by embedding an increased number of implants on different specimens.

3. Conduct similar tests using a fabric instead of a layup consisting of unidirectional plies. Since splits will not be able to form in the fabric even though the ply is delaminated, strain readings could be taken on and around the delamination. This will also serve to separate the reduction in strength due to splits from that due to bending.

4. Examine methods for determining post first ply failure effects so as to establish a better failure model to improve predictions of fracture strength.

5. Investigate the effect of implant thickness in compression. Current compression studies assume the implant itself does not have any affect on sublaminate buckling or delamination growth.

REFERENCES

1. Labor, J. D., and Bhatia, N. M., "Impact Resistance of Graphite and Hybrid Configurations," Fibrous Composites in Structural Design, 1978, pp. 293-312.

2. Pagano. N. J., and Pipes, R. B., "Some Observations on the Interlaminar Strength of Composite Laminates," International Journal of Mechanical Sciences, Vol. 15, 1973, pp. 679-688.

3. Pagano, N. J., Soni, S. R., "Global-Local Laminate Variational Model," International Journal of Solids and Structures, Vol. 19, No. 3, 1983.

4. Puppo, A. H., and Evensen, H. A., "Interlaminar Shear in Laminated Composites Under Generalized Plane Stress," Journal of Composite Materials, Vol. 4, 1970, pp. 204-220.

5. Pipes, R. B., and Pagano, N. J., "Interlaminar Stresses in Composite Laminates Under Uniform Axial Extension," Journal of Composite Materials, Vol. 4, 1970, pp. 538-548.

6. Whitney, J. M., "Free-Edge Effects in the Characterization of Composite Materials," Analysis of the Test Methods for High Modulus Fibers and Composites, ASTM STP 521, American Society for Testing and Materials, 1973, pp. 167-180.

7. Pagano, N. J., and Pipes, R. B., "The Influence of Stacking Sequence on Laminate Srength," Journal of Composite MateriaLs, Vol. 5, 1971, pp. 50-57.

8. O'Brien, T. K., "Characterization of Delamination Onset and Growth in a Composite Laminate," Damage in Composite Materials, ASTM STP 775, K. L. Reifsnider, Ed., American Society for Testing and Materials, 1982, pp. 140-167.

9. Herakovich, C. T., "Influence of Layer Thickness on the Strength of Angle-Ply Laminates," Journal of Composite Materials, Vol. 16, May 1982, pp. 216-226.

10. Rybicki, E. F., Schmueser, D W., and Fox, J., "An Energy Release Rate Approach For Stable Crack Growth in the Free-Edge Delamination Problem," Journal of Composite Materials, Vol. 11, 1977, pp. 470-486.

11. Wang, S. S., "Delamination Crack Growth in Unidirectional Fiber-Reinforced Composites under Static and Cyclic Loading," Composite Materials: Testing and Design (Fifth Conference), ASTM STP 674, S. W. Tsai, Ed., American Society for Testing and Materials, 1979, pp. 642-663.

12. Crossman, F. W., Warren, W. T., Wang, A. S. D., and Law, G. E., "Initiation and Growth of Tranverse Cracks and Edge Delamination in Composite Laminates," Journal of Composite Materials, Supplemental Volume (1980), pp. 88-106.

13. Talug, A., and Reifsnider, K. L., " Analysis of Stress Fields in Composite Laminates With Interior Cracks," Fibre Science and Technology, Vol. 12, 1979, pp. 201-215.

14. Reifsnider, K. L., and Talug, A.,"Analysis of Fatigue Damage in Composite Laminates," International Journal of Fatigue, Vol. 3, No. 1, January 1980, pp. 3-11.

15. O'Brien, T. K., "Analysis of Local Delaminations And Their Influence On Composite Laminate Behavior," USAAVSCOM Technical Report 83-B-6, NASA Technical Memorandum 85728, January, 1984.

16. Wang, A. S. D., and Slomiana, M., "Fracture Mechanics of Delamination Initiation and Growth," Report No. NADC-79056-60, Contract No. N62269-79-C-0270, Drexel University, Philadelphia, Pa., January, 1982.

17. Chai, H., and Babcock, C. D., "Two-Dimensional Modeling of Compressive Failure in Delaminated Laminates," Journal of Composite Materials, Vol. 19, 1985, pp. 67-98.

18. Ramkumar, R. L., "Compression Fatique Behavior of Composites in the Presence of Delaminations," Damage in Composite Materials, ASTM STP 775, K. L. Reifsnider, Ed., American Society for Testing and Materials, 1982, pp. 184-210.

19. Lagace, P. A., and Brewer, J. C., TELAC Manufacturing Course Notes, Edition 0-2, Technology Laboratory for Advanced Composites, TELAC Report 81-14, Massachusetts Institute of Technology, September 1981.

20. "Standard Test Method for Tensile Properties of Fiber-Resin Composites," ASTM Designation D 3039-76.

21. Lagace, P. A., Static Tensile Fracture of Graphite/Epoxy, Technology Laboratory for Advanced Composites, TELAC Report No. 82-5, Ph. D. Thesis, Department of Aeronautics and Astronautics, Massachusetts Institute of Technology, June, 1982.

22. Kassapoglou, C., Interlaminar Stresses at Straight Free Edges of Composite Laminates, Technology Laboratory for Advanced Composites, TELAC Report No. 84-18, S. M. Thesis, Department of Aeronautics and Astronautics, Massachusetts Institute of Technology, October, 1984.

23. Operating Instructions and Technical Manual, Measurements Group, Photoelastic Division, 1977.

24. Vizzini, A. J., and Lagace, P. A., "Tebas-Telac Software User's Manual," Telac Report No. 84-14-2, 1984.

25. Jenkins, C. F., "Report on Materials of Construction Used in Aircraft and Aircraft Engines," Great Britain Aeronautical Research Committee, 1920.

26. Lagace, P. A., "Nonlinear Stress-Strain Behavior of Graphite/Epoxy Laminates," AIAA Journal, Vol. 23, No. 10, October 1985, pp. 1583-1589.

27. Flaggs, D. L., and Kural, M. H., "Experimental Determination of the In Situ Transverse Lamina Strength in Graphite/Epoxy Laminates," Journal of Composite Materials, Vol. 16, 1982, pp. 103-114.

28. Chou, C., Orringer, O., and Rainey, J. H., "Post-Failure Behavior of Laminates I - No Stress Concentration," Journal of Composite Materials, Vol. 10, 1976, pp. 371-381.

DATA TABLE 1

SUMMARY OF DATA FOR $[\pm 45/0]_s$ SPECIMENS

SPECIMEN	THICKNESS		LONG. MODULUS [GPa]	σ_f [MPa]	STRAIN GAGE
	AWAY FROM IMPLANT [mm]	OVER IMPLANT [mm]			
0-45A1-1	0.836	N/A	65.7	831	C
0-45A1-2	0.833	N/A	62.7	931	C
0-45A1-3	0.841	N/A	62.1	836	C
0-45A1-4	0.834	N/A	57.0	706	C
0-45A1-5	0.841	N/A	65.6	828	C
C1-45A1-11G	0.836	0.848	59.0	817	A-E
C1-45A1-21G	0.843	0.856	60.6	809	A-E
C1-45A1-31G	0.856	0.896	60.5	850	A-E
C1-45A1-41G	0.850	0.890	63.6	878	A-E
C1-45A1-51G	0.855	0.868	62.0	911	A-E
S2-45A1-22F	0.841	0.841	*	838	C
S2-45A1-32F	O.843	0.843	58.1	845	C
S2-45A1-42F	0.831	0.831	61.3	815	C
S2-45A1-52F	0.845	0.845	61.0	857	C
S2-45A1-62F	0.834	0.834	61.4	771	C
S3-45A1-1G	0.889	0.889	57.7	683	B
S3-45A1-2G	0.899	0.899	60.0	801	B
S3-45A1-3G	0.897	0.897	62.7	782	B
S3-45A1-4G	0.904	0.904	58.3	864	B
S3-45A1-5G	0.900	0.900	57.4	792	B

* DENOTES INOPERATIVE STRAIN GAGE

DATA TABLE 2

SUMMARY OF DATA FOR $[\pm 45/0]_s$ SPECIMENS

SPECIMEN	THICKNESS		LONG. MODULUS [GPa]	σ_f [MPa]	STRAIN GAGE
	AWAY FROM IMPLANT [mm]	OVER IMPLANT [mm]			
C4-45A1-11F	0.835	0.900	53.7	717	C
C4-45A1-21F	0.833	0.889	61.9	800	C
C4-45A1-31F	0.854	0.891	61.8	860	C
C4-45A1-41F	0.834	0.858	55.6	787	C
C4-45A1-51F	0.841	0.920	62.5	746	C
S4-45A1-11F	0.849	0.891	60.8	779	C,F
S4-45A1-21F	0.846	0.900	57.8	848	C,F
S4-45A1-31F	0.847	0.910	61.0	839	C,F
S4-45A1-41F	0.847	0.900	60.0	791	C,F
S4-45A1-61F	0.863	0.890	59.4	840	C,F
S4-45A1-22F	0.869	0.895	62.5	699	C
S4-45A1-32F	0.860	0.900	63.2	735	C
S4-45A1-42F	0.867	0.890	56.9	684	C
S4-45A1-52F	0.840	0.885	55.5	674	C
S4-45A1-62F	0.856	0.893	60.7	730	C

DATA TABLE 3

SUMMARY OF DATA FOR $[\pm 45/0]_s$ SPECIMENS

SPECIMEN	THICKNESS AWAY FROM IMPLANT [mm]	THICKNESS OVER IMPLANT [mm]	LONG. MODULUS [GPa]	σ_f [MPa]	STRAIN GAGE
C4-45A1-11G	0.876	1.097	55.7	649	A-E
C4-45A1-21G	0.896	1.110	61.8	686	A-E
C4-45A1-31G	0.913	1.145	61.7	648	A-E
C4-45A1-41G	0.885	1.170	60.9	616	A-E
C4-45A1-51G	0.899	1.110	61.2	659	A-E
C4-45A1-61G	0.862	1.090	55.1	580	C
C4-45A1-71G	0.868	1.080	61.4	532	C
C4-45A1-81G	0.869	1.070	61.9	625	C
C4-45A1-91G	0.866	1.110	58.9	637	C
C4-45A1-101G	0.868	1.070	61.1	5.5	C
S4-45A1-11G	0.880	1.122	59.5	582	C,F
S4-45A1-21G	0.871	1.076	61.0	615	C,F
S4-45A1-31G	0.874	1.120	61.7	716	C,F
S4-45A1-41G	0.866	1.102	60.5	536	C,F
S4-45A1-51G	0.877	1.105	57.3	544	C,F
S4-45A1-12G	0.985	1.137	62.9	694	C
S4-45A1-22G	0.977	1.145	62.5	690	C
S4-45A1-32G	0.985	1.149	62.6	740	C
S4-45A1-42G	0.989	1.149	61.7	706	C
S4-45A1-52G	0.971	1.134	65.4	778	C
S4-45A1-72G	0.993	1.150	61.8	460	C
S4-45A1-82G	1.011	1.135	65.1	446	C
S4-45A1-92G	1.028	1.153	63.0	624	C
S4-45A1-102G	1.003	1.144	61.3	535	C
S4-45A1-112G	0.964	1.118	60.9	530	C
S4-45A1-122G	0.926	1.146	69.6	390	C
S4-45A1-132G	0.960	1.134	61.0	430	C
S4-45A1-142G	0.975	1.131	62.8	523	C
S4-45A1-152G	0.992	1.143	61.9	466	C
S4-45A1-162G	0.965	1.150	62.4	402	C

DATA TABLE 4

SUMMARY OF DATA FOR $[0/\pm45]_s$ SPECIMENS

SPECIMEN	THICKNESS		LONG. MODULUS [GPa]	σ_f [MPa]	STRAIN GAGE
	AWAY FROM IMPLANT [mm]	OVER IMPLANT [mm]			
0-45B1-1	0.828	N/A	61.0	741	C
0-45B1-2	0.822	N/A	62.1	745	C
0-45B1-3	0.837	N/A	60.0	841	C
0-45B1-4	0.822	N/A	62.7	843	C
0-45B1-5	0.821	N/A	62.1	806	C
S4-45B1-11G	0.906	1.902	58.9	677	C,F
S4-45B1-21G	0.881	1.101	60.3	599	C,F
S4-45B1-31G	0.882	1.099	62.3	822	C,F
S4-45B1-41G	0.875	1.096	60.3	659	C,F
S4-45B1-51G	0.890	1.148	61.6	810	C,F
S4-45B1-12G	0.944	1.148	59.0	563	C
S4-45B1-22G	0.953	1.118	64.3	796	C
S4-45Ba-32G	0.976	1.133	62.6	773	C
S4-45B1-42G	0.941	1.141	59.5	674	C
S4-45B1-52G	0.989	1.150	61.4	756	C


FILMED
0-8